# Nature of Large Vesicle Exocytosis in Pancreatic -cells: Release of ATP and GABA

Karanauskaite, Jovita

2008

# NATURE OF LARGE VESICLE EXOCYTOSIS IN PANCREATIC B-CELLS: RELEASE OF ATP AND GABA

**JOVITA KARANAUSKAITE**

**DOCTORAL THESIS**

THIS THESIS WILL BE DEFENDED ON 30TH OCTOBER 2008 AT 13.00 IN OSCE LECTURE HALL, CRC, ENTRANCE 93, MALMÖ, SWEDEN

**FACULTY OPPONENT:**

ASOCIATE PROFESSOR CHRISTINA BARK,
DEPARTMENT OF MOLECULAR MEDICINE AND SURGERY, KAROLINSKA INSTITUTE,
KAROLINSKA UNIVERSITY HOSPITAL, STOCKHOLM, SWEDEN


LUND UNIVERSITY

**DEPARTMENT OF CLINICAL SCIENCES**

**LUND 2008**

# CONTENTS

# ORIGINAL PUBLICATIONS

This thesis is a summary of the following papers, which will be referred to in the text by their Roman numerals:

I. Karanauskaite J, Hoppa ME, Braun M, Galvanovskis J and Rorsman P. (2008) Quantal ATP release in rat β-cells by exocytosis of insulin-containing LDCVs. *(Manuscript)*.

II. Braun M, Wendt A, Karanauskaite J, Galvanovskis J, Clark A, MacDonald PE, Rorsman P. (2007) Corelease and differential exit via the fusion pore of GABA, serotonin, and ATP from LDCV in rat pancreatic beta cells. J *Gen Physiol* 129(3):221-31.

III. Obermuller S, Lindqvist A, Karanauskaite J, Galvanovskis J, Rorsman P and Barg S. (2005) Selective nucleotide-release from dense-core granules in insulin-secreting cells. *J Cell Sci* 118(Pt 18): 4271-82.

IV. Hoppa MB, Karanauskaite J, Eliasson L, Hanna S, Clark A, MacDonald PE, Rorsman P. (2008) Global elevations in cytoplasmic $Ca^{2+}$ elicit compound exocytosis in rat pancreatic β–cells and Ins-1 cells. (*Manuscript).*

# ABBREVIATIONS

| | |
|---|---|
| **5-HT** | 5-hydroxytryptamine (serotonin) |
| **ADP** | Adenosine diphosphate |
| **ATP** | Adenosine triphosphate |
| **EGFP** | Enhanced green fluorescent protein |
| **EPSCs** | Excitatory post synaptic current |
| **ER** | Endoplasmic reticulum |
| **GABA** | Gamma-aminobutyric acid |
| **IAPP** | Islet amyloid polypeptide |
| **IDDM** | Insulin-dependent diabetes (Type-1 diabetes) |
| **Ins-1** | Rat insulinoma cell line |
| **LDCV, LV** | Large dense core vesicles, large vesicles |
| **NIDDM** | Non-insulin-dependent diabetes mellitus (Type-2 diabetes) |
| **NSF** | N-ethylmaleimide-sensitive factor |
| **$P2X_2R$** | Purinergic ATP sensitive receptor-channel, type-2 |
| **RRP** | Readily releasable pool |
| **SLMV, SV** | Synaptic like micro vesicles, small vesicles |
| **SNARE** | Soluble NSF attachment receptor |
| **TIC** | Transient inward currents |
| **TIRF** | Total internal reflection microscopy |
| **VAMP** | Vesicle-associated membrane protein |

# INTRODUCTION

The blood sugar-regulating hormone insulin is synthesized, stored and released from the pancreatic islets of Langerhans. These were named in honour of the German pathological anatomist Paul Langerhans who discovered these tiny structures of the pancreas in 1869. Usually about a million islets of various sizes are found in a healthy adult pancreas. Allthough the combined weight of these small roughly spherical cell clusters in humans is only from 1 to 1.5 grams, they play a crucial role in the metabolism of the whole body and have a profound effect on human health (Spellman, 2007). The decrease in islet cell mass brought about by their autoimmune destruction, initiates Type-1 or insulin-dependent diabetes mellitus (IDDM). Although this form of diabetes causes severe and hard to repair health problems in the affected individual, much greater harm for modern society results from another type of illness attributed to insulin. This non-insulin-dependent form of diabetes mellitus (NIDDM or Type-2 diabetes) is much more common than IDDM. It affects ~6% of the world population, and its prevalence is persistently rising, especially in developing countries. NIDDM is characterised by insulin resistance and hyperinsulinaemia and eventually glucose resistance and hyperglycaemia. In individuals suffering from Type-2 diabetes, pancreatic islets and insulin-containing β-cells do not differ morphologically from those found in healthy subjects and they contain the same quantities of insulin as healthy cells but it is not released, most likely because of impaired secretion mechanisms (Kahn and Porte, 1988). In order to understand why a diabetic pancreatic β-cell, fully loaded with insulin and ultrastructually undistinguishable from a healthy one, retains its cargo and does not respond to physiological stimuli of secretion and to find ways to restore normal secretion in these cells, it is important to unravel the subcellular and molecular mechanisms that normally ensure the release of insulin and other substances into extracellular space.

## Cell types found in islets of Langerhans

The focus of this thesis is the insulin-secreting β-cells. They constitute the majority of cells found in pancreatic islets of Langerhans. In rat, the animal model used throughout this study, 65 - 80% of all islet cells are insulin-producing β-cells; 15 - 20% of islet cells secrete glucagon (α-cells), 3 - 10% secrete somatostatin (δ-cells). The rest consists of pancreatic peptide-containing PP-cells and ghrelin-containing GH-cells. Knowledge about the two last cell types is currently very limited. Even though α– and δ–cells are believed to provide an essential contribution

to the regulation of blood sugar levels, most research on islets conducted to date has been performed on β-cells.

## Secretion process in β-cells

Pancreatic β-cells, like all endocrine cells, possess a highly developed secretory process. Proteins or peptides, including insulin, targeted for delivery to the outside the cell are synthesized in the rough endoplasmic reticulum, then folded and moved to the Golgi apparatus. There the peptides are biochemically modified and, finally, tightly packed into secretory vesicles or granules. These are small spherical bodies of ~350 nm diameter surrounded by a membrane made of a lipid bilayer. Each β-cell contains more than 10,000 granules (Dean, 1973, Olofsson et al., 2002) with insulin organized into a dense crystal core stabilized by Zn ions. This core is electronically opaque and appears in electron micrographs as a dark dot contrasted by a surrounding white halo. This characteristic appearance has led to these granules being named large dense core vesicles (LDCVs). Insulin is neither the only compound, nor the only type of substances produced by β-cells. Apart from insulin, β-cells release C-peptide and amylin or islet amyloid polypeptide (IAPP) into the extracellular space. To make the picture even more complicated, a number of low-molecular weight transmitter molecules, such as amino acids, nucleotides and amines, are present in the granules and co-released with insulin. This complex mixture of substances is often referred to as 'granular cargo'. It is fascinating that LDCVs contain and release millimolar concentrations of ATP which is known to be a universal source of energy in most living organisms. There is some experimental evidence that implicates ATP released from pancreatic β-cells in paracrine signalling (Salehi et al., 2005). However, its impact on hormone secretion from pancreatic cells is far from being fully understood.

In common with neurones, pancreatic β-cells also possess small vesicles with a diameter of ~90 nm and called synaptic-like-microvesicles (SMLVs) (Braun et al., 2004, Reetz et al., 1991). At present, the relative roles of SVs, LDCVs and different substances released from them, their interactions while responding to secretion stimuli, ways of their differential regulation etc. remain largely unknown.

Release of insulin from LDCVs is triggered by an increase in blood glucose levels. Glucose molecules are rapidly carried across the β-cell membrane by highly expressed high-capacity low-affinity glucose transporter glut-2 (Newgard and McGarry, 1995). Glucokinase, which is considered to be an intracellular 'glucose sensor' (Matschinsky, 1996), phosphorylates glucose to glucose-6-phosphate catalyzing the first steps of its metabolism

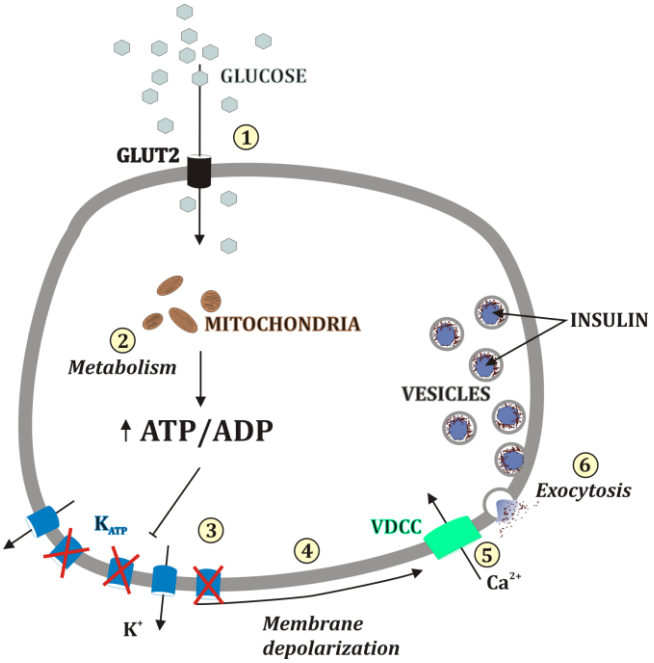


**Figure 1. Glucose stimulated exocytosis from insulin secreting cells.**

(Iynedjian, 1993, Matschinsky, 1996, Newgard and McGarry, 1995). During subsequent steps of glucose metabolism, ATP is produced in mitochondria, thus increasing the ATP/ADP ratio in the cell cytoplasm. This leads to the closure of ATP sensitive $K^+$ channels ($K_{ATP}$ channels) on the cell membrane (Fig. 1). In pancreatic β-cells these channels are responsible for creating a resting membrane potential of about -70mV. The closure of these channels is associated with membrane depolarization and ultimately activates voltage-gated L-type $Ca^{2+}$ channels. The ensuing influx of $Ca^{2+}$ accelerates the cell membrane depolarization, initiates action potentials and triggers the fusion of the granule membrane with the plasma membrane. Thus, granular cargo is discharged into the blood stream in an oscillatory manner (Ashcroft and Rorsman, 1989, Lang, 1999). Over physiological concentrations, electrical activity of β-cells and the resulting stimulation of insulin secretion are approximately proportional to glucose concentration in the cell environment. Finally, at 20 mM glucose (and above), the β-cells respond electrically with uninterrupted action potential firing and continuous release of cargo.

## Exocytosis of insulin granules

The fusion of vesicle/granule and cell membranes that results in the formation of a fluid pathway between the two aqueous compartments, the granule lumen and extracellular space, is called exocytosis. This pathway begins as a

microscopic water-filled pore and later evolves in a way that ensures the discharge of composite granular cargo. The complex process of exocytosis is usually devided into several steps depending on how the term "exocytosis" is understood. In our treatment of exocytosis we shall include the following six steps: 1) adhesion or tethering, 2) docking, 3) priming, 4) membrane fusion and fusion pore formation, 5) pore widening, and 6) content/cargo discharge (Zimmerberg, 1987).

An increasing number of proteins have been implicated in the exocytosis of secretory vesicles. The most important of these are: 1) the soluble NSF attachment receptors, or SNAREs, a group of proteins that include vesicular synaptobrevin (VAMP), synaptosome associated protein of 25 kDa (SNAP-25) and syntaxin which are located on the cell membrane (Jahn and Scheller, 2006); 2) NSF (a soluble *N*-ethylmaleimide-sensitive factor), an ATPase that binds to SNARE complexes via adaptor proteins called "SNAPs" (NSF adaptor proteins); NSF functions in a way similar to a chaperones, in that it mediates an ATP-dependent conformational change in its substrate (Tagaya et al., 1993); 3) Rabs and Sec1/Munc18-like (SM proteins proteins) (Abderrahmani et al., 2006, Lang, 1999); and 4) the $Ca^{2+}$-sensing protein synaptotagmin (Meldolesi and Chieregatti, 2004). Several isoforms of this protein has been detected of which synaptotagmins III, V, VII, VIII and IX are expressed in β-cells (Mizuta et al. 1997; Brown et al. 2000; Gao et al. 2000; Gut et al. 2001; Iezzi et al. 2004). It is known that SNARE proteins syntaxin and SNAP-25 interact with voltage-dependent calcium channels (Catterall, 1999), and that this interaction mediates the tight coupling of $Ca^{2+}$ entry and the fusion of vesicles that belong to the readily releasable pool (RRP) (Barg and Rorsman, 2004).

A schematic view showing the relative positions of these proteins inside a β-cell during the different exocytotic steps can be found in Fig. 2.

**Adhesion or tethering.** It is useful to distinguish between the initial loose *tethering* of vesicles/granules to their targets from the more stable *docking* interactions. This follows from the fact that the initial contact between fusing biological membranes is fundamentally different from one between two protein-free bilayers. Usually the distance between bilayers of biological membranes is as wide as 10–25 nm, and the contact zone is crowded with a multitude of membrane-associated proteins. These proteins have to be removed so that lipid bilayers of fusing membranes can establish a physical contact. The displacement of proteins that are not involved in the building of the exocytotic machinery is almost always mediated by specific tethering molecules. In pancreatic β-cells this is done with the help of F-actins, a specific eight-subunit protein complex known as the "exocyst", and the plasma membrane-associated small

GTPase protein, Ra1A (Lopez et al., 2008, Varadi et al., 2005). Tethering interactions are likely to be involved in the concentration of secretory vesicles at sites of exocytosis (Fig. 2B ).

**Docking.** The term *docking* refers usually to the holding of two membranes within a bilayer's distance of one another (<5-10 nm). Stable docking comprises several distinct molecular states, since the molecular interactions underlying the close and tight association of a vesicle with its target should include the molecular rearrangements needed to trigger bilayer fusion. A common feature of many proteins that function in vesicle tethering and docking is their tendency to form highly extended, coiled-coil structures. Physical docking occurs when VAMP attached to the granule membrane, binds to two proteins on the cell membrane, syntaxin and SNAP-25. Other proteins such as α-SNAP and NSF also attach. The granule membrane protein synaptotagmin, which is also included in the docking protein complex, binds four Ca ions per molecule, so it may act as the calcium sensor for the exocytotic machinery.

When tethering and docking have

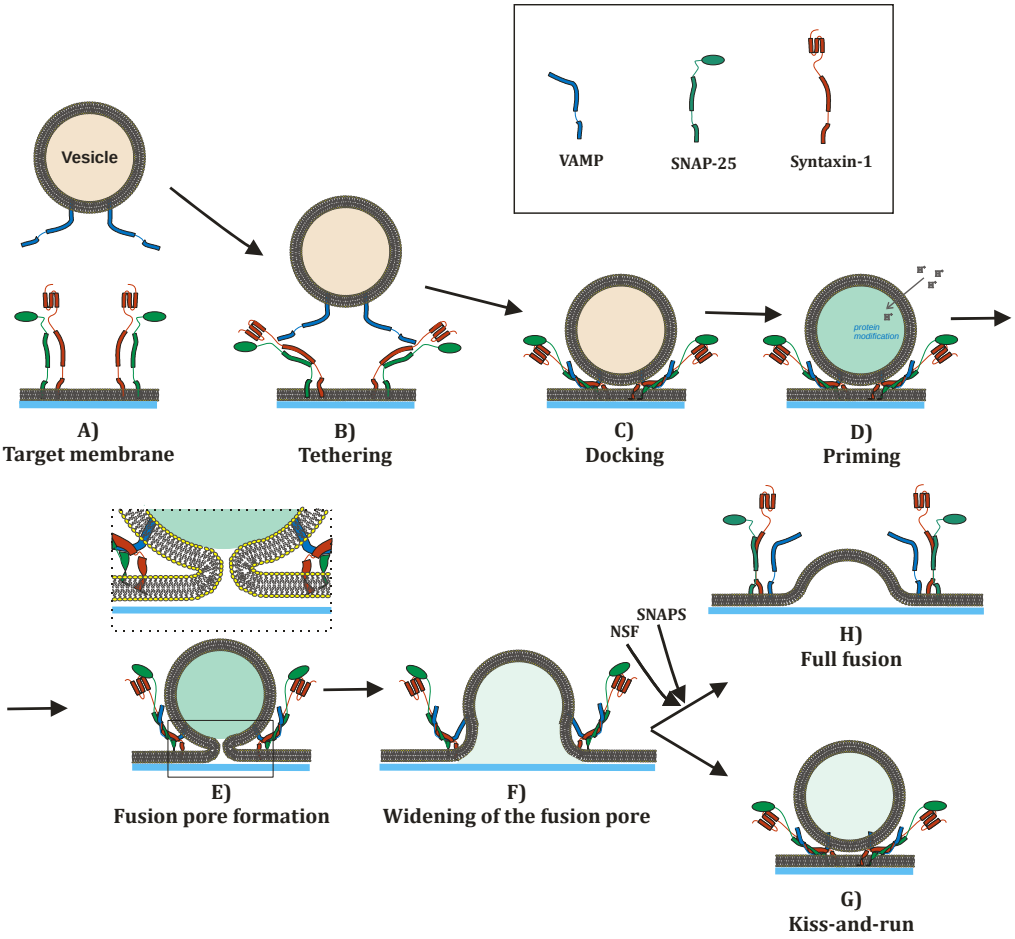


**Figure 2. Main steps in LDCV exocytosis with relative positions of proteins involved.** The SNARE complex is formed by VAMP (blue), SNAP-25 (green) and Syntaxin-1 (red).

been completed (Fig. 2C), the secretory granule is ready for priming and the formation of a tight-core SNARE complex.

**Priming.** This step includes all of the molecular rearrangements and ATP-dependent protein and lipid modifications that take place after initial docking of a secretory vesicle until membrane fusion. After this step the influx of $Ca^{2+}$ ions is all that is needed to trigger nearly instantaneous cargo release. Different priming reactions and enzymes have been proposed (Lang, 1999) but the exact nature and extent of this final preparation step before membrane fusion remains unresolved. One of the central events here may well be intragranular acidification dependent on simultaneous operation of the V-type $H^+$-ATPase and the ClC-3 $Cl^-$-channel (Barg et al., 2001a). This acidification may facilitate the conformational changes in SNARE proteins that are necessary to render these proteins fusogenic (Sutton et al., 1998) (Fig. 2D).

In other cell types, in which secretion is constitutive (i.e. continuous, $Ca^{2+}$ ion independent, non-triggered secretion) priming of granules is not recquired.

**Membrane fusion and fusion pore formation.** In pancreatic β-cells the fusion of fully primed granules with the cell membrane occurs in response to elevated cytosolic $Ca^{2+}$ concentrations in the immediate vicinity of the core complex of proteins that comprise the exocytotic machinery. High $[Ca^{2+}]_i$ causes a conformational change within the core complex that forces the granule membrane into physical contact with the cell membrane (Fig. 2E). What happens immediately after the contact has been formed is not yet fully understood and is the subject of much controversy. The end result of this transformation is, however, the formation of a water-filled channel or pore that spans the lipid bilayers of both the plasma and vesicular membranes. What remains unresolved is whether the fusion pore is lined by proteins or lipids. All fusion pore models that have been proposed as yet fall into two distinct classes based on this. There is experimental evidence that supports both possibilities. Though important, these considerations are irrelevant to topics discussed in this thesis. It is critical, however, that the fusion pore is created after the $Ca^{2+}$ signal has reached the exocytotic core complex, and that it stays stable for time intervals of various duration and at a variety of widths (Fig.2F) (Breckenridge and Almers, 1987, Ardiles et al., 2007).

Two distinct modes of the fusion pore behaviour have been detected in a variety of secretory systems: “kiss-and-run fusion” and “full fusion”.

**Kiss-and-run exocytosis.** As mentioned above, fusion of a secretory granule with the plasma

membrane begins with the formation of a narrow water-filled pore. The initial pore size can be as small as 2-3 nm. Later on, the pore can widen, then stay stable for a comparatively long time (from tens of ms to several seconds) or its diameter can oscillate around a certain average value. In many cases it closes without the granule losing its integrity (Fig. 2G). A critical pore size of 10-20 nm may not be exceeded for the re-closure to happen (Alvarez de Toledo et al., 1993, Lollike et al., 1998, Spruce et al., 1990). This behavior of secretory vesicles is referred to "kiss-and-run" exocytosis. After being detected, this type of granule fusion raised a plethora of interesting and important questions about secretion. These include, for example, the differential release of substances depending on their molecular weight and structure; the regulation of the pore size and recapture, and the exchange of lipid between the two membranes involved. Many aspects of these processes have been intensely studied during recent years but several important questions remain to be answered.

**Full fusion exocytosis.** Another sequence of events detected in secretory cells after the membrane fusion involves full fusion of the vesicle/granule with the cell membrane. In this scenario, the fusion pore, after its formation, expands irreversibly and all the granule content is released into the extracellular space. Simultaneously, the membrane lipids of the granule integrate into the plasma membrane by rapid lateral diffusion (Fig. 2H) (Detimary et al., 1995, Kirshner et al., 1966). This type of fusion event – referred as 'full fusion' - is important in situations when fast release of peptide hormones is required or when components of granular membrane are to be incorporated into the cell membrane. Many factors affect the dynamics of the fusion pore. It has been shown that both cytosolic and extracellular $Ca^{2+}$ concentration have a significant impact on the type of fusion that granules undergo (Ales et al., 1999, Hartmann and Lindau, 1995). Other compounds of interest in this context are protein kinase C (Scepek et al., 1998), proteins of the exocytotic machinery, such as complexin (Archer et al., 2002), synaptotagmin (Wang et al., 2001), and syntaxin (Han et al., 2004).

**Release of cargo.** The release of granular cargo is the final step of the exocytotic event. In case of insulin secretion, it is noteworthy that granules in β-cells contain substances of highly variable molecular size: from ~2 nm for ATP to more than 10 nm for the insulin-Zn crystals. Additionally, each substance within a granule is embedded in a specific matrix consisting of a number of glycoproteins. The matrix acts as an ion-exchanger (Westphal et al., 1999) that facilitates the packing of a large amount of charged molecules into the comparatively small

granule. The electrochemical properties of the matrix directly influence the release rate of all substrates, charged or neutral, once fusion pore has been formed. It may also have an indirect effect on the dynamics of the fusion pore, through swelling after the loss of bound counter-ions (Tabares et al., 2003).

## Mobilization of LDCVs

Exocytosis in isolated β-cells elicited by membrane depolarization or photorelease of caged $Ca^{2+}$ follows a biphasic time course; it exhibits a rapid early and a slow late phase. Interestingly, a similar biphasic secretion response to glucose stimulation is present in isolated whole islets as well as systemically. The similarity of these responses led to the suggestion that 1st phase insulin secretion may correspond to the fast early component of exocytosis in single β-cells detected in capacitance measurements (Barg et al., 2001b, Gillis and Misler, 1992).

In single β-cells, the biphasic exocytotic response has been used to argue the exisence of several granule pools, which differ functionally and/or morphologically. The initial fast exocytotic component is usually referred to as RRP, which contains docked and fully primed granules. The granules in this pool are located on or close to the intracellular side of the cell membrane, though not all granules that are morphologically docked belong to this pool. This pool is responsible for the fast physiological response to an increase in blood glucose. The second phase of insulin secretion depends on the priming of vesicles that are, in part, already situated close to the cell membrane (Rorsman and Renstrom, 2003). However, more persistent stimulation may require new granules to be recruited and mobilized to the cell membrane from deeper parts of the cell. Glucose, ATP and cAMP stimulate cytoplasmic granule movements (Hisatomi et al., 1996, Pouli et al., 1998, Varadi et al., 2002) along the microtubule network using motor protein myosin 5A (Varadi et al., 2005). Disruption of this network impairs granule movements and the refilling of the RRP (Ivarsson et al., 2004). The docking of delivered granules is also controlled by a dense actin web that covers the intracellular side of the cell membrane.

To respond adequately to physiological stimuli, β-cells must be equipped with enough release-competent granules, and there has to be an effective mechanism to ensure their fresh supply. Failure at any stage of the granule mobilization will result in suppression of 1st phase and reduction in the 2nd phase of insulin secretion. Such changes in the secretory response are typically observed in Type-2 diabetes.

## Multi-vesicular and compound exocytosis

The pancreatic β-cell, like many other secreting cells, contains a large number of granules packed with cargo (in this case insulin). Many granules are in physical contact with their neighbors, raising the intriguing possibility that vesicle-to-vesicle membrane fusion may occur in several ways depending on surrounding conditions. Vesicles/granules may pre-fuse to form a granule conglomerate. This could occur after global elevation of $Ca^{2+}$ concentration in the cytoplasm, before any of members of the conglomerate has established a contact with the cell membrane. Alternatively, a vesicle already fused to the cell membrane is then subsequently joined by a number of other release competent granules (Kishimoto et al., 2005). The pre-fusion of granules and the release of cargo from a resulting conglomerate is called *compound exocytosis*. This is in contrast to the *sequential release* from granules joining a row of earlier fused granules. Exocytosis that involves release of cargo simultaneously from multiple granules demonstrates, once again, the plasticity and complexity of the secretion process in pancreatic islet cells. The relative physiological role of these types of exocytosis, their incidence rates, modes of regulation etc. remain unknown, but one may imagine that under certain conditions these mechanisms may become quantitatively important to allow rapid and massive release of substances stored in the LDCVs.

# AIMS OF THE STUDY

The general objective of this study was to expand our knowledge about LDCV exocytosis in pancreatic β-cells and the mechanisms involved in cargo release. The specific aims were to:

1. establish and characterize a highly sensitive electrophysiological method for the detection of ATP release from individual LDCVs in insulin-secreting cells;
2. characterize the release of nucleotides and peptides from LDCVs in insulin-secreting cells;
3. investigate whether GABA is stored in LDCVs and co-released with ATP;
4. estimate the relative contribution of SVs in the release of ATP in rat pancreatic β-cells;
5. investigate if compound exocytosis occurs in insulin-secreting cells.

# METHODS

A range of sensitive, and high-precision methods are available to study exocytosis from single cells. Roughly, they can be divided into two groups; 1) *electrophysiological* methods that are based on measurements of electric currents across the cell membrane, and 2)

various *imaging* methods (such as confocal and total internal reflection microscopy (TIRF), two-photon microscopy, atomic force microscopy etc.) that attempt to visualize individual cellular components and steps that comprise an exocytotic event. In this study methods from both types of measurements were used, separately or in combination, to detect exocytotic events in pancreatic β-cells and in Ins-1 cells.

## Detection of ATP release from individual granules

In pancreatic β-cells, ATP is stored and released together with insulin and many other low molecular weight substances into the extracellular space during LDCV exocytosis. (Hutton, 1994). In this thesis, a novel method was established that permits the electrical detection of minute (amoles) quantities of ATP. This allowed measurement of the ATP released from an insulin granule after its fusion with the cell membrane (Figure 3.). To achieve this, insulinoma or primary β-cells were transfected/infected with an EGFP labelled purinergic $P2X_2$ receptor ($P2X_2R$). The fluorescent probe that is attached to the receptor allows one to perform two procedures: 1) to visualize transfected cells under a microscope using UV light in order to select them for further investigation; 2) to evaluate the quality of transfection by assessing the character of the distribution of fluorescence over the cell surface. Imaging experiments confirmed that the construct is

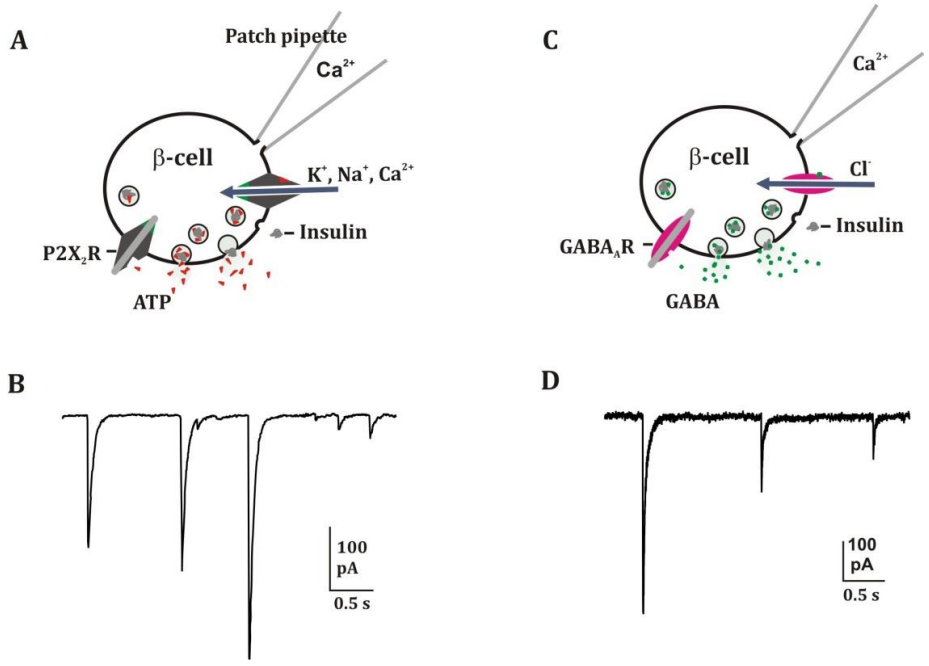


**Figure 3. Quantal ATP and GABA release detection in rat pancreatic β-cells.** Schematic pictures of protocols used in $P2X_2$-EGFP (*A*) and $GABA_A$ (*C*) transfected rat β-cells. Cells were held at −70 mV and exocytosis elicited by intracellular application of 0.2 μM free [$Ca^{2+}$]. Examples of ATP- (*B*) and GABA-activated (*D*) TICs recorded.

efficiently expressed and correctly targeted to the plasma membrane. Each molecule of this receptor is a cationic channel that contains an ATP-sensitive sequence exposed to the extracellular space. The channel is activated by an increase in the extracellular concentration of ATP (Khakh *et al.*, 1999). The transfected/infected cells were patched and their membrane potential clamped at -70 mV (Fig. 3A). Exocytosis in these cells was then stimulated by elevated levels of $[Ca^{2+}]_i$ introduced through the patch pipette or by the photorelease of caged $Ca^{2+}$. Finally, the fusion of secretory granules with the cell membrane and subsequent release of ATP into the extracellular space was detected as transient inward currents (TICs) through $P2X_2$ receptor channels activated by the ATP (Fig. 3B). Brief applications of external ATP on $P2X_2$ expressing β-cells evoked a substantial (≤5 nA) inward currents that were sensitive to the purinergic antagonist suramin (50 μM). The latter result shows that the transients recorded are indeed produced by the action of ATP upon $P2X_2$-receptor.

A similar method was used to detect GABA release from pancreatic β-cells. In order to do this the ionotropic $GABA_A$ receptor was expressed (Fig. 3C and D).

## Patch-clamp technique

The fusion of a granule with the cell membrane and the release of its cargo is a fast process that is usually completed within a few milliseconds. This event is so fast because of the small size and volume of sub-cellular components involved. If the details of an exocytotic event are to be clarified, methods of high temporal resolution need to be employed. An electrophysiological solution to this problem is the patch-clamp technique developed by Neher and Sakmann in the late 1970s (Neher et al., 1978). The essence of this method lies in creating conditions where full control over the electrical potential across the cell membrane is achieved. Then, with the help of specific electronic circuitry, the potential across the cell membrane is altered in a controlled way and the response of the cell membrane

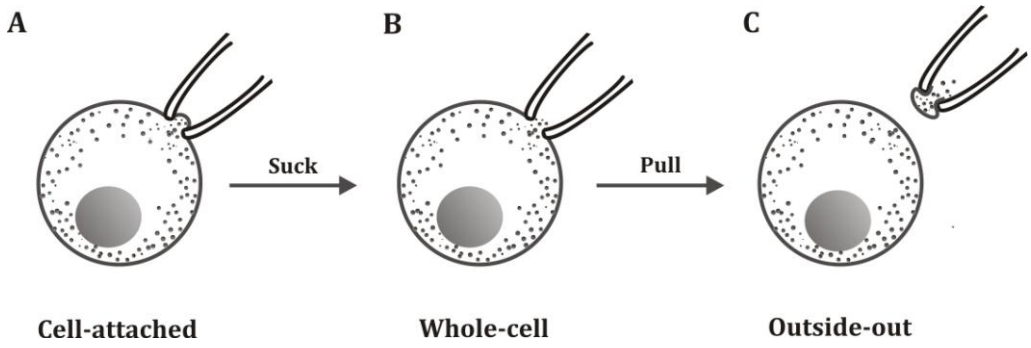


**Figure 4. Patch-clamp configurations.** *A*, Cell-attached; *B*, Whole-cell; *C*, Outside-out.

recorded. Subsequent analysis of this response yields information about different properties of the cell membrane and its comprising components such as the membrane capacitance, conductance and presence of ion channels etc.

There exist at least four patch-clamp recording configurations of which three were used in this study (Fig. 4). All of those are based upon the formation of a gigaseal of the order of 10 GΩ between the glass electrode and the cell membrane. A patch-clamp experiment usually starts in a *cell-attached* configuration (Fig. 4A), during which the gigaseal is established. The s*tandard whole-cell* configuration (Fig. 4B), which is the configuration used for the majority of electrical measurements in this study, is formed by applying a gentle pulse of negative pressure to the interior of the patching pipette. The cell membrane enclosed within the tip of the pipette is then ruptured, thus creating a low-resistance connection between the electrode and the cell interior that allows control of the electrical potential and current across the whole cell membrane. An additional advantage of this configuration is the possibility to dialyze the cell cytosol through the pipette and thus introduce into the cell different compounds of interest. This configuration is especially convenient in studies of electrically excitable cells. These cells can be stimulated by depolarizing pulses and the resulting (ionic) currents across the cell membrane measured. In addition exocytosis/endocytosis can be investigated by monitoring changes in cell membrane capacitance (See below).

Another recording configuration that employs *outside-out patches* (Fig. 4C) was used in this thesis to investigate some specific features of insulin granule fusion from a small area of the cell membrane. This configuration is achieved by pulling the electrode away from the cell in whole-cell mode. This action results in forming a small patch of the cell membrane over the tip of the electrode with the external surface directed outwards, i.e. a miniature version of the whole-cell configuration.

## Capacitance measurements

As mentioned above, the membrane capacitance can be measured in the whole-cell configuration of the patch-clamp technique. To analyze electrical data recorded on live cells and extract information about their various parts, the cell is replaced by an equivalent electrical circuit (Fig. 5). In case of capacitance measurements, this circuit consists of three elements: 1) an access resistor (Rs), 2) a resistor representing the cell membrane (Rm), and 3) a capacitor that takes care of the membrane capacitance (Cm). To determine these parameters several methods have been proposed. In this thesis, the sine+DC method was used. It

employs sinusoidal voltage (500 Hz) in combination with DC voltage in order to detect all three parameters of the equivalent electrical circuit of the cell. The technique was used to monitor exocytosis from single β-cells as well as individual Ins-1 cells. In this, advantage was taken of the fact that during the fusion of LDCVs or SLMVs with the plasma membrane, the cell surface area increases. This increase can be measured electrically as a corresponding increase in membrane capacitance (Cm) since the capacitance of any capacitor is directly proportional to its surface area. For biological membranes, which consist mainly of a lipid bilayer, the coefficient of proportionality between the area and capacitance is ~10 $fF\mu m^{-2}$ (Pethig et al., 2005). Thus, a vesicle that fuses with the cell membrane will cause an increase in cell capacitance while recapture of the cell membrane during an endocytotic event will result in a decrease of similar size in cell membrane capacitance. Because endocytosis is a comparatively slow process, it does not normally influence the measurement of exocytosis (Eliasson et al., 1996). Still, it is not possible to fully separate two processes from each other.

For capacitance measurements, the cell membrane is usually stimulated by depolarizing voltage pulses of different length and amplitude. Since the depolarization activates voltage-gated $Ca^{2+}$ channels and causes large and fast changes of the membrane permeability, the detection of the membrane capacitance is not possible during the depolarization pulse if sine+DC method is used onsequenly photorelease of caged $Ca^{2+}$ was used for the investigation of granule fusion events immediately after the rapid increase in intracellular $Ca^{2+}$ (See below.).

Changes in capacitance of the cell membrane caused by fusion of a

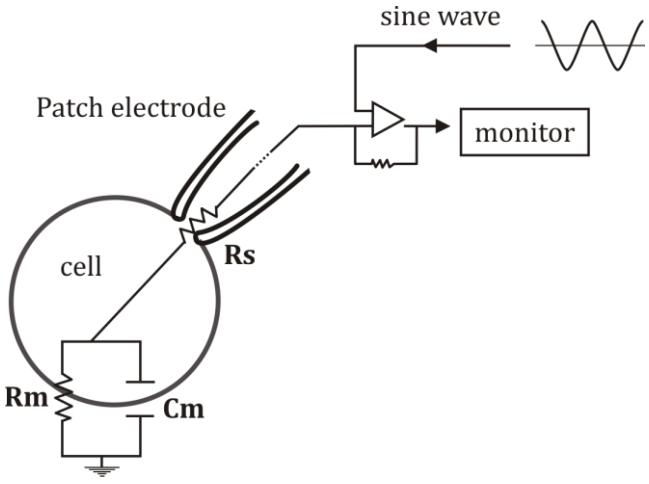


**Figure 5. A schematic diagram of cell capacitance measurement circuit.** Rm - cell membrane resistance, Rs – series resistance and Cm – cell membrane capacitance.

single granule were detected in this thesis with the help of the cell-attached configuration (Fig. 4A) that permits low-noise capacitance measurements. The main difference from the capacitance measurements in the whole-cell configuration is that, to resolve individual fusion pores in the relevant size range, higher sine wave frequencies (the sine+DC method) are applied (typically about 20 kHz versus 500 Hz in the whole-cell configuration).

## Amperometry

Carbon fibre amperometry is another electrophysiological method which is used for detailed investigation of exocytosis of LDCVs with a single event resolution (Fig. 6). An amperometric signal, that marks an exocytotic event, is formed by chemically oxidizing the released secretory products on the surface of the carbon electrode at a fixed potential. Electrons freed by oxidized molecules are transferred through the volume of the carbon fibre to the electronic circuit thus creating a current transient whenever an oxidizable substance is adjacent to the electrode surface. It is obvious then that amperometry can be performed only on cells that secrete oxidizable molecules. Unfortunately, vesicles in pancreatic cells do not contain enough such molecules. To overcome this difficulty, β-cells were loaded with exogenous neurotransmitter serotonin (5-HT) that is readily oxidized by a carbon fibre. In this study the carbon electrode was connected to the head stage of an amplifier and held at +650 mV. The detection of exocytosis relied on current generated when serotonin was oxidized on the surface of

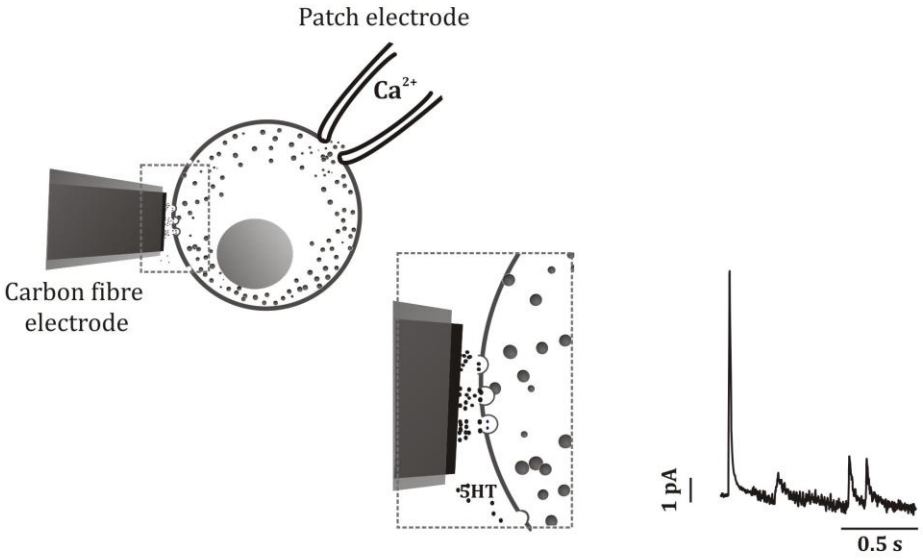


**Figure 6. A schematic diagram of amperometric measurements of serotonin release from pancreatic β-cells.** Cells were preloaded with 5-HT (small black dots) and stimulated with $Ca^{2+}$ containing buffer through the patch pipette. Release of serotonin (left and insert)from LDCVs was detected as an amperometric current (right).

electrode positioned as close as possible to the cell. Such positioning was necessary to maximize the detection of released serotonin molecules. We have shown that 5-HT release from pancreatic β-cells as detected by this method reflects exocytosis from LDCVs (Aspinwall et al., 1999, Bokvist et al., 2000, Smith et al., 1995). A weakeness of this method is that only 30-50% of events taking place on the surface of a single cell can be detected because of the loss of 5-HT during the diffusion process to the surface of carbon fibre.

## Photorelease of caged $Ca^{2+}$ and $[Ca^{2+}]_i$ measurements

The application of caged $Ca^{2+}$ compounds to rapidly and uniformly increase intracellular $Ca^{2+}$ levels is important to establish the dynamics of vesicle fusion. As explained above, it is not possible to monitor the capacitance of cell membrane during a depolarization pulse. Another problem is that $Ca^{2+}$ entry during depolarization is not uniform but concentrated to certain areas of the cell (Bokvist et al., 1995). In adition, there are steep gradients of $[Ca^{2+}]_i$ below the plasma membrane making it difficult to reliably measure $[Ca^{2+}]_i$. By contrast, the elevation of $[Ca^{2+}]_i$ by photorelease of caged $Ca^{2+}$ loaded into cells through the patch pipette does not increase the conductance of the cell membrane, and so does not interfere with the capacitance measurements. In this thesis NP-EGTA was used as a source of caged $Ca^{2+}$.

During a typical experiment, caged $Ca^{2+}$ was released by a brief (~1 ms) flash of UV-light delivered to a β-cell preloaded with NP-EGTA via the microscope objective with the help of a special spot illumination adaptor. It should be noted that the delivery of UV light through the objective is essential in this type of experiments that employ a carbon fibre with an outer protective plastic layer. Initial experiments revealed that UV light knocks out of the carbon fibre a considerable number of electrons that are caught in the volume of protective plastic. After UV flash, these electrons are retracted by carbon fibre. This backward movement of electrons is detected as a huge current artefact that obscures any biologically relevant signal. The delivery of UV light through the objective limited this artefact to an acceptable degree. The remnant of it could be removed digitally off-line by fitting and subsequent subtracting of an exponential grom the initial part of the current recording. Intracellular level of $Ca^{2+}$ was continuously observed by monitoring the fluorescence of Fura-FF (loaded into the cell via the recording electrode) at two wavelengths on a microfluorimetric system installed on an inverted microscope Axiovert 200. The excitation and emission wavelengths used for Fura-FF were 340/380 and >505 nm respectively. To convert the fluorescence ratio at

these two excitation wavelengths into $[Ca^{2+}]_i$ (Grynkiewicz et al., 1985), the minimum value of the ratio was determined at basal $[Ca^{2+}]_i$ for each experiment. The maximum value of the ratio was recorded immediately after experiment rupturing the cell by briefly clamping the membrane voltage at +500 mV. The $K_d$ for the binding of $Ca^{2+}$ to Fura-FF was assumed of 5.5 μM.

## Imaging of an exocytotic event

Direct visualisation or imaging of cell structures and the dynamic processes such as exocytosis is a powerful and versatile tool that is widely used in many branches of life sciences. Of many imaging methods available, two were used in this thesis to clarify the character of an exocytotic event: TIRF and confocal microscopy. Both techniques were used to image insulin granules and to make the exocytotic event visible on a computer screen.

To render the relevant structures and components of the β-cell visible, they were labelled with a set of fluorescent probes such as enhanced green fluorescent protein (EGFP), monomeric red fluorescent protein (RFP), pH-insensitive emerald fluorescent protein (EMD) and cyan fluorescent protein (CFP). For example, IAPP, the marker of water-soluble cargo peptides within insulin granules, was labelled with EGFP and used to monitor granule movements inside cell cytoplasm as well as to observe the release of peptides. Also VAMP, a protein that is attached to granule membrane, was labelled at the luminal side with pHluorin, a variant of GFP that is sensitive to pH of surrounding solution (Tsuboi and Rutter, 2003). Since exocytosis of insulin granules involves a drastic change of intra-luminal pH, the presence of this construct allowed us to monitor the penetration of protons (and presumably low molecular weight substances) through the fusion pore. The VAMP-pHluorin signal is initially "silent" due to the low luminal pH of granules that have not yet fused with the cell membrane. Following exocytosis, there is fast increase in fluorescence, reflecting the opening of the fusion pore and the equilibration of $H^+$ concentration between extracellular space and the lumen of the insulin granule.

# SUMMARY OF RESULTS AND DISCUSSION

## Detection of ATP release

In this thesis we introduce a novel method for studying exocytosis in insulin-secreting cells based on the expression of a high density of ATP-sensitive $P2X_2$ receptors in the plasma membrane. The technique is conceptually related to the "sniffer cell"-approach, also based on $P2X_2$ receptors, used previously by

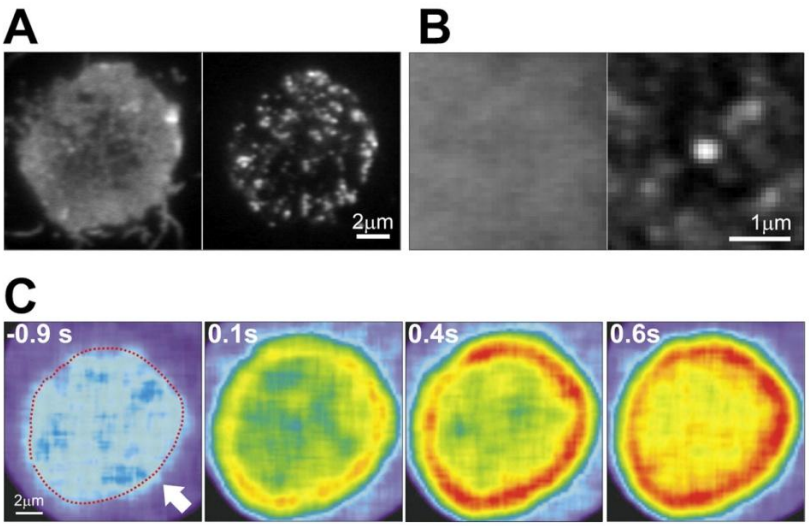


**Figure 7. $P2X_2R$ expression.** (A) TIRF images of a cell transfected with $P2X_2R$-RFP (left panel) and IAPP-EGFP (right panel). (B) Average image of 23 small frames taken from images like those shown in A and centered on the location of granules (right panel, IAPP-EGFP spots). The left panel is the average image of similar frames cut at the same locations from the red channel. (C) Sequence of confocal images showing Fluo-5F fluorescence in a cell that expressed $P2X_2$-mRFP. At t=0 seconds, ATP (2 mM) was applied to the cell via a puffer pipette from the direction indicated with an arrow.

Hazama et al. (Hazama *et al.*, 1998) with the important difference that the ATP releasing β-cell is used as its own "sniffer" cell.

Here we have shown that the autaptic use of $P2X_2$ receptors to detect the release of ATP from β-cells is a valuable complement to amperometry. ATP is a natural component of the secretory granules in β-cells, so it is not necessary to load them with exogenous ATP before experiment as is the case with serotonin in amperometric studies. Another essential advantage is that exocytosis can be monitored over the entire cell surface whereas amperometry only detects secretion on the 30-50% of the cell surface area adjacent to the carbon fibre (Braun et al., 2007a). Moreover, the shape of amperometric signals is modified by the diffusion of released molecules in a manner dependent on the position of an exocytotic event relative to the tip of the carbon fibre. Only sophisticated correction methods allow reconstruction of the true nature of the release events.

The new approach is fully compatible with other methods used in cellular studies of exocytosis and has been successfully combined with amperometry, the measurements of cell membrane capacitance, different patch-clamp configurations, calcium imaging, and confocal microscopy.

**The distribution of $P2X_2$ receptor over the cell surface.** The uniform distribution of $P2X_2$ receptor on the cell surface is important in the context of experiments conducted in

this study since any irregularities in their distribution over the cell surface will distort the detected electrical signal.

TIRF microscopy was used to establish whether there was a correlation between the localization of $P2X_2$ receptor molecules and granule release sites. Analysis of cell footprint images recorded on rat insulinoma (Ins-1) cells transfected with $P2X_2$-mRFP1 and the granule marker IAPP-EGFP (Fig. 7A) revealed the presence of receptors at high and uniform levels in the immediate vicinity of granule docking sites (Fig. 7B).

Additional test was performed by confocal microscopy in order to find out whether the fluorescent label observed on the cell surface represented functionally active molecules of the receptor. In this we took an advantage of the fact that $P2X_2$ is somewhat permeable to $Ca^{2+}$ and imaged exogenous ATP-evoked $Ca^{2+}$-influx into cells that expressed $P2X_2$-mRFP. These cells were loaded with low-affinity $Ca^{2+}$-indicator Fluo-5F (Zenisek et al., 2003) through a patching pipette and voltage-clamped at -70 mV in the whole-cell configuration. External application of 2mM ATP through a local puffer pipette activated practically all $P2X_2$-channels present on the cell surface and caused a massive influx of $Ca^{2+}$ into the cell. By confocal imaging, this influx was detected as a continuous fluorescent ring just below the plasma membrane as expected in the case of uniform distribution of functional $P2X_2$-channels over the cell surface (Fig. 7C).

The surface density of active $P2X_2$-channels was found to be of ~8500 per cell in experimental conditions of this study as evaluated on the basis of whole-cell current (5.1±0.5 nA) measurements and taking into account the reported single-channel properties: conductance (15-30 pS) and open probability (0.6) (Ding and Sachs, 1999, Whitlock et al., 2001). The cell capacitance of the rat β-cells used for these experiments averaged 10.6±1.0 pF. Since the specific membrane capacitance is ~10 $fF\mu m^{-2}$, we can estimate the receptor density to be 80 $\mu m^{-2}$ what corresponds to an average distance between two adjacent receptors of 0.11 μm. Thus the distance between the opening of a fusion pore and the closest receptor molecule is ≈50 nm. Such small distance ensures that the shape of the inward current spike evoked by the release of ATP from a fused granule is practically independent on the specific localization of the release site on the cell surface.

**Release of adenine nucleotides from pancreatic β-cells.** With $P2X_2$ receptors expressed in β-cells, any exocytotic event associated with ATP release is detected as a current transient across the cell membrane (Fig. 3B). Consequently electrical monitoring of the cell membrane allows us to detect the number of

release events as well as their dependence on the presence of different agents. Such data can be acquired by simply counting the current transients. However, as explained below, the amount and depth of information that can be extracted from this type of recordings is not limited to determination of the number of vesicle counts.

An individual current transient is shaped by specific conditions and physical parameters that define an exocytotic event. The main of these are the amount of ATP in the granule, the rate of ATP diffusion in intragranular matrix, the size of the fusion pore, the dynamic behavour of the pore, the size of granule and the cell etc. Information about these conditions is contained in the characteristics of an individual spike such as the spike amplitude, the rising time, the decay time, the half time, the presence or absence of a spike foot and others. Therefore effective use of this method implies a thorough analysis of spike properties (Fig. 8).

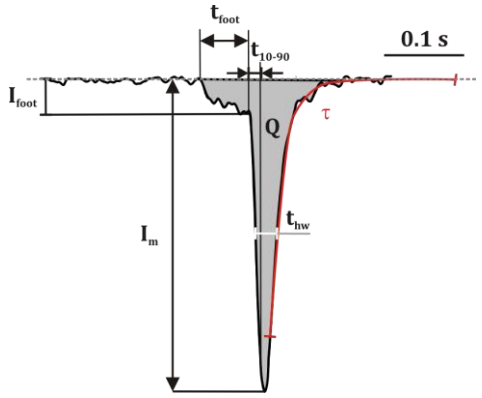


**Figure 8. Definition of parameters often used in the analysis of ATP current spikes.** Spike baseline – dashed line, $I_m$- spike amplitude; $Q$ – overall charge moved into the cell by the current spike equal to the integral of current over the duration of the spike; $t_{10\text{-}90\%}$ - 10 to 90% rise time; $t_{hw}$ – the halfwidth of the spike measured at 50% of $I_m$; $\tau$ – the decay time of the spike measured between 75% of $I_m$ and baseline; $I_{foot}$ – the foot current amplitude; $t_{foot}$ – foot duration.

A convenient and useful way of presenting data on ATP current transients is histograms of charge $Q$ brought into the cell by a single spike (Fig. 9). The intragranular concentration of ATP is mainly determined by electrochemical conditions in cell cytoplasm and therefore can be expected to be roughly similar in all granules. If this is the case, then the charge of a spike is proportional to the volume of the granule of $4\pi R^3/3$, where $R$ is the granule radius. The cubic root of c**h**arge ($Q^{1/3}$) is therefore proportional to the granule diameter. Thus, substituting the cubic root of charge $Q^{1/3}$ for charge $Q$ gives physical meaning to these histograms as reflecting the granule size distribution (note that the granule diameters are normally distributed) (Fig. 9). Such way of presenting charge data will also reveal the presence of granule populations of different size.

The histogram shown in Fig. 9 reveals that the majority of events observed in this experiment belong to a single population of events and can be reasonably fit by a Gausian. However approximately 20% of TICs exhibit very large charge indicating

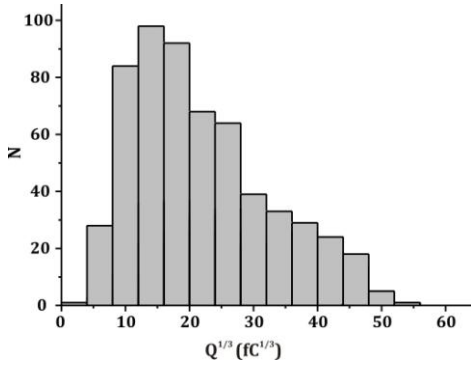


**Figure 9. Distribution of $Q^{1/3}$ of ATP evoked currents in pancreatic β-cells.** Exocytosis was evoked by 2 μM $[Ca^{2+}]_i$ and 0.1 mM cAMP via patch electrode.

the release of vast amounts of ATP during a single fusion event. The size of large events was found to be dependent on levels of $[Ca^{2+}]_i$ and cAMP in the intracellular buffer. Removing cAMP and stimulating cells with lower levels of $[Ca^{2+}]_i$ – (0.1-0.2 μM) - decreased the numbers of large spikes and their frequency fell to ~3%.

When combined with simultaneous measurements of the cell membrane capacitance, the $P2X_2$ method yielded a capacitance change per single exocytotic event. The values - 1.0 fF for Ins-1 cells and 3.4fF for β-cells - are in good agreement with those obtained by on-cell capacitance studies of single-vesicle exocytosis (MacDonald et al., 2006).

## Selective release from LDCVs

Exocytosis in β-cells is initiated with a delay as short as 5-10 milliseconds after $Ca^{2+}$-influx (Barg et al., 2001b). However the release of peptide cargo takes on average much longer time (up to ~2 seconds) to be fully finished (Barg, 2003). Here we explore events that take place in between pore opening and the release of peptide, i.e. different stages of exocytosis, with the aim to find out whether the release of cargo is regulated beyond the moment of membrane fusion, and, specifically, whether a transient fusion mechanism may enable cells to release selectively low-molecular-weight transmitters from LDCVs.

**Time course of nucleotide release.**

We compared the time course of nucleotide and peptide release by a combination of high-resolution cell membrane capacitance measurements, the $P2X_2$ receptor-based assay for the detection of ATP release and confocal imaging of

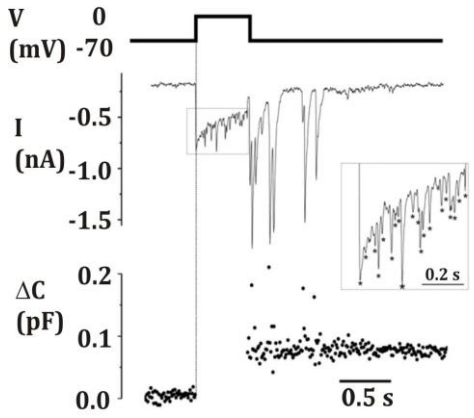


**Figure 10. Time course of nucleotide release.** The 500 ms depolarization pulse to 0mV (*above*), ATP currents (*middle*) and cell capacitance recording (*below*). The inset shows the expanded indicated part (highlighted by square). Asterisks indicate current spikes superimposed on the inward $Ca^{2+}$-current (identified by eye).

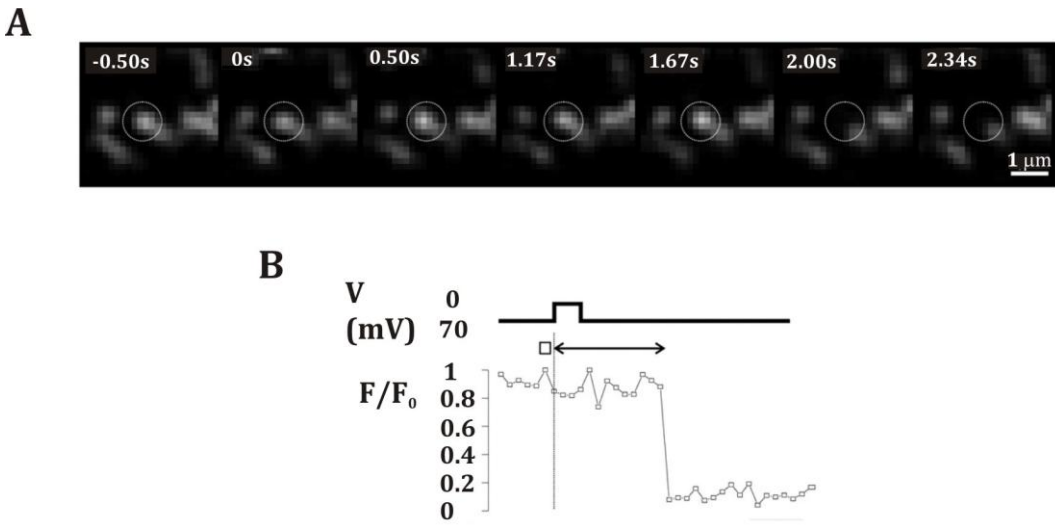


**Figure 11. Time course of peptide release.** Ins-1 cells expressing IAPP-emerald (IAPP-EMD) were voltage-clamped and their footprint imaged at 10 Hz. (A) Images taken at the indicated times relative to the onset of a 500 millisecond depolarization from -70 mV to zero mV. (B) Time course of IAPP-EMD fluorescence (lower trace) in the ROI indicated by the circle in A in response to a 500 millisecond depolarization (top trace).

single-granules.

To determine the time course of nucleotide release, we recorded membrane capacitance and currents in Ins-1 cells expressing $P2X_2$-EGFP receptors, and applied a single depolarization pulse to zero mV lasting 500ms. The type of data obtained in these experiments is demonstrated in Fig. 10. A series of transient inward currents were detected in parallel to increase in membrane capacitance. In the experiment shown, the observed capacitance increase was 70 fF and was confined to the duration of depolarization pulse. This change in capacitance corresponds to the release of 88 granules (conversion factor of 0.8 fF per granule (MacDonald et al., 2005). The main result obtained by these measurements is the cumulative histogram of the time of the current spikes relative to the onset of depolarization (Fig. 14, dotted line). After correcting this histogram for lost points it was found that ATP was released in Ins-1 cells with a time constant of 280 milliseconds. This time constant is longer than that for capacitance increase. It was concluded that the release of adenine nucleotides is slightly delayed in relation to membrane fusion.

**Time course of peptide release.** It is interesting to compare the rate of nucleotide release with that of peptides which have a considerably larger molecular size. To achieve this, we monitored the time course of peptide release from Ins-1 cells using chimeric constructs of IAPP with fluorescent protein emerald (EMD). Thus labelled IAPP is a soluble protein which is correctly targeted to LV lumen (Michael et al., 2004) and acts as a fluorescent

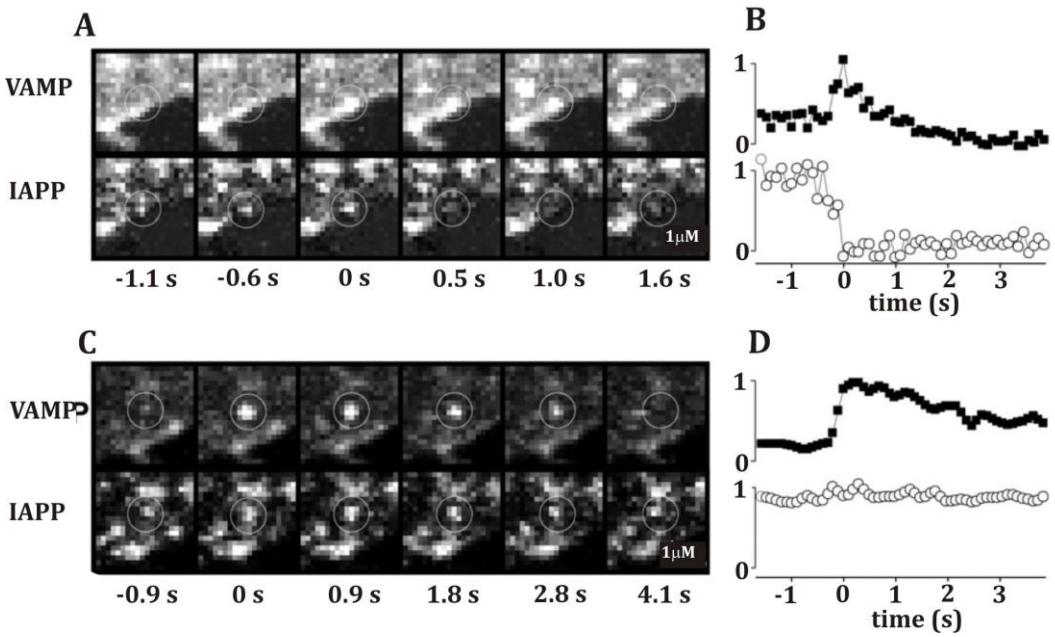


**Figure 12. Simultaneous imaging of VAMP-pHluorin (top) and IAPP-ECFP (lower) in double-transfected cells.** The cell (imaged at 10 Hz) was stimulated with a 3 second puff of solution containing 87 mM KCl. Times quoted below the images are relative to the peak in the VAMP-pHluorin signal. (A) Example of a granule (highlighted by a circle) that showed a transient increase in VAMP-pHluorin fluorescence and that culminated in the loss of IAPP-ECFP fluorescence. (B) Fluorescence intensities of IAPP-ECFP (open circles) and VAMP-pHluorin (black squares) within ROIs centered on the granule highlighted in A. (C) Example where the increase in VAMP-pHluorin fluorescence was not associated with the rapid loss of IAPP-ECFP fluorescence. (D) As in B, but for the granule shown in C.

marker of peptide release during exocytotic event. Additionally, this fluorescent label is essentially pH-insensitive which is important in view of large changes in intragranular pH during exocytosis.

Confocal imaging of IAPP-EMD transfected Ins-1 cells (Fig. 11) revealed that depolarizing pulses to 0 mV for 500 miliseconds caused sudden disappearance of fluorescence from several IAPP-EMD labelled granules localized just below the cell membrane. The cumulative histogram of disappearance times relative to the stimulation showed that granules are fusing with the cell membrane with the time constant of 2.2 s (Fig 14, square markers). The speed of fluorescence decay in these granules, once they underwent exocytosis, was very high and completed in 100ms. This clearly indicates that the fluorescent cargo was lost by its extrusion into extracellular space and not by vertical granule displacement. This is in accordance with the data reported previously (Barg et al., 2002) but ~6-fold slower that the time constant for nucleotide release.

**Exocytosis does not always lead to release of peptides.** Next, we attempted to detect if pore opening was always associated with peptide release. In these experiments, cells were co-transfected with VAMP-

pHluorin and IAPP fused to the pH-insensitive enhanced cyan fluorescent protein (IAPP-ECFP). By combining these two probes, we took advantage of visualizing simultaneously granular pH changes and release of a peptide marker throughout an exocytotic event. Under high $K^+$ (87 mM) stimulation, there were events that showed an increase in pHluorin fluorescence that were clearly associated with the abrupt disappearance of fluorescence from the corresponding spot in the IAPP-ECFP channel (Fig. 12A). It can be seen from analysis of associated fluorescence intensities (Fig. 12B) that the IAPP-ECFP fluorescence vanished in <0.3 seconds and at the same time as the increase in VAMP-pHluorin. In other cases (Fig. 12C and D), the increase in pHluorin fluorescence occurred without concomitant decrease in ECFP-fluorescence. The VAMP-pHluorin signal reached a peak within a fraction of a second, and then decayed slowly towards the original level. No significant changes were detected in the IAPP-ECFP channel. This clearly indicates two separate patterns of exocytotic granule behaviour: complete release of peptide cargo (39% of events) and intragranular retention of the cargo until the re-closure of the fusion pore (61%).

**Nucleotides are released independently of peptides.** Finally we tested if nucleotides can be released from granules that retain their peptide content. To test this possibility, we combined the electrophysiological detection of nucleotide release with $P2X_2$ and the optical detection of exocytosis and release. For the latter measurements, we used IAPP-pHluorin as probe, which combines the advantages of being sensitive to the pH-change after pore opening and being a soluble peptide that is potentially released from the granule. It was first ascertained that the IAPP-pHluorin reports exocytosis. We imaged the footprint of cells expressing both IAPP-pHluorin and $P2X_2$-mRFP. The cells were then voltage-clamped at –70 mV and exocytosis was evoked by dialyzing the cell interior through the patch pipette with a solution containing 2 μM free $Ca^{2+}$. Soon after establishing the whole cell configuration, discrete spots of transient increases in fluorescence were observed. The events could be classified into two classes. In the first type of events (52%), there was a rapid loss of fluorescence that often coincided with the appearance of a short-lived cloud of fluorescence centered at the original spot (Fig. 13A). In the second type, the fluorescence remained elevated for several seconds and then slowly decayed towards the baseline (Fig. 13B). We defined fluorescence increases that decayed with time constants ($\tau$) of <350 milliseconds and >350 miliseconds as rapid and persistent events, respectively (Fig 13G). Based on the rapid decay and the association with a cloud of

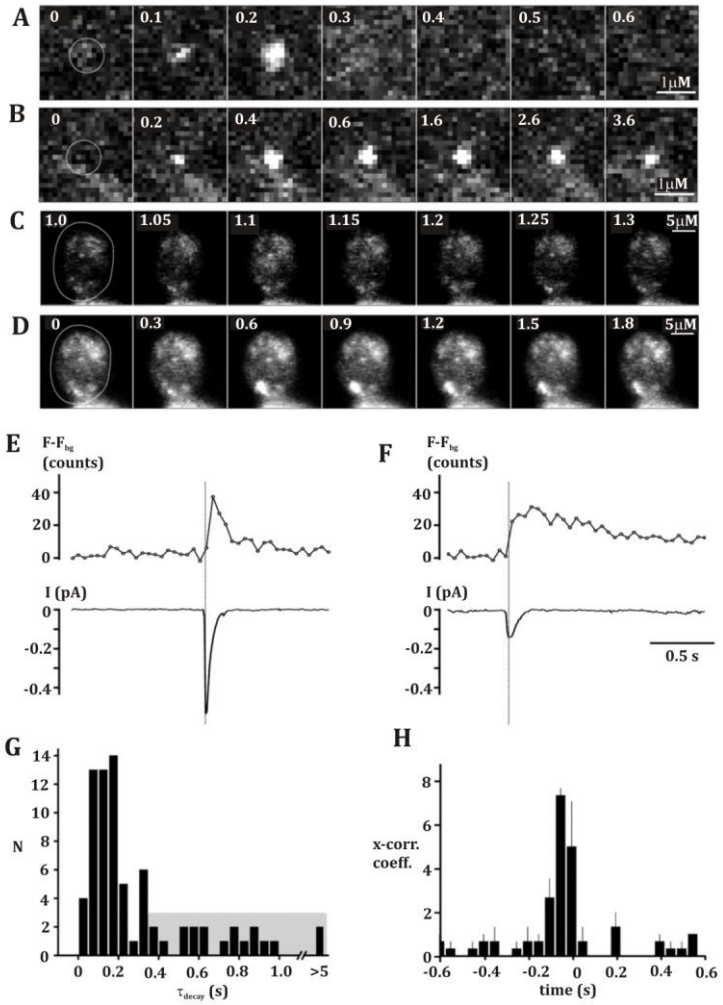


**Figure 13. Parallel recording of nucleotide and peptide release from individual granules.** (A,B) Confocal images of a section of the footprint of a voltage-clamped cell expressing both IAPP-pHluorin and $P2X_2$-mRFP. The images were recorded at the indicated times relative the onset of the IAPP-pHluorin flash. Exocytosis was elicited by intracellular dialysis with a buffer containing 2 μM $[Ca^{2+}]_i$. (C,D) Image sequences of a cell co-transfected with IAPP-pHluorin and $P2X_2$-mRFP1 and stimulated as in A and B. ATP activated current were recorded in parallel. Examples of a short-lived fluorescence transient in C, and a long-lasting event in D. (E,F) Time course of the average fluorescence intensity in the ROIs indicated by the white circle in C and D (top) and inward membrane currents associated with the events (lower). (G) Histogram of the decay constants of 56 events as in C and D. The shaded area indicates decay constants greater than 350 milliseconds. (H) Cross-correlation histogram of the times of fluorescence peaks vs the times of current peaks in three experiments similar to that shown in C and D.

fluorescence (Fig. 13A, third frame) it seems justifiable to interpret the rapid events as release of IAPP-pHluorin. The persistent events are consistent with granules that retain IAPP-pHluorin after exocytosis and dim slowly because of a combination of bleaching and re-acidification. We demonstrated that single exocytotic events can be resolved optically even at the level of entire cell (Fig. 13C and D).

Imaging of transfected cells was done with parallel recording of transient ATP-activated currents in the same cells (Fig. 13E and F). Combined analysis of optical and electrophysiological data revealed that: 1) the peak of the IAPP-pHluorin fluorescence lagged behind that of the current spikes by 50 milliseconds (Fig. 13H); confirming the earlier observation that pH-equilibration during exocytosis is somewhat slower than nucleotide release; 2) 68±14% of the current spikes were associated with either transient or persistent changes in fluorescence suggesting that release of ATP by exocytosis of insulin granules was detected, rather than from other types of secretory vesicles. The lack of complete correlation was expected because in transiently transfected cells, not all granules would contain IAPP-pHluorin; 3) 52 granules undergoing exocytosis as detected by both methods were not different from the entire sample of 75 granules, and the ratio of rapid (full) events (71 %,) and persistent (kiss-and-run) events (29±5%) was similar.

Taken together, these data indicate that exocytosis of insulin granules can take two functionally different routes following membrane fusion: either complete emptying of the granule content, or selective release of ions and small low-molecular-weight compounds with (at most) partial release of peptides.

## Is differential release mediated via transient fusion?

Traditionally, insulin granules have been thought to collapse into the plasma membrane during exocytosis (full fusion). This may have been the case for some of the granules we studied; most notably those where the VAMP-pHluorin signal had a rapid decay phase (Fig. 12 A and B). However, we often observed a plateau phase in the VAMP-pHluorin signal, which indicates that the granules did not collapse immediately. Indeed, there is now good evidence that a significant fraction of granules remains structurally intact after exocytosis (Barg et al., 2002, Perrais et al., 2004, Taraska and Almers, 2004, Taraska et al., 2003, Tsuboi et al., 2004, Tsuboi et al., 2000, Vo et al., 2004). In agreement with these observations we found that in up to two thirds of the exocytotic events the labelled IAPP remained at the

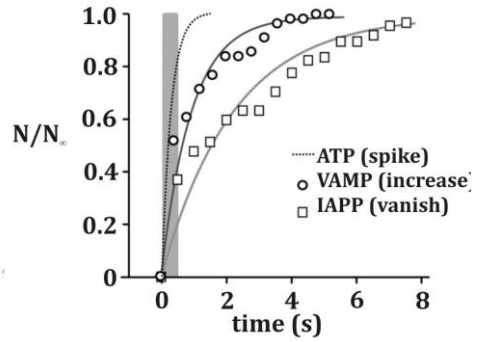


**Figure 14.** Cumulative histograms showing the time, relative to stimulation, of the loss of IAPP-EMD fluorescence (squares), the increase in VAMP-pHluorin fluorescence (circles).

site of the granule. Furthermore, the extracellular tracer dye uptake experiments (Paper I, this thesis) demonstrated that granules, still containing the release marker IAPP-EGFP, accumulated the dye in a stimulus-dependent manner. Together with the fact that dye accumulation was insensitive to extensive washing, this indicates that the granules had undergone exocytosis, released small compounds like nucleotides and then closed their pores and became pinched off from the plasma membrane.

How is the mode of exocytosis (full fusion vs. transient exocytosis) related to the mode of release from a granule (partial or complete)? It is tempting to equate transient exocytosis with partial cargo release because the duration of the transient fusion pore openings is long in relation to the time it takes for nucleotide release (Fig. 14). In addition, we observed nucleotide release from granules engaged in transient exocytosis (Fig. 13F).

Assuming that the duration of the plateau phase in VAMP-pHluorin experiments (1 second) reports the time during which the pore remains open, premature closure of the pore is a likely mechanism by which release of peptides (delay of 2.2 seconds after exocytosis) is prevented (Fig. 15A and B). There is evidence that granules that are retrieved intact in this manner remain fusion competent and are able to bypass the endosomal recycling pathway (Vo et al., 2004). The presence of nucleotide transporters in insulin granules supports the idea that such recaptured granules can be recycled by simple refilling with the

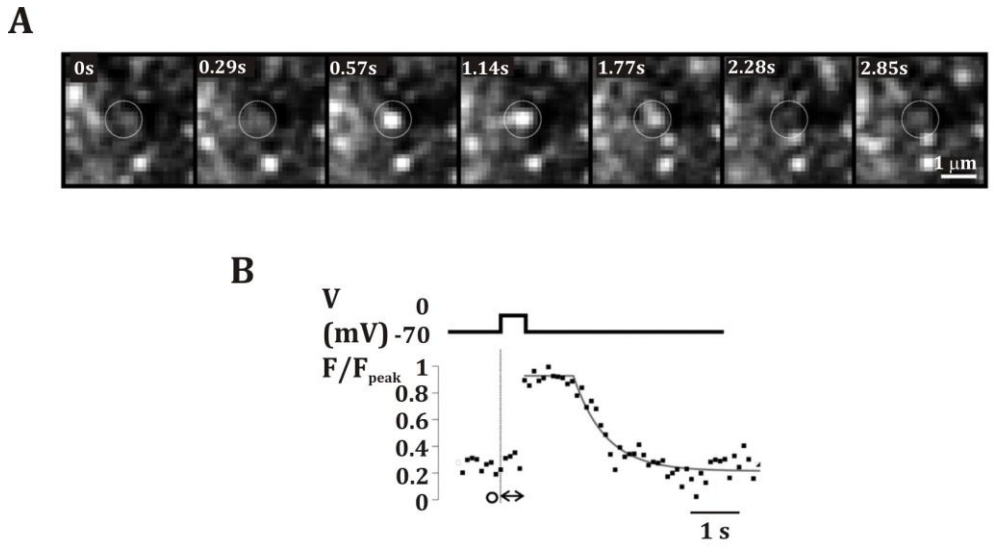


**Figure 15. Premature closure of fusion pore without peptide release.** Ins-1 cells expressing VAMP-pHluorin were voltage-clamped and their footprint imaged at 10 Hz. (A) Images taken at the indicated times relative to the onset of a 500 millisecond depolarization from -70 mV to zero mV. (B) Time course of VAMP-pHluorin fluorescence (lower trace) in the ROI indicated by the circle in A in response to a 500 millisecond depolarization (top trace).

nucleotide (Bankston and Guidotti, 1996). A similar mechanism has been postulated for chromaffin granules (Tabares et al., 2001). Granule recycling by transient exocytosis and refilling with transmitter provides the cell with a secretory pathway that avoids sorting, concentration and internalization of the granular components.

## Corelease of GABA and ATP from LDCVs

Gamma-aminobutyric acid (GABA) is the chief inhibitory neurotransmitter in the mammalian central nervous system. It plays an important role in regulating neuronal excitability throughout the nervous system. It is also found in pancreatic β-cells (Rorsman et al., 1989) though its role in coordinating processes in the pancreas is unknown. It was believed that GABA is stored in SLMVs (Reetz et al., 1991). However, there is some ultra-structural evidence that indicates the presence of GABA in LDCVs as well (Braun et al., 2007b). $GABA_A$ (Wendt et al., 2004, Rorsman et al., 1989) and $GABA_B$ receptors (Braun et al., 2004) have been identified in islets of Langerhans. This suggests that GABA, released by regulated exocytosis from the β-cell, can serve as paracrine/autocrine regulator.

To explore if GABA is released by exocytosis of LDCVs, we combined amperometric monitoring of serotonin release with patch-clamp measurements of GABA and ATP release in β-cells over-expressing $GABA_A$ and $P2X_2$ receptors, respectively. We observed that 22 ± 5% (n = 8) of GABA-induced current transients associated with simultaneous serotonin release (Fig. 16). This value was not statistically different from 29 ± 4% of ATP-induced transients associated with serotonin release and was sevenfold larger ($P < 0.01$) than that expected for simultaneous release of GABA and serotonin by independent events. These observations argue that at least some GABA is released by exocytosis of LDCVs. The last conclusion was reinforced by the

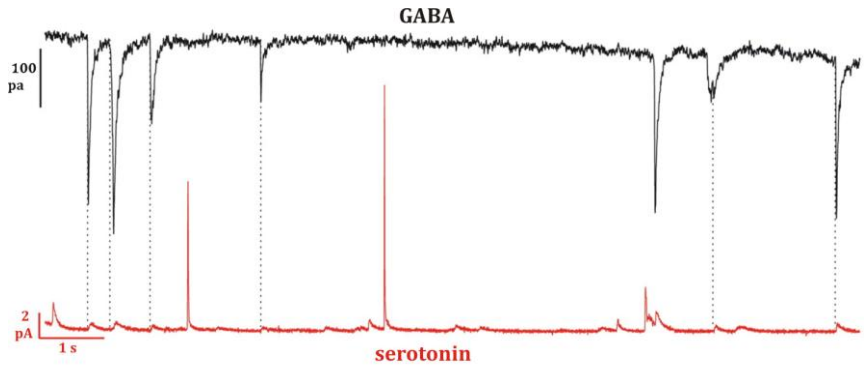


**Figure 16. Corelease of GABA and serotonin.** Parallel recording of GABA-induced TICs (top) and serotonin release (bottom) in a single ß-cell. The cell was held at –70 mV and exocytosis elicited by intracellular application of 2 µM free $Ca^{2+}$.

observation that there were no differences in the rise time, halfwidth, and charge between amperometric events that associated with GABA release and those that did not. If a subpopulation of the amperometric events were due to exocytosis of SLMVs, this should be reflected in different amplitudes and kinetics of the events (compare (Bruns et al., 2000)). The conclusion that GABA is released by exocytosis

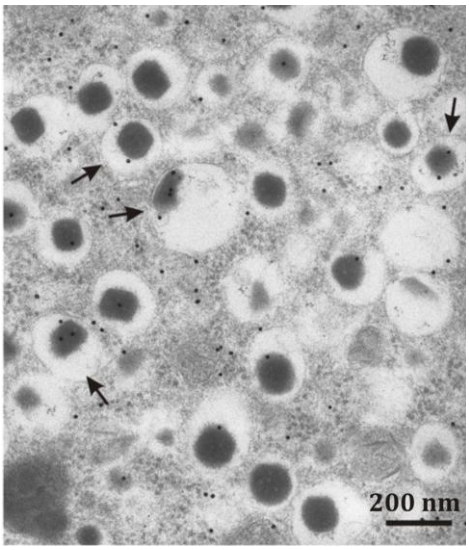


**Figure 17. Immunogold labeling of GABA in rat pancreatic ß-cells.** Arrows indicate labeling over the insulin-containing LDCVs.

of the insulin granules is also underpinned by ultrastructural data indicating that β-cell LDCVs do contain GABA (Fig. 17).

How big is the relative contribution of LDCVs to the GABA release observed? If we take the 29% of the ATP-induced current transients that associated with serotonin release as the maximum, then at least 75% of the GABA release events (i.e., 22%/29%) are attributable to exocytosis of LDCVs. Thus, we conclude that exocytosis of LDCVs accounts for most (if not all) depolarization-evoked GABA release.

## Low molecular weight granule constituents are differentially released via the fusion pore

Simultaneous measurements of GABA and ATP release from pancreatic β-cells combined with amperometric serotonin monitoring provided additional information about the dynamics of the fusion pore and its role in the secretion of low molecular weight substances.

Amperometric measurements on chromaffin and pancreatic β-cells have revealed the presence of a small foot in front of many amperometric events (Chow et al., 1992, Zhou and Misler, 1996). It is understood that the foot occurs because transmitter is released at a slow rate through a relatively narrow pore. In this thesis, such feet were observed during parallel recordings of ATP/serotonin and GABA/serotonin (Paper II) for both amperometric spikes and the simultaneously recorded ATP and GABA induced TICs. Interestingly, the foot signals of ATP- and GABA-induced TICs (Fig. 18) contributed substantially less to the total charge of the event than the corresponding amperometric foot currents: 3.6 ± 1% for ATP, 6.4 ±1% for GABA and 20 ±5% for serotonin detected

amperometrically. Also, the foot signal of ATP-induced TICs had lower amplitude relative to the spike phase than the corresponding amperometric currents: 12 ± 2% for ATP vs. 28 ± 3% for serotonin. This indicates that the fusion pore restricts the passage of ATP significantly more than that of serotonin. The dimensions of ATP and serotonin are ~1.6 × 1.1 × 0.5 nm and ~1.0 × 0.5 × 0.2 nm respectively. The diameter of the β-cell LDCV fusion pore is ~1.4 nm (MacDonald et al., 2006). This predicts that whereas serotonin will be easily accommodated within the fusion pore, the movements of ATP will be more restricted. The occurrence of isolated GABA-induced TICs in our recordings without simultaneous ATP release we attribute to partial opening of the fusion pore, sufficient to allow the exit of the GABA but not of the bigger ATP molecule. Evidence for the fusion pore to "filter" small molecules has also been obtained in synaptic vesicles (Gandhi and Stevens, 2003). Thus, exocytosis through fusion pores ("kiss-and-run") provides cells with a mechanism to differentially release small molecular weight transmitters from individual vesicles.

## What are the large ATP events? Compound exocytosis

Charge histograms of ATP release events discussed above (Fig. 9) revealed the presence of some

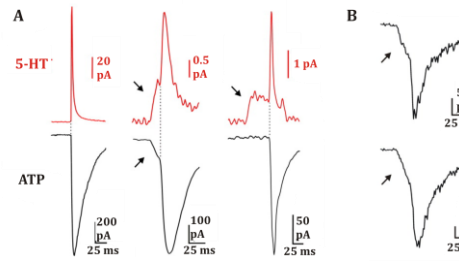


**Figure 18. Examples of 5-HT, ATP and GABA release recordings from pancreatic β-cells.** (A) Examples of simultaneous 5-HT and ATP events. (B) GABA current spikes. Feet indicated by arrows.

unusually large events. In most cases, large charge values were also reflected in uncommonly large amplitudes of current spikes that might reach several nA in size rather than the more typical amplitude of ~100 pA. Large current transients were persistently re-occurring and were not a recording artefact. One may suggest several possible causes for the intriguing appearance of such large spikes.

The most straightforward explanation would be that several LDCVs fuse simultaneously at different locations on the cell surface. The tight packing of insulin granules in the volume of the β-cell seems to support a coincidental occurrence of such multiple fusions. Fortunately, this can be verified comparatively simply with the help of outside-out configuration of patch-clamp technique (Fig. 4C). When this configuration is used, the bulk of the cytoplasm with the majority of insulin granules is lost, so that the probability for several fusion events to occur

simultaneously decreases significantly. In our experiments the size of the patch comprised 8.9% of the whole cell surface of Ins-1 cells used. However, the obtained data revealed that some of the events exhibited amplitudes ~3 times larger than the mean. This corresponds to an increase in the charge transfer associated with the event by a factor of ~27. If the fusion of a single granule causes transfer of mean charge, then this event asks for simultaneous fusion of 27 granules which is unrealistic in the outside-out patch configuration.

Mathematical modeling suggested that the response of a single fusion event can be considerably enhanced by release in the limited space that can be created between the cell surface and the glass coverslip or even between two cells of a small cell cluster. To exclude such possibility, cells were patched in the whole cell configuration and, after establishing gigaseal, moved away from the bottom of the culture dish. Current transients recorded in this way did not differ in their characteristics (amplitude, rise and decay time) from those observed while cells were attached to the bottom of the culture dish. Nevertheless it was verified by propidium iodide staining of the nucleus that the measurements were conducted on single cells.

Moreover, mathematical modelling of ATP release showed that the rise time of the current transient associated with the release depended only slightly on intragranular ATP concentration. This is not the case for large spikes observed in experiment: the average rising time for these events is ~10 times bigger.

Having considered and excluded all these possibilities, we focused our attention on the possibility of multivesicular compound exocytosis in the pancreatic β-cell. There is evidence that this occurs in eosinophils (Scepek and Lindau, 1993, Hafez et al., 2003, Hartmann et al., 2003), neutrophils (Lollike et al., 2002) and mast cells (Pickett and Edwardson, 2006). Though there is some early ultrastructural (Dahl and Henquin, 1978) and electrochemical (Bokvist et al., 2000) evidence that this occurs in β-cells as well, more recent investigations have yielded conflicting results (Kwan and Gaisano, 2005, Takahashi and Kasai, 2007).

First, we looked for evidence of compound exocytosis in the β-cell by recording small capacitance changes of a cell membrane patch in the on-cell or cell-attached configuration (Fig 4A and Fig. 19). The majority of detected capacitance steps had the same size (3fF) as that reported earlier (MacDonald et al., 2006). An example of event of this class is marked by the arrow in Fig 20A. However, more extensive analysis revealed that ~7% of all recorded events in rat β-cells (8 events out of 110 events in 43 cells) were associated with a capacitance jump

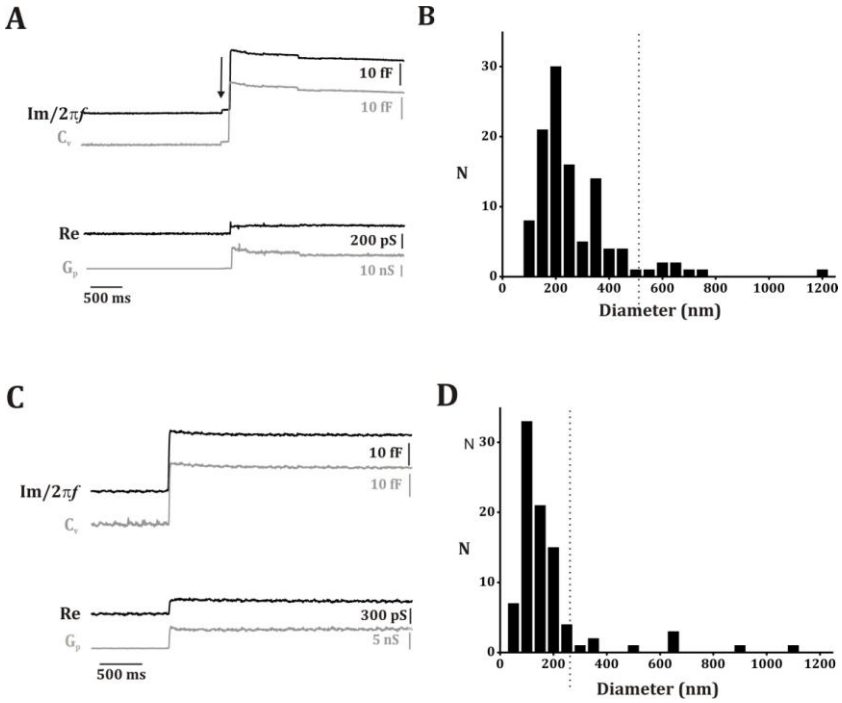


**Figure 19. Exocytosis of granules in cell-attached membrane patches of Ins-1 and primary rat β-cells have a varied distribution in single step size.** (A-C) Representative capacitance (Im/2π*f*) and conductance (Re) recordings from membrane patches of intact rat β- (A) and Ins-1 (C) cells stimulated with 10 mM glucose. Upward steps in Im/2π*f* result from the fusion of single vesicles within the patch. The arrow in A highlights a small event (1.7 fF) preceding a large event producing a capacitance increase of 26.6 fF. (B-D) The size distribution of exocytotic events in rat β-cells (B) and Ins-1 cells (D) shown as vesicle diameter. The vertical dashed lines indicates the diameter of a vesicle producing a capacitance increase 3-fold higher than the mean value (7.2 fF in B and 2.4 fF in D).

3-fold larger than the average event size (to the right of the dotted line in Fig. 19B). In Ins-1-cells, 11% of all events (i.e. 9 out of 80 events in 22 cells) displayed similarly large capacitance steps (Fig. 19C and D). Given the millisecond time resolution of these recordings, it is unlikely that these large events represent the sequential fusion of granules with the plasma membrane.

TIRF microscopy with its capability to visualize events immediately below the cell membrane should be very helpful for detection of compound events. We used this technique to visualize exocytosis in a cell expressing VAMP-pHluorin (a VAMP being granule-specific transmembrane protein with pHluorin exposed to the granule lumen) (Tsuboi and Rutter, 2003). As has been discussed above, exocytosis can be stimulated in several ways: by glucose, by application of high $K^+$, by cell depolarization, by perfusing the cell via the patch pipette etc. Though all of these methods lead to an increased rate of $Ca^{2+}$-dependent exocytosis, they are not identical in their ways of how the fusion of granules is stimulated. The main difference is the distribution of $Ca^{2+}$ within the cell cytoplasm created by

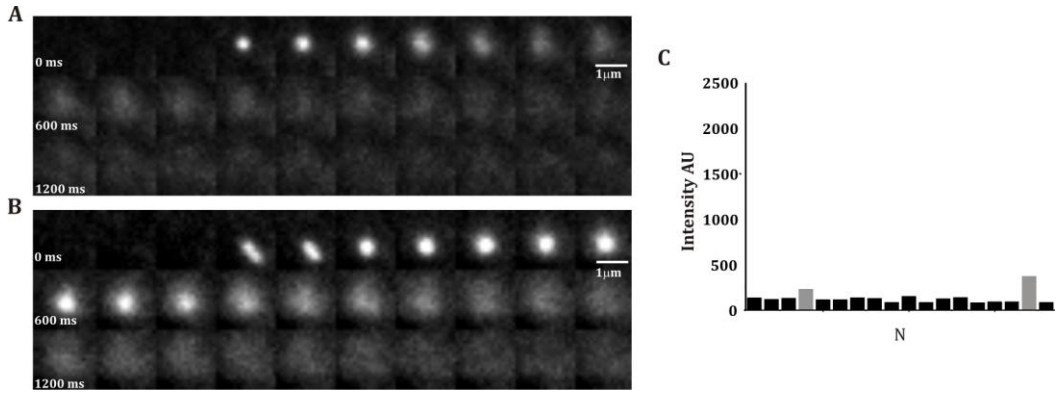


**Figure 20. TIRF images of LDCV exocytosis.** These images obtained by TIRF microscopy in an Ins-1 cell transfected with VAMP-pHluorin. Exocytosis was evoked by superfusion with a buffer containing 70 mM $K^+$. (A) A representative montage of a single exocytotic event (image interval: 60 ms). (B) Montage of a compound exocytotic event of two interconnected granules. (C) Distribution of integrated intensity of pHlourin fluorescence. n=18 events recorded from 7 cells. The grey bars show the two events associated with a fluorescence increase 2-to 3-fold greater than average.

each of these methods with some of them giving rise to a rapid global elevation of $Ca^{2+}$ (by infusion through patch electrode or by flash photolysis) and with others causing only a local increase of $Ca^{2+}$ in the vicinity of the cell membrane (by depolarization pulses or extracellular application of high glucose or $K^+$ concentrations). For example, Fig. 20A shows images of exocytotic events in cells expressing VAMP-pHluorin and stimulated by high $K^+$ (70 mM). The exocytotic event starts to be seen after membrane fusion leads to intragranular $H^+$ equilibration with the extracellular space. Next, the VAMP-pHluorin-labeled granule membrane spreads laterally within the plasma membrane. Most of the observed events exhibited similar amounts of fluorescence with roughly the same amplitude (Fig. 20C). Occasionally, events of larger amplitude were seen. Fig. 20 B, shows an example of an event consisting of the simultaneous appearance of an oblong structure with the dimensions of two single granules ($4^{th}$ frame from left), which merge over the subsequent two frames into a circular shape from which VAMP-pHluroin subsequently diffuses. Fig. 21 A shows granules undergoing exocytosis in response the muscarinic agonist carbachol which , at concentrations used, causes sharp increase of $[Ca^{2+}]_i$ all over the cell cytoplasm (Martin et al., 1997). In this case 29% of all events were of "compound" type and some of them were very large involving more than 10 secretory granules (Fig. 21B).

We also obtained electron micrographs of β-cells stimulated with 20 mM glucose in both the absence and presence of 100 μM carbachol. Upon glucose stimulation alone, single granules predominated, but when islets were stimulated with carbachol for 10 min prior to

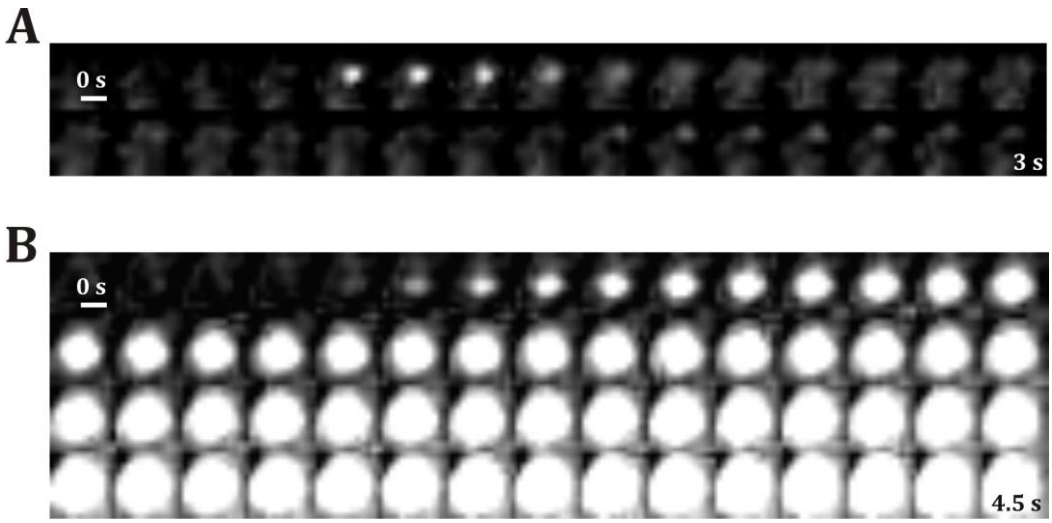


**Figure 21. Carbachol-induced stimulation of exocytosis in Ins-1 cells.** (A,B) As in Fig. 20 A and B but the image interval is 100 ms and secretion was evoked by puffer ejection of 60 nl of 1 mM carbachol close to the cell.

fixation, multivesicular structures of connected granules could be observed.

On the basis of data obtained in this study we conclude that compound exocytosis does happen in pancreatic β-cells. The frequency of such events is normaly low but it increases drastically under conditions of global $[Ca^{2+}]_i$ elevation such as muscarinic stimulation.

What is the functional significance of compound exocytosis? The low density of $Ca^{2+}$ channels in the β-cells can be envisaged to limit the number of secretory granules that are sufficiently close to the $Ca^{2+}$-channel to undergo exocytosis upon depolarization. If several granules can prefuse, then a large exocytotic response may initiated by $Ca^{2+}$ influx via a single (cluster of) $Ca^{2+}$-channels (Barg et al., 2001b).

## Do SVs contribute to ATP release and in $\Delta C_m$?

In addition to insulin-containing LDCVs, pancreatic β-cells also contain SVs (Reetz et al., 1991, Braun et al., 2004) that undergo regulated exocytosis (MacDonald et al., 2006). It has been reported that there is a temporal dissociation between the increase in membrane capacitance and the detection of extracellular serotonin (5-HT), which is co-released with insulin from β-cells preloaded with the amine (Aspinwall et al., 1999, Bokvist et al., 2000, Smith et al., 1995). Thus, an early component of capacitance was seen without any concomitant serotonin release (Takahashi et al., 1997) and it was proposed that this early component reflects exocytosis of SVs (Kasai, 1999). It should be noted, however, that not all studies on β-cells have

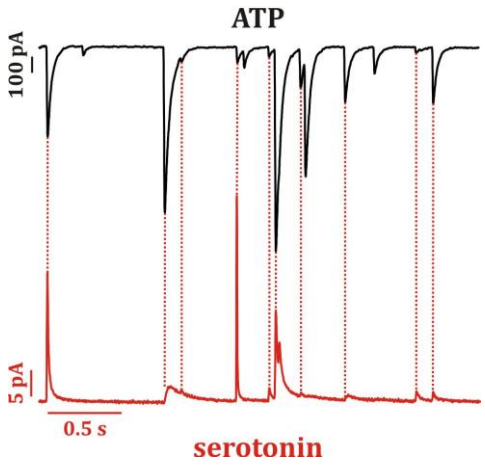


**Figure 22. An example of a parallel recording of ATP (black) and 5-HT (red) release in rat primary cells.** Red dotted lines indicate simultaneous events..

observed a dissociation between the capacitance increase and the release of 5-HT (Smith et al., 1995, Bokvist et al., 2000, Smith et al., 1999). More recently, it was reported (based on advanced two-photon extracellular polar-tracer image quantification) that photorelease of caged $Ca^{2+}$ leads to the rapid release of ~4000 SVs (Hatakeyama et al., 2007). A dissociation between capacitance measurements and LDCV exocytosis studied by amperometry (Haller et al., 1998) and TIRF imaging of cargo release (Becherer et al., 2007) has also been observed in chromaffin cells.

We addressed this unresolved problem by parallel recordings of ATP and 5-HT release in primary rat β-cells engineered to express purinergic ionotropic $P2X_2$ receptors ($P2X_2R$) combined with cell membrane capacitance measurements. Parallel recordings of ATP and 5-HT release revealed that at both 0.2 and 2 μM $[Ca^{2+}]_i$ there is an excess of small events not associated with detectable co-release of serotonin whereas there was a better agreement for larger current amplitudes (Fig. 22). However, there is reason to assume that these events do not represent a release of SVs. Rather, this is a consequence of the lower resolution of amperometry: some events associated with the release of 5-HT will not be detected by the carbon fibre because they are too small and/or occur too far away from the carbon fibre. This skews the distribution of ATP currents associated with 5-HT release towards the larger events. When the original histogram of the ATP-evoked TICs was corrected for the failure to detect the smallest events (see paper I, Methods), the difference became less apparent

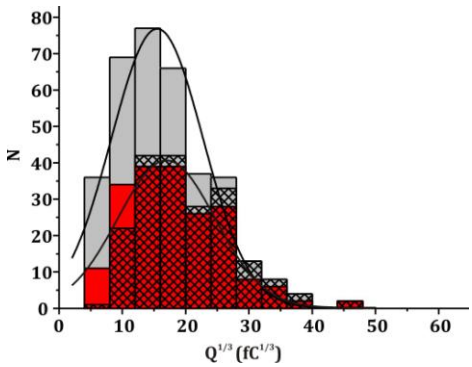


**Figure 23. Cubic root of charge distributions of $P2X_2$ currents from the parallel ATP and 5-HT release recordings in primary β-cells.** Grey bars – all $P2X_2$ events, red bars – events associated with 5-HT release, stippled bars – a histogram obtained from the distribution of all events (grey bars) by assuming that ATP was detected amperometrically and by taking into account the diffusion time of ATP from the release site to the carbon fibre. (Haller et al., 1998).

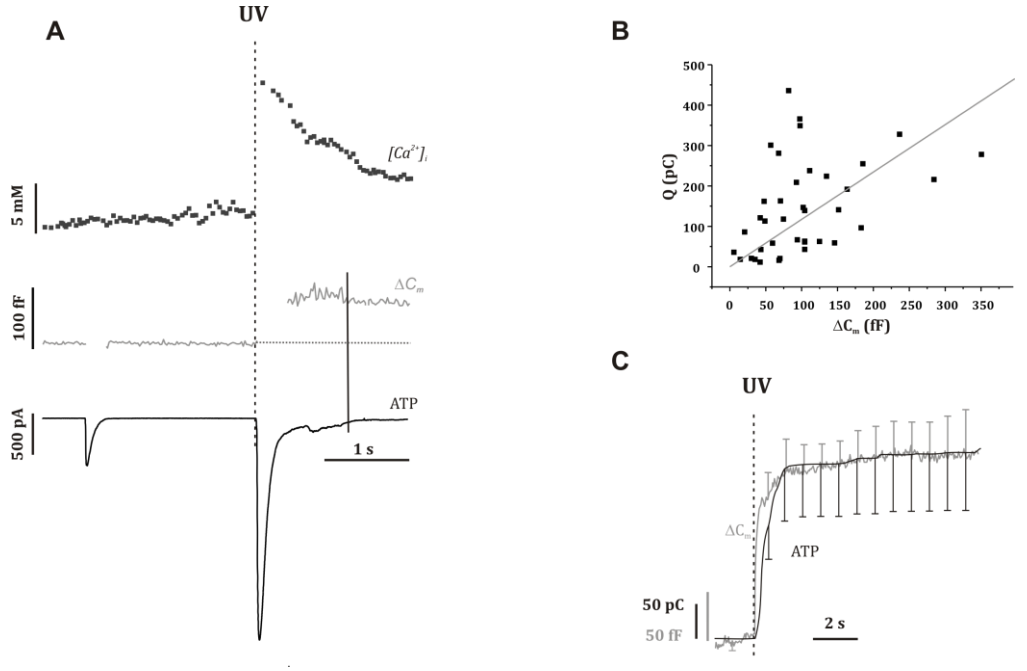


**Figure 24. $P2X_2$ receptor currents and changes in β-cell membrane capacitance evoked by photorelease of caged $Ca^{2+}$.** (A) Increase in $[Ca^{2+}]_i$ (top), change in membrane capacitance (middle) and associated $P2X_2R$ currents (bottom) transients recorded from a rat β-cell. (B) Relationship between capacitance increase ($\Delta C_m$) and total TIC charge ($Q$) evoked by photorelease of caged $Ca^{2+}$. A straight line was fitted to the data points with a slope of 1.2±0.2 pC/fF ($r$=0.8: $P$<0.001). The charge and capacitance was measured over the period indicated by dashed vertical line in (A). (C) Cumulative charge of TICs (black; n=6) superimposed on the mean capacitance increase in untransfected cells (grey; n=5).

(Fig. 23). Collectively, the parallel measurements of ATP and 5-HT release provide no evidence for a separate class of vesicles that contain ATP but no 5-HT and that might represent an exocytotic pathway distinct from the LDCVs.

The contribution of SVs to both the increase of cell capacitance and ATP response was further evaluated in experiments with the photoliberation of caged $Ca^{2+}$ (Fig. 24A). In a series of 37 pulses in 22 cells, it was found that the initial current transient reached its maximum value in 137±31 ms with the total charge ($Q$) transferred into the cell on average equal to 139±19 pC. This ATP release correlated with an increase in membrane capacitance ($\Delta C_m$) which averaged to 105±13 fF over an 545±49 ms. As is seen in Fig. 24B, $Q$ is linearly related to $\Delta C_m$ ($r$=0.8; $P$<0.001). The relationship has a slope of 1.2±0.2 pC/fF.

To estimate the relative input each type of vesicles, we assume that the initial current transient is created by ATP released from both SVs and LDCVs. Further, we denote the total number of SVs involved as $a$ and the total number of LDCVs as $b$. Experimentally detected values for charge ($Q$) of the ATP-evoked current and increase in membrane capacitance ($\Delta C_m$) allows us to form a system of two linear equations for

these two unknown values of *a* and *b*:

$$\begin{cases} \Delta C_m = c_{m,SV} \cdot a + c_{m,LDCV} \cdot b \\ Q = q_{SV} \cdot a + q_{LDCV} \cdot b \end{cases}$$

Single-vesicle capacitance increases for SVs ($c_{m,\,SV}$) and LDCVs ($c_{m,\,LDCV}$) have been measured to be on the scale of 0.2 fF and 2.9 fF, respectively (MacDonald et al., 2006). We have estimated in this thesis the unitary charge of the current associated with the ATP release during exocytosis of an LDCV ($q_{LDCV}$) to be of 4.2 pC. Unfortunately, the unitary charge evoked by ATP release due to exocytosis of SVs ($q_{SV}$) is not known. That does not allow us to solve the above system of equations straightforwardly. Instead, we consider here three limiting possibilities in order to estimate the largest possible input of SVs in observed values of charge and capacitance increase. These are: 1) SVs contain no ATP at all (i.e. $q_{SV}=0$) and does not affect the value of *Q* though their input is present in $\Delta C_m$ ; 2) SVs contain ATP at the same concentration as the LDCVs but because the volume of an SV is only 2% of the LDCVs (as predicted from the diameters of 90 nm and 330 nm; (Braun et al., 2004)), the amount of ATP released during SV exocytosis will be correspondingly reduced (i.e. $q_{SV}=0.02*q_{LDCV}$); and 3) the concentration of ATP in SVs is such that these vesicles release approximately the same amount of nucleotide as LDCVs ($q_{SLMV}=q_{LDCV}$); this is achieved if SVs contain ATP at an ~50-fold higher concentration than the LDCVs.

Our experimental data exclude from further consideration case 2 as leading to the presence of a second peak at 3.6-4.5 $fC^{1/3}$ in the charge histogram which was not observed.

For the two remaining cases, inserting of the experimentally observed values of $\Delta C_m$ and *Q* (105 fF and 139 pC) into the above equations yields values for *b* and *a* of ~33 and 45 for case 1 ($q_{SV}=0$), and 36 and 0 for case 3 ($q_{SV}=q_{LDCV}$). Taking into account the small volume of SVs, these values indicate that exocytosis of SVs accounts for maximally <0.05% of the ATP release. In terms of capacitance increase, exocytosis of SVs will contribute not more than 10% of the changes observed.

Additionally, there was a good temporal correlation between the kinetics of capacitance increase and ATP release (Fig. 24C). However, the capacitance started to increase at around 33 ms after $Ca^{2+}$ stimulus and preceded the cumulative TIC charge by 40ms. It is possible, that this delay reflects the time-dependent expansion of the fusion pore. At the first stages of the pore formation its size may be restrictive for the release of ATP molecules. Indeed, there are fewer pedestals in the ATP-release measurements than what can be detected by a amperometry. This is consistant

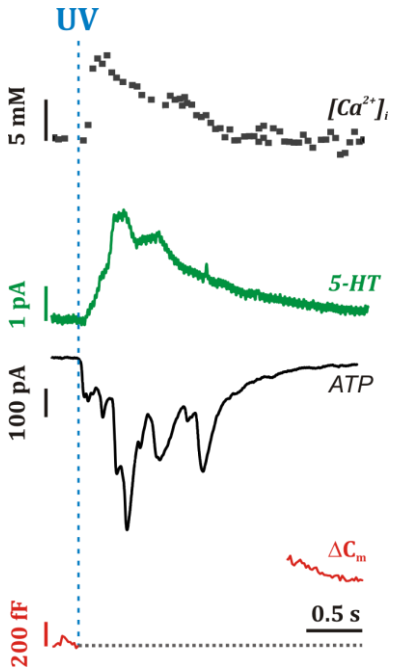


**Figure 25. $Ca^{2+}$-evoked exocytosis monitored by 5-HT amperometry, ATP release and capacitance measurements.** Increase in $[Ca^{2+}]_i$ (top), amperometric transients (2nd from top, green), associated TICs (3rd from top) and change in membrane capacitance (bottom, red) recorded from a rat β-cell.

with a restrictive passage of ATP. The presence of charged matrix in granules may also hinder fast exit of other charged substances when the pore has not yet expanded fully. ATP was co-released with the insulin granule marker 5-HT (Fig. 25) and there was only a small (if any) delay between ATP and 5-HT release. The small delay that occurs may be attributed to the time needed for 5-HT to diffuse from the release site to the carbon fibre.

Collectively, these data suggest that measurements of membrane capacitance and ATP release principally reflect exocytosis of LDCVs. Thus, capacitance measurements remain a valid and useful technique to study the cellular regulation of insulin exocytosis. The data presented here also illustrate the power of combining capacitance measurements with electrophysiological detection of substances released during exocytosis. Methods similar to those described here for β-cells may be also possible to apply to other secretory cells to address similar questions on the nature of exocytosis.

# CONCLUSIONS

We explored the nature of LDCV exocytosis in pancreatic β-cells by employing a variety of electrophysiological and imaging methods. The following conclusions were reached:

1. Expression of $P2X_2$ receptors in pancreatic β-cells in combination with patch-clamp technique provides a highly sensitive and accurate method for measurements of ATP release from individual LDCVs.

2. In rat insulinoma cells, peptides and low molecular weight compounds are released independently and with different time course. Nucleotides are released with delay of 280 ms after the membrane depolarization. The granular peptide marker IAPP release was detected 2.2 s after the same stimulus. In

72% of all exocytotic events nucleotide release is not followed by the discharge of peptide cargo.

3. At least 75% of GABA release events are attributable to the exocytosis of LDCVs in rat pancreatic β-cells and its selective release is regulated by fusion pore size.

4. In rat pancreatic β-cells ATP is stored and released by LDCVs. The contribution of small synaptic like vesicles is below detection levels of methods used. Rapid increase of $[Ca^{2+}]_i$ by flash photolysis in rat β-cells triggered an increase in membrane capacitance followed by approximately parallel release of ATP and 5HT. No evidence was detected in these conditions of cell capacitance increase not linked to exocytosis of LDCVs.

5. Global increase in $[Ca^{2+}]_i$ promotes the formation of complexes of interconnected granules within cell cytoplasm that subsequently undergo exocytosis as one unit. This may lead to exocytosis of up to 15 granules simultaneously (compound exocytosis).

# ACKNOWLEDGEMENTS

I would like to express my sincere gratitude to all those who gave me the chance to complete this thesis.

I want to thank my supervisor Patrik Rorsman for inviting me to Lund to start my PhD studies in his lab. Thanks for your trust, inspiration, freedom you gave me and your endless enthusiasm.

Thanks to my former colleagues in Lund and Malmö for being helpful and friendly: Sebastian Barg for introducing me to electrophysiology at a very early stage of my PhD. The rest was 'easy'. I am also grateful to Stefanie Obermüller and Anders Lindqvist for being so understanding and supportive. I thank Kristina Borglid and Brit-Marie Nilsson for making high quality cell preps and for being extremely helpful when help was what was needed the most. I want to thank Lena Eliasson, Erik Renström and Bryndis Birnir for valuable advice and comments. Thanks to Charlotta, Rosita, Catta, Anna, Yang, Anders R. and Sven. It was fun and a great pleasure to study and work with you!

I also would like to express my gratitude to all my colleagues and friends in Oxford, especially to Matthias Braun for sharing his knowledge and scientific experience. Also thanks for being a helpful colleague and a good family friend. I am grateful to Michael Hoppa for his enthusiasm and friendship. It was fun to work with you and I am looking forward more fun in the future! I am extremely grateful to David Wiggins for helping me with excellent preps on the shortest possible notice; to Reshma Ramracheya for being such a good friend; to Caroline Ward for patiently correcting my English especially while writing this thesis; all my other colleagues for their understanding and support.

I am especially thankful to my best friend Sandra for being such a great friend. Niekada nesu turejusi tokios geros, nuosirdzios, tiesiog ypatingos draugsės kaip tu. Be galo esu tau ir likimui dėkinga už mūsų laiką praleistą kartu.

I want to thank my family in Lithuania who have been so supportive and caring. Dėkoju visai savo šeimai Lietuvoje, už pagalbą, palaikymą ir paramą. Esu be galo visiems dėkinga ir skolinga. Myliu jus visus. Rimgaile, tu irgi prie lietuvos šeimos ar ne? Dėkui tau, superpusseseryte, ir linkiu sėkmės. Be galo dėkoju Močiutei ir Diedukui už parama ir maldą. Tėčiui, Mamai, Dianai ir mano ypatingajai sesei Eglytei esu dėkinga už tai, kas esu.

And most of all I would like to thank my close family: Juris, for your eternal patience, persistent guidance, sharp critiques and your endless love. I am incredibly lucky to have you by my side; Simonas, my such a special boy, thanks for making me so happy. I love both of you deeply

# REFERENCES


ABDERRAHMANI, A., PLAISANCE, V., LOVIS, P. & REGAZZI, R. (2006) Mechanisms controlling the expression of the components of the exocytotic apparatus under physiological and pathological conditions. *Biochem Soc Trans*, 34**,** 696-700.

ALES, E., TABARES, L., POYATO, J. M., VALERO, V., LINDAU, M. & ALVAREZ DE TOLEDO, G. (1999) High calcium concentrations shift the mode of exocytosis to the kiss-and-run mechanism. *Nat Cell Biol*, 1**,** 40-4.

ALVAREZ DE TOLEDO, G., FERNANDEZ-CHACON, R. & FERNANDEZ, J. M. (1993) Release of secretory products during transient vesicle fusion. *Nature*, 363**,** 554-8.

ARCHER, D. A., GRAHAM, M. E. & BURGOYNE, R. D. (2002) Complexin regulates the closure of the fusion pore during regulated vesicle exocytosis. *J Biol Chem*, 277**,** 18249-52.

ARDILES, A. O., GONZALEZ-JAMETT, A. M., MARIPILLAN, J., NARANJO, D., CAVIEDES, P. & CARDENAS, A. M. (2007) Calcium channel subtypes differentially regulate fusion pore stability and expansion. *J Neurochem*, 103**,** 1574-81.

ASHCROFT, F. M. & RORSMAN, P. (1989) Electrophysiology of the pancreatic beta-cell. *Prog Biophys Mol Biol*, 54**,** 87-143.

ASPINWALL, C. A., HUANG, L., LAKEY, J. R. & KENNEDY, R. T. (1999) Comparison of amperometric methods for detection of exocytosis from single pancreatic beta-cells of different species. *Anal Chem*, 71**,** 5551-6.

BANKSTON, L. A. & GUIDOTTI, G. (1996) Characterization of ATP transport into chromaffin granule ghosts. Synergy of ATP and serotonin accumulation in chromaffin granule ghosts. *J Biol Chem*, 271**,** 17132-8.

BARG, S. (2003) Mechanisms of exocytosis in insulin-secreting B-cells and glucagon-secreting A-cells. *Pharmacol Toxicol*, 92**,** 3-13.

BARG, S., HUANG, P., ELIASSON, L., NELSON, D. J., OBERMULLER, S., RORSMAN, P., THEVENOD, F. & RENSTROM, E. (2001a) Priming of insulin granules for exocytosis by granular Cl(-) uptake and acidification. *J Cell Sci*, 114**,** 2145-54.

BARG, S., MA, X., ELIASSON, L., GALVANOVSKIS, J., GOPEL, S. O., OBERMULLER, S., PLATZER, J., RENSTROM, E., TRUS, M., ATLAS, D., STRIESSNIG, J. & RORSMAN, P. (2001b) Fast exocytosis with few Ca(2+) channels in insulin-secreting mouse pancreatic B cells. *Biophys J*, 81**,** 3308-23.

BARG, S., OLOFSSON, C. S., SCHRIEVER-ABELN, J., WENDT, A., GEBRE-MEDHIN, S., RENSTROM, E. & RORSMAN, P. (2002) Delay between fusion pore opening and peptide release from large dense-core vesicles in neuroendocrine cells. *Neuron*, 33**,** 287-99.

BARG, S. & RORSMAN, P. (2004) Insulin secretion: a high-affinity Ca2+ sensor after all? *J Gen Physiol*, 124**,** 623-5.

BECHERER, U., PASCHE, M., NOFAL, S., HOF, D., MATTI, U. & RETTIG, J. (2007) Quantifying exocytosis by combination of membrane capacitance measurements and total internal reflection fluorescence microscopy in chromaffin cells. *PLoS ONE*, 2**,** e505.

BOKVIST, K., ELIASSON, L., AMMALA, C., RENSTROM, E. & RORSMAN, P. (1995) Co-localization of L-type Ca2+ channels and insulin-containing

secretory granules and its significance for the initiation of exocytosis in mouse pancreatic B-cells. *EMBO J,* 14**,** 50-7.

BOKVIST, K., HOLMQVIST, M., GROMADA, J. & RORSMAN, P. (2000) Compound exocytosis in voltage-clamped mouse pancreatic beta-cells revealed by carbon fibre amperometry. *Pflugers Arch,* 439**,** 634-45.

BRAUN, M., WENDT, A., BIRNIR, B., BROMAN, J., ELIASSON, L., GALVANOVSKIS, J., GROMADA, J., MULDER, H. & RORSMAN, P. (2004) Regulated exocytosis of GABA-containing synaptic-like microvesicles in pancreatic beta-cells. *J Gen Physiol,* 123**,** 191-204.

BRAUN, M., WENDT, A., KARANAUSKAITE, J., GALVANOVSKIS, J., CLARK, A., MACDONALD, P. E. & RORSMAN, P. (2007a) Corelease and Differential Exit via the Fusion Pore of GABA, Serotonin, and ATP from LDCV in Rat Pancreatic {beta} Cells. *J Gen Physiol,* 129**,** 221-31.

BRAUN, M., WENDT, A., KARANAUSKAITE, J., GALVANOVSKIS, J., CLARK, A., MACDONALD, P. E. & RORSMAN, P. (2007b) Corelease and differential exit via the fusion pore of GABA, serotonin, and ATP from LDCV in rat pancreatic beta cells. *J Gen Physiol,* 129**,** 221-31.

BRECKENRIDGE, L. J. & ALMERS, W. (1987) Final steps in exocytosis observed in a cell with giant secretory granules. *Proc Natl Acad Sci U S A,* 84**,** 1945-9.

BRUNS, D., RIEDEL, D., KLINGAUF, J. & JAHN, R. (2000) Quantal release of serotonin. *Neuron,* 28**,** 205-20.

CATTERALL, W. A. (1999) Interactions of presynaptic Ca2+ channels and snare proteins in neurotransmitter release. *Ann N Y Acad Sci,* 868**,** 144-59.

CHOW, R. H., VON RUDEN, L. & NEHER, E. (1992) Delay in vesicle fusion revealed by electrochemical monitoring of single secretory events in adrenal chromaffin cells. *Nature,* 356**,** 60-3.

DAHL, G. & HENQUIN, J. C. (1978) Cold-induced insulin release in vitro: evidence for exocytosis. *Cell Tissue Res,* 194**,** 387-98.

DEAN, P. M. (1973) Ultrastructural morphometry of the pancreatic -cell. *Diabetologia,* 9**,** 115-9.

DETIMARY, P., JONAS, J. C. & HENQUIN, J. C. (1995) Possible links between glucose-induced changes in the energy state of pancreatic B cells and insulin release. Unmasking by decreasing a stable pool of adenine nucleotides in mouse islets. *J Clin Invest,* 96**,** 1738-45.

DING, S. & SACHS, F. (1999) Single channel properties of P2X2 purinoceptors. *J Gen Physiol,* 113**,** 695-720.

ELIASSON, L., PROKS, P., AMMALA, C., ASHCROFT, F. M., BOKVIST, K., RENSTROM, E., RORSMAN, P. & SMITH, P. A. (1996) Endocytosis of secretory granules in mouse pancreatic beta-cells evoked by transient elevation of cytosolic calcium. *J Physiol,* 493 ( Pt 3)**,** 755-67.

GANDHI, S. P. & STEVENS, C. F. (2003) Three modes of synaptic vesicular recycling revealed by single-vesicle imaging. *Nature,* 423**,** 607-13.

GILLIS, K. D. & MISLER, S. (1992) Single cell assay of exocytosis from pancreatic islet B cells. *Pflugers Arch,* 420**,** 121-3.

GRYNKIEWICZ, G., POENIE, M. & TSIEN, R. Y. (1985) A new generation of Ca2+ indicators with greatly improved fluorescence properties. *J Biol Chem,* 260**,** 3440-50.

HAFEZ, I., STOLPE, A. & LINDAU, M. (2003) Compound exocytosis and

cumulative fusion in eosinophils. *J Biol Chem,* 278**,** 44921-8.

HALLER, M., HEINEMANN, C., CHOW, R. H., HEIDELBERGER, R. & NEHER, E. (1998) Comparison of secretory responses as measured by membrane capacitance and by amperometry. *Biophys J,* 74**,** 2100-13.

HAN, X., WANG, C. T., BAI, J., CHAPMAN, E. R. & JACKSON, M. B. (2004) Transmembrane segments of syntaxin line the fusion pore of Ca2+-triggered exocytosis. *Science,* 304**,** 289-92.

HARTMANN, J. & LINDAU, M. (1995) A novel Ca(2+)-dependent step in exocytosis subsequent to vesicle fusion. *FEBS Lett,* 363**,** 217-20.

HARTMANN, J., SCEPEK, S., HAFEZ, I. & LINDAU, M. (2003) Differential regulation of exocytotic fusion and granule-granule fusion in eosinophils by Ca2+ and GTP analogs. *J Biol Chem,* 278**,** 44929-34.

HATAKEYAMA, H., TAKAHASHI, N., KISHIMOTO, T., NEMOTO, T. & KASAI, H. (2007) Two cAMP-dependent pathways differentially regulate exocytosis of large dense-core and small vesicles in mouse beta-cells. *J Physiol,* 582**,** 1087-98.

HISATOMI, M., HIDAKA, H. & NIKI, I. (1996) Ca2+/calmodulin and cyclic 3,5' adenosine monophosphate control movement of secretory granules through protein phosphorylation/dephosphorylation in the pancreatic beta-cell. *Endocrinology,* 137**,** 4644-9.

HUTTON, J. C. (1994) Insulin secretory granule biogenesis and the proinsulin-processing endopeptidases. *Diabetologia,* 37 Suppl 2**,** S48-56.

IVARSSON, R., OBERMULLER, S., RUTTER, G. A., GALVANOVSKIS, J. & RENSTROM, E. (2004) Temperature-sensitive random insulin granule diffusion is a prerequisite for recruiting granules for release. *Traffic,* 5**,** 750-62.

IYNEDJIAN, P. B. (1993) Mammalian glucokinase and its gene. *Biochem J,* 293 ( Pt 1)**,** 1-13.

JAHN, R. & SCHELLER, R. H. (2006) SNAREs--engines for membrane fusion. *Nat Rev Mol Cell Biol,* 7**,** 631-43.

KAHN, S. E. & PORTE, D., JR. (1988) Islet dysfunction in non-insulin-dependent diabetes mellitus. *Am J Med,* 85**,** 4-8.

KASAI, H. (1999) Comparative biology of Ca2+-dependent exocytosis: implications of kinetic diversity for secretory function. *Trends Neurosci,* 22**,** 88-93.

KIRSHNER, N., SAGE, H. J., SMITH, W. J. & KIRSHNER, A. G. (1966) Release of catecholamines and specific protein from adrenal glands. *Science,* 154**,** 529-31.

KISHIMOTO, T., LIU, T. T., HATAKEYAMA, H., NEMOTO, T., TAKAHASHI, N. & KASAI, H. (2005) Sequential compound exocytosis of large dense-core vesicles in PC12 cells studied with TEPIQ (two-photon extracellular polar-tracer imaging-based quantification) analysis. *J Physiol,* 568**,** 905-15.

KWAN, E. P. & GAISANO, H. Y. (2005) Glucagon-like peptide 1 regulates sequential and compound exocytosis in pancreatic islet beta-cells. *Diabetes,* 54**,** 2734-43.

LANG, J. (1999) Molecular mechanisms and regulation of insulin exocytosis as a paradigm of endocrine secretion. *Eur J Biochem,* 259**,** 3-17.

LOLLIKE, K., BORREGAARD, N. & LINDAU, M. (1998) Capacitance flickers and pseudoflickers of small granules, measured in the cell-attached configuration. *Biophys J,* 75**,** 53-9.

LOLLIKE, K., LINDAU, M., CALAFAT, J. & BORREGAARD, N. (2002) Compound exocytosis of granules

in human neutrophils. *J Leukoc Biol*, 71**,** 973-80.

LOPEZ, J. A., KWAN, E. P., XIE, L., HE, Y., JAMES, D. E. & GAISANO, H. Y. (2008) The RalA GTPase is a central regulator of insulin exocytosis from pancreatic islet beta cells. *J Biol Chem*, 283**,** 17939-45.

MACDONALD, P. E., BRAUN, M., GALVANOVSKIS, J. & RORSMAN, P. (2006) Release of small transmitters through kiss-and-run fusion pores in rat pancreatic beta cells. *Cell Metab*, 4**,** 283-90.

MACDONALD, P. E., OBERMULLER, S., VIKMAN, J., GALVANOVSKIS, J., RORSMAN, P. & ELIASSON, L. (2005) Regulated exocytosis and kiss-and-run of synaptic-like microvesicles in INS-1 and primary rat beta-cells. *Diabetes*, 54**,** 736-43.

MARTIN, F., RIBAS, J. & SORIA, B. (1997) Cytosolic Ca2+ gradients in pancreatic islet-cells stimulated by glucose and carbachol. *Biochem Biophys Res Commun*, 235**,** 465-8.

MATSCHINSKY, F. M. (1996) Banting Lecture 1995. A lesson in metabolic regulation inspired by the glucokinase glucose sensor paradigm. *Diabetes*, 45**,** 223-41.

MELDOLESI, J. & CHIEREGATTI, E. (2004) Fusion has found its calcium sensor. *Nat Cell Biol*, 6**,** 476-8.

MICHAEL, D. J., GENG, X., CAWLEY, N. X., LOH, Y. P., RHODES, C. J., DRAIN, P. & CHOW, R. H. (2004) Fluorescent cargo proteins in pancreatic beta-cells: design determines secretion kinetics at exocytosis. *Biophys J*, 87**,** L03-5.

NEHER, E., SAKMANN, B. & STEINBACH, J. H. (1978) The extracellular patch clamp: a method for resolving currents through individual open channels in biological membranes. *Pflugers Arch*, 375**,** 219-28.

NEWGARD, C. B. & MCGARRY, J. D. (1995) Metabolic coupling factors in pancreatic beta-cell signal transduction. *Annu Rev Biochem*, 64**,** 689-719.

OLOFSSON, C. S., GOPEL, S. O., BARG, S., GALVANOVSKIS, J., MA, X., SALEHI, A., RORSMAN, P. & ELIASSON, L. (2002) Fast insulin secretion reflects exocytosis of docked granules in mouse pancreatic B-cells. *Pflugers Arch*, 444**,** 43-51.

PERRAIS, D., KLEPPE, I. C., TARASKA, J. W. & ALMERS, W. (2004) Recapture after exocytosis causes differential retention of protein in granules of bovine chromaffin cells. *J Physiol*, 560**,** 413-28.

PETHIG, R., JAKUBEK, L. M., SANGER, R. H., HEART, E., CORSON, E. D. & SMITH, P. J. (2005) Electrokinetic measurements of membrane capacitance and conductance for pancreatic beta-cells. *IEE Proc Nanobiotechnol*, 152**,** 189-93.

PICKETT, J. A. & EDWARDSON, J. M. (2006) Compound exocytosis: mechanisms and functional significance. *Traffic*, 7**,** 109-16.

POULI, A. E., EMMANOUILIDOU, E., ZHAO, C., WASMEIER, C., HUTTON, J. C. & RUTTER, G. A. (1998) Secretory-granule dynamics visualized in vivo with a phogrin-green fluorescent protein chimaera. *Biochem J*, 333 ( Pt 1)**,** 193-9.

REETZ, A., SOLIMENA, M., MATTEOLI, M., FOLLI, F., TAKEI, K. & DE CAMILLI, P. (1991) GABA and pancreatic beta-cells: colocalization of glutamic acid decarboxylase (GAD) and GABA with synaptic-like microvesicles suggests their role in GABA storage and secretion. *Embo J*, 10**,** 1275-84.

RORSMAN, P., BERGGREN, P. O., BOKVIST, K., ERICSON, H., MOHLER, H., OSTENSON, C. G. & SMITH, P. A. (1989)

Glucose-inhibition of glucagon secretion involves activation of GABAA-receptor chloride channels. *Nature,* 341**,** 233-6.

RORSMAN, P. & RENSTROM, E. (2003) Insulin granule dynamics in pancreatic beta cells. *Diabetologia,* 46**,** 1029-45.

SALEHI, A., QADER, S. S., GRAPENGIESSER, E. & HELLMAN, B. (2005) Inhibition of purinoceptors amplifies glucose-stimulated insulin release with removal of its pulsatility. *Diabetes,* 54**,** 2126-31.

SCEPEK, S., COORSSEN, J. R. & LINDAU, M. (1998) Fusion pore expansion in horse eosinophils is modulated by Ca2+ and protein kinase C via distinct mechanisms. *EMBO J,* 17**,** 4340-5.

SCEPEK, S. & LINDAU, M. (1993) Focal exocytosis by eosinophils--compound exocytosis and cumulative fusion. *EMBO J,* 12**,** 1811-7.

SMITH, P. A., DUCHEN, M. R. & ASHCROFT, F. M. (1995) A fluorimetric and amperometric study of calcium and secretion in isolated mouse pancreatic beta-cells. *Pflugers Arch,* 430**,** 808-18.

SMITH, P. A., PROKS, P. & ASHCROFT, F. M. (1999) Quantal analysis of 5-hydroxytryptamine release from mouse pancreatic beta-cells. *J Physiol,* 521 Pt 3**,** 651-64.

SPELLMAN, C. W. (2007) Islet cell dysfunction in progression to diabetes mellitus. *J Am Osteopath Assoc,* 107 Suppl**,** S1-5.

SPRUCE, A. E., BRECKENRIDGE, L. J., LEE, A. K. & ALMERS, W. (1990) Properties of the fusion pore that forms during exocytosis of a mast cell secretory vesicle. *Neuron,* 4**,** 643-54.

SUTTON, R. B., FASSHAUER, D., JAHN, R. & BRUNGER, A. T. (1998) Crystal structure of a SNARE complex involved in synaptic exocytosis at 2.4 A resolution. *Nature,* 395**,** 347-53.

TABARES, L., ALES, E., LINDAU, M. & ALVAREZ DE TOLEDO, G. (2001) Exocytosis of catecholamine (CA)-containing and CA-free granules in chromaffin cells. *J Biol Chem,* 276**,** 39974-9.

TABARES, L., LINDAU, M. & ALVAREZ DE TOLEDO, G. (2003) Relationship between fusion pore opening and release during mast cell exocytosis studied with patch amperometry. *Biochem Soc Trans,* 31**,** 837-41.

TAGAYA, M., WILSON, D. W., BRUNNER, M., ARANGO, N. & ROTHMAN, J. E. (1993) Domain structure of an N-ethylmaleimide-sensitive fusion protein involved in vesicular transport. *J Biol Chem,* 268**,** 2662-6.

TAKAHASHI, N., KADOWAKI, T., YAZAKI, Y., MIYASHITA, Y. & KASAI, H. (1997) Multiple exocytotic pathways in pancreatic beta cells. *J Cell Biol,* 138**,** 55-64.

TAKAHASHI, N. & KASAI, H. (2007) Exocytic process analyzed with two-photon excitation imaging in endocrine pancreas. *Endocr J,* 54**,** 337-46.

TARASKA, J. W. & ALMERS, W. (2004) Bilayers merge even when exocytosis is transient. *Proc Natl Acad Sci U S A,* 101**,** 8780-5.

TARASKA, J. W., PERRAIS, D., OHARA-IMAIZUMI, M., NAGAMATSU, S. & ALMERS, W. (2003) Secretory granules are recaptured largely intact after stimulated exocytosis in cultured endocrine cells. *Proc Natl Acad Sci U S A,* 100**,** 2070-5.

TSUBOI, T., MCMAHON, H. T. & RUTTER, G. A. (2004) Mechanisms of dense core vesicle recapture following "kiss and run" ("cavicapture") exocytosis in insulin-secreting cells. *J Biol Chem,* 279**,** 47115-24.

TSUBOI, T. & RUTTER, G. A. (2003) Multiple forms of "kiss-and-run" exocytosis revealed by evanescent

wave microscopy. *Curr Biol,* 13**,** 563-7.

TSUBOI, T., ZHAO, C., TERAKAWA, S. & RUTTER, G. A. (2000) Simultaneous evanescent wave imaging of insulin vesicle membrane and cargo during a single exocytotic event. *Curr Biol,* 10**,** 1307-10.

VARADI, A., AINSCOW, E. K., ALLAN, V. J. & RUTTER, G. A. (2002) Involvement of conventional kinesin in glucose-stimulated secretory granule movements and exocytosis in clonal pancreatic beta-cells. *J Cell Sci,* 115**,** 4177-89.

VARADI, A., TSUBOI, T. & RUTTER, G. A. (2005) Myosin Va transports dense core secretory vesicles in pancreatic MIN6 beta-cells. *Mol Biol Cell,* 16**,** 2670-80.

VO, Y. P., HUTTON, J. C. & ANGLESON, J. K. (2004) Recycling of the dense-core vesicle membrane protein phogrin in Min6 beta-cells. *Biochem Biophys Res Commun,* 324**,** 1004-10.

WANG, C. T., GRISHANIN, R., EARLES, C. A., CHANG, P. Y., MARTIN, T. F., CHAPMAN, E. R. & JACKSON, M. B. (2001) Synaptotagmin modulation of fusion pore kinetics in regulated exocytosis of dense-core vesicles. *Science,* 294**,** 1111-5.

WENDT, A., BIRNIR, B., BUSCHARD, K., GROMADA, J., SALEHI, A., SEWING, S., RORSMAN, P. & BRAUN, M. (2004) Glucose inhibition of glucagon secretion from rat alpha-cells is mediated by GABA released from neighboring beta-cells. *Diabetes,* 53**,** 1038-45.

WESTPHAL, C. H., MULLER, L., ZHOU, A., ZHU, X., BONNER-WEIR, S., SCHAMBELAN, M., STEINER, D. F., LINDBERG, I. & LEDER, P. (1999) The neuroendocrine protein 7B2 is required for peptide hormone processing in vivo and provides a novel mechanism for pituitary Cushing's disease. *Cell,* 96**,** 689-700.

WHITLOCK, A., BURNSTOCK, G. & GIBB, A. J. (2001) The single-channel properties of purinergic P2X ATP receptors in outside-out patches from rat hypothalamic paraventricular parvocells. *Pflugers Arch,* 443**,** 115-22.

ZENISEK, D., DAVILA, V., WAN, L. & ALMERS, W. (2003) Imaging calcium entry sites and ribbon structures in two presynaptic cells. *J Neurosci,* 23**,** 2538-48.

ZHOU, Z. & MISLER, S. (1996) Amperometric detection of quantal secretion from patch-clamped rat pancreatic beta-cells. *J Biol Chem,* 271**,** 270-7.

ZIMMERBERG, J. (1987) Molecular mechanisms of membrane fusion: steps during phospholipid and exocytotic membrane fusion. *Biosci Rep,* 7**,** 251-68.

# Quantal ATP release in rat β-cells by exocytosis of insulin-containing LDCVs

**Jovita Karanauskaite, Michael B. Hoppa, Matthias Braun, Juris Galvanovskis, Patrik Rorsman**

***OCDEM, University of Oxford, Churchill Hospital, Oxford OX3 7LJ, U.K***

**Abstract** Quantal release of ATP was monitored in rat pancreatic β-cells expressing $P2X_2$ receptors. Stimulation of exocytosis evoked rapidly activating and deactivating ATP-dependent transient inward currents (TICs). The unitary charge (*q*) of the events recorded at 0.2 μM $[Ca^{2+}]_i$ averaged 4.3 pC. The distribution of the $\sqrt[3]{q}$ of these events could be described by a single Gaussian. The rise times averaged ~5 ms over a wide range TIC amplitudes. In β-cells preloaded with 5-HT (accumulating in insulin granules) ATP was co-released with 5-HT during >90% of the release events. Following step elevation of $[Ca^{2+}]_i$ to ~5 μM by photorelease of caged $Ca^{2+}$, an increase in membrane capacitance was observed after 33 ms, whereas ATP release first became detectable after 43 ms. The step increase in $[Ca^{2+}]_i$ produced an initial large TIC followed by a series of smaller events that echoed the changes in membrane capacitance ($\Delta C_m$). Mathematical modelling suggests that the large initial TIC reflects the superimposition of many unitary events. Exocytosis, measured as $\Delta C_m$ or TICs, was complete within 2 s after elevation of $[Ca^{2+}]_i$ with no sign of endocytosis masking the capacitance increase The relationship between total charge (*Q*) and $\Delta C_m$ was linear with a slope of ~1.2 pC/fF. The latter value predicts a capacitance increase of 3.6 fF for the observed mean value of *q*, close to that expected for exocytosis of individual insulin granules. Our results indicate that measurements of ATP release and $\Delta C_m$ principally (≥85-95%) report exocytosis of insulin granules.

**Key words** insulin • exocytosis • LDCV • ATP

## Introduction

Capacitance measurements and amperometry are widely used to study single-vesicle release from endocrine cells [1, 2]. Secretory cells contain both large dense core vesicles (LDCVs) and small synaptic-like microvesicles (SVs) [3]. Whole-cell capacitance measurements monitor the increase in cell surface area that occurs when the vesicular membranes are inserted into the plasma membrane. However, it is not possible to discriminate between exocytosis of SVs and LDCVs and their relative contributions to the observed changes in membrane capacitance remain unknown.

Pancreatic β-cells are electrically excitable and changes in blood glucose translate into changes of insulin secretion via electrical activity [4]. In addition to insulin-containing LDCVs, they also contain SVs [5, 6] capable of undergoing exocytosis [7]. It has been reported that there is a temporal dissociation between the increase in membrane capacitance and the detection of extracellular serotonin (5-HT), which is co-released with insulin from β-cells preloaded with the amine [8-10]. Thus, some (but not all [10, 11]) studies report an early component of capacitance increase that occurs without any detectable release of serotonin. A dissociation between capacitance measurements and LDCV exocytosis studied by amperometry [12] and

TIRF imaging of cargo release [13] has also been observed in chromaffin cells. Clearly, these discrepant observations have great impact on the interpretation and validity of data obtained by capacitance measurements and merit further analyses.

The insulin granules constitute an important intracellular ATP depot [14-16]. Synaptic vesicles also contain ATP [17] but whether this also applies to the SVs in β-cells is not known. We have engineered primary rat β-cells to express purinergic ionotropic $P2X_2$ receptors ($P2X_2R$). These ligand-gated channels are activated by extracellular ATP [18]. Exocytosis of ATP-containing secretory vesicles can therefore be expected to transiently elevate extracellular ATP sufficiently to activate the in $P2X_2Rs$ in β-cells expressing these receptors. Indeed, stimulation of exocytosis in β-cells expressing $P2X_2Rs$ is associated with large current transients [19, 20]. We have previously demonstrated that ATP is co-released with 5-HT [21], consistent with the idea that ATP is released during exocytosis of the LDCVs. However, it remains to be determined whether ATP is also released by exocytosis of the SVs and, if this is the case, how much of the observed capacitance increase reflects fusion of such vesicles with the membrane.

Here we confirm that ATP is co-released with the insulin granule marker 5-HT preloaded into pancreatic β-cells. We further demonstrate that the amplitude distribution of the ATP-induced current transients and kinetics of these events are consistent with the release of a single class of vesicles. Finally, we show that ATP and serotonin are released in parallel with exocytosis detected as increases in membrane capacitance and that there is no temporal dissociation between the processes. We conclude that capacitance increases in rat β-cells upon stimulation of exocytosis principally reflect exocytosis of insulin-containing LDCVs.

## Results

### $P2X_2R$-based detection of extracellular ATP

Rat pancreatic β-cells were infected with ionotropic $P2X_2$ receptors ($P2X_2Rs$). Secretory vesicles in a variety of secretory cells including β-cells contain ATP [15, 16, 22]. Exocytosis of insulin granules will therefore be associated with the co-release of ATP [7, 23] and result in transient inward currents (TICs). Importantly, exocytotic ATP release will activate $P2X_2Rs$ and give rise to TICs regardless of the location of the release events (Fig. 1a). By contrast, measurements of exocytosis by amperometry only detect events that occur close to the carbon fibre [21].

In successfully infected β-cells (as judged by GFP fluorescence) held at -70 mV, application 100 μM ATP elicited an inward current with a peak amplitude ($I$) averaging 5.1±0.5 nA (n=19) (Fig 1b; trace ii); no ATP-activated currents were observed in non-infected β-cells (n=17) (Fig. 1b, trace i). The spontaneous decline in the amplitude during the application is due to slow ($\tau$ >5 s) desensitization of the receptors. At -70 mV, the $P2X_2R$ single-channel amplitude ($i$) is ~1 pA [24]. The open probability ($P_o$) of the channel at a maximally activating concentration of ATP has been reported to be ~0.6 [25]. The number of receptors per cell ($N$) can be estimated from the relationship $N=I/(i_*P_o)$. Using the above values of $I$, $P_{open}$ and $i$, $N$ can thus be estimated to be ~8500. The cell capacitance averaged 10.6±1.0 pF (n=19). Since the specific membrane capacitance is ~10 fF $\mu m^{-2}$ [26], the above value of $N$ corresponds to a receptor density of 80 $\mu m^{-2}$. This predicts an average distance between two adjacent receptors of 0.11 μm.

### Exocytosis detected by the $P2X_2R$-based assay

Fig. 1c shows recordings of ATP-induced transient inward currents (TICs) when exocytosis was stimulated by intracellular dialysis with a buffer containing 0.2 μM $Ca^{2+}$ (i) and 2 μM $Ca^{2+}$ in the absence (ii) and presence (iii) of 0.1 mM cAMP. These events were suppressed by suramin (50 μM), confirming that they are due to activation of $P2X_2Rs$ (not shown). The $P2X_2Rs$ respond principally to extracellular ATP and to a much lesser extent to ADP [27]. The frequency of the TICs averaged 9±1 $min^{-1}$ (n=8) at 0.2 μM $[Ca^{2+}]_i$, 37±4 $min^{-1}$ at 2 μM $[Ca^{2+}]_i$ alone (n=7;

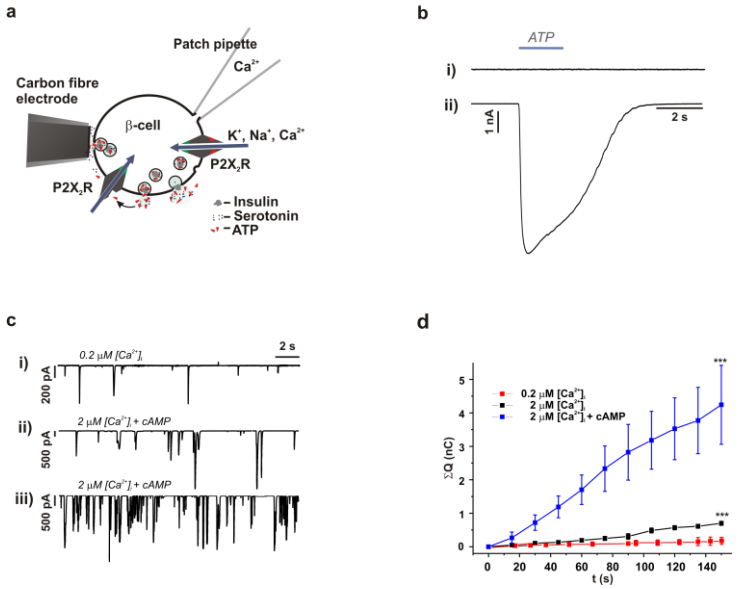


**Fig. 1.** Expression of purinergic $P2X_2$ receptors and ATP release in rat β-cells. **a** Schematic of infected β-cell and ATP release evoked by intracellular $Ca^{2+}$ application during standard whole-cell patch-clamp and amperometric measurements. Note that the $P2X_2R$ receptors will detect exocytosis-associated ATP-release across the entire cell surface area, whereas amperometry principally reports release in the close proximity of the carbon fibre. **b** Membrane current evoked by application of 100 μM ATP (as indicated by horizontal bar above current trace) to a non-infected rat β-cell (i) and a β-cell infected with $P2X_2$ receptor-GFP ($P2X_2R$-GFP) (ii). **c** TICs observed in a β-cell dialyzed with intracellular buffer containing 0.2 μM $[Ca^{2+}]_i$ (i), 2 μM $[Ca^{2+}]_i$ (ii) and 2 μM $[Ca^{2+}]_i$ + 100 μM cAMP (iii). **d** Time-dependent increase in cumulative charge (Σ*Q*) measured in cells dialyzed with 0.2 μM $[Ca^{2+}]_i$ (red; n=8), 0.2 μM $[Ca^{2+}]_i$ + 100 μM cAMP (green), 2 μM $[Ca^{2+}]_i$ (black; n=5) and 2 μM $[Ca^{2+}]_i$ + 100 μM cAMP (n=5). ***$P$<0.001 for the differences between the total increase in $Q$ over 150 s between the low and high $[Ca^{2+}]_i$ and absence and presence of cAMP at the higher $[Ca^{2+}]_i$.

$P$<0.001 *vs.* the lower $Ca^{2+}$ concentration) and 69±8 $min^{-1}$ at the higher $[Ca^{2+}]_i$ and in the presence of 100 μM cAMP (n=6: $P$<0.001 vs. 2 μM $Ca^{2+}$ alone).

Fig. 1d shows the cumulative charge (Σ*Q*) displayed against time after establishment of the whole-cell configuration. Increasing $[Ca^{2+}]_i$ from 0.2 μM to 2 μM stimulated exocytosis ~4-fold (from 185 pC to 700 pC). The inclusion of 100 μM cAMP in the intracellular medium resulted in a further 6-fold enhancement of exocytosis. The average unitary event size ($q$) was estimated by dividing Σ*Q* by the oberved number of events. It averaged 4.3±0.4 pC (n=8) and 5.3±0.6 (n=8) at 0.2 μM $[Ca^{2+}]_i$ in the absence and presence of 100 μM cAMP, respectively. At the tenfold higher $[Ca^{2+}]_i$, $q$ averaged 6.6±0.5 pC (n=5; $P$<0.05 vs. 0.2 μM $[Ca^{2+}]_i$) under control conditions and 19.2±4.2 pC (n=5) in the presence of 100 μM intracellular cAMP ($P$<0.05 vs. 2 μM $[Ca^{2+}]_i$ alone). The latter effect is reminiscent of the ~5-fold increase in the amplitude and charge of the exocytotic events previously documented by amperometry in mouse β-cells following elevation of intracellular cAMP levels by activation of adenylate cyclase by forskolin [9].

### Properties of quantal ATP release in β-cells

At 0.2 μM $[Ca^{2+}]_i$, the frequency of the TICs is low enough to allow the resolution of the individual events. Fig. 2a shows the distribution of the $\sqrt[3]{q}$ values. It can be described by a single Gaussian. The mean charge ($\bar{q}$) of these events was 4.3±0.3 pC. The peak amplitude and the charge of the smallest events (i.e. those in the leftmost bin) averaged 8±1 pA and 52±3 fC (n=11). The latter value corresponds to a $\sqrt[3]{q}$ of 3.7 $fC^{1/3}$. The inset in Fig. 2a shows the five smallest events with the baseline RMS noise given above the traces. The smallest event we observed had an amplitude of 3.2 pA and a charge of 33.4 fC.

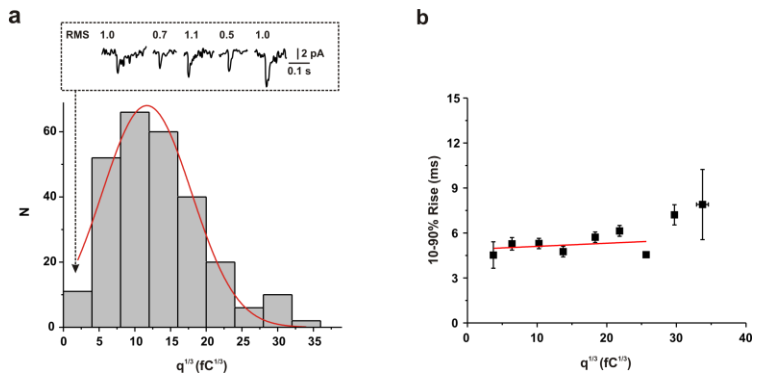


**Fig. 2. a** Distribution of $^3\sqrt{q}$ obtained in cells dialyzed with 0.2 µM $[Ca^{2+}]_i$. The red curve is a Gaussian fit to the distribution of $^3\sqrt{q}$-values. The TICs in the insert above the histogram are five examples of smallest events observed (i.e. within the first bin). The numbers above the selected events represent the baseline RMS noise level (in pA) for each trace. **b** Rise times displayed against $^3\sqrt{q}$. Data are presented as mean values ± S.E.M. for the events within the same bins as used in a. The line was obtained by least-squares analysis of the original data (rise time = 4.9 + 0.02*$^3\sqrt{q}$: $r^2$=0.11)

We characterised the TICs further by measuring the rise times of the events (i.e. the time it takes to go from 10 to 90% of the peak amplitude). These data are displayed against $^3\sqrt{q}$ in Fig. 2b. This analysis revealed that the rise time was constant and ~5 ms for $^3\sqrt{q}$ values of ≤25 $fC^{1/3}$ (≤15.6 pC).

**Parallel release of ATP and 5-HT**

Exocytosis of insulin-containing LDCVs can be studied by amperometry following preloading of the β-cell and the LDCVs with 5-HT [8]. Fig. 3a shows parallel recordings of ATP (black trace) and 5-HT release (red trace). Exocytosis was elicited by intracellular dialysis of 0.2 µM $[Ca^{2+}]_i$ and 100 µM cAMP. In a series of five experiments, 92±6% of the release events detected by amperometry associated with simultaneous ATP release. ATP-dependent TICs not associated with 5-HT release represent events occurring too far away from the carbon fibre to be detected. Fig. 3b shows the distribution of $^3\sqrt{q}$-values for all TICs (grey) and the subset of events (56% in this experiment) that were associated with simultaneous 5-HT release (red). The amplitude of both types of events exhibited close to normal distribution. It can be seen whereas >70% of the ATP-dependent TICs are associated with detectable co-release of 5-HT for $^3\sqrt{q}$-values >20 $fC^{1/3}$, the correlation is weaker for smaller events (28% for $^3\sqrt{q}$-values <8 $fC^{1/3}$). However, when the effects of amplitude and diffusional loss of 5-HT were taken into account (stippled bars; see Methods), the distributions of TICs with and without simultaneous 5-HT release became

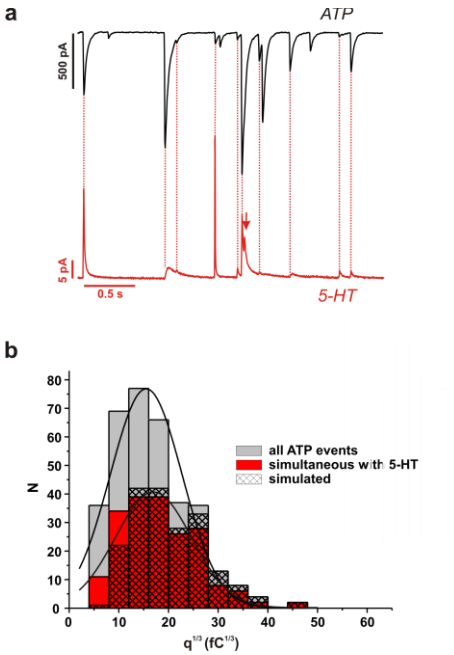


**Fig. 3.** $P2X_2R$ currents associated with serotonin release. **a** Examples of amperometric events (red) with parallel recordings of TICs (black). Red lines indicate simultaneous events. A single amperometric event not associated with a detectable TICs has been highlighted by the arrow. **b** Distribution of $^3\sqrt{q}$ of all events (grey) and the events associated with serotonin release (red) when exocytosis was evoked by 0.2 µM $[Ca^{2+}]_i$ and 100 µM cAMP. The stippled bars represent the distribution obtained from the original one (grey bars) when allowance is made for the diffusion of ATP and assuming detection of the ATP-dependent TICs been by an amperometric sensor (cf. [12]).

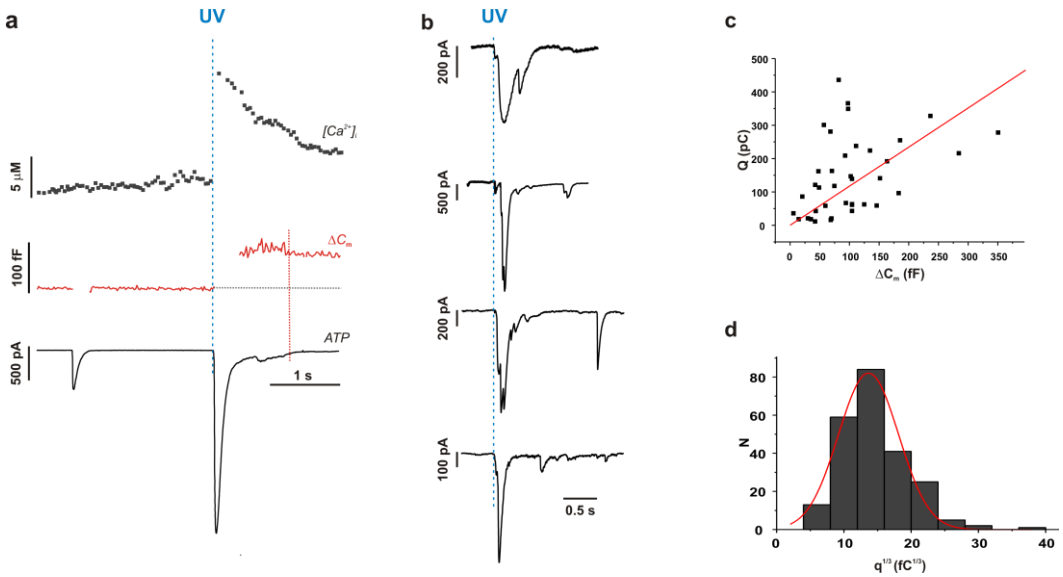


**Fig. 4.** $P2X_2$ receptor currents and changes in β-cell membrane capacitance evoked by photorelease of caged $Ca^{2+}$. **a** Increase in $[Ca^{2+}]_i$ (top), change in membrane capacitance (middle) and associated $P2X_2R$ currents (bottom) transients recorded from a rat β-cell. The capacitance measurements are not shown during the period associated with the TIC to remove large artefactual transients. **b** Examples of TIC responses following photorelease of $Ca^{2+}$ in another 4 cells. **c** Relationship between capacitance increase ($\Delta C_m$) and total TIC charge ($Q$) evoked by photorelease of caged $Ca^{2+}$. A straight line was fitted to the data points with a slope of 1.2±0.2 pC/fF ($r$=0.8: $P$<0.001). The charge and capacitance was measured over the period indicated by dashed vertical line in (a). **d** Distribution of spontaneous events observed prior to photorelease of $[Ca^{2+}]_i$. A Gaussian has been superimposed.

more similar. Thus, both the location and amplitude of the release events influence the detection of the amperometric events.

## Correlation between ATP release and exocytosis detected by capacitance measurements

Exocytosis in β-cells is normally triggered by $Ca^{2+}$-entry during glucose-induced action potentials. Because of the strongly inwardly rectifying properties of the $P2X_2Rs$ [24], the TICs become small and difficult to resolve during membrane depolarization. The time course of $Ca^{2+}$-induced exocytosis and ATP release was therefore instead determined by photoliberation of caged $Ca^{2+}$ ($Ca^{2+}$—NP-EGTA). Using this approach, exocytosis can proceed even when the membrane potential is held constant at -70 mV (Fig. 4a). In a series of 37 experiments carried out on 22 cells, in which $[Ca^{2+}]_i$ rose to 5.3±0.5 µM, the first TIC spike started on average 43±7 (n=37) ms after the flash. This is only slightly longer than delay between photorelease of $Ca^{2+}$ and a detectable increase in membrane capacitance which averaged 31±3 ms (n=9) in β-cells not infected with $P2X_2Rs$. Non-infected β-cells were used for the latter measurement as time course of the capacitance increase cannot be reliably determined in infected cells because the large increase in membrane conductance resulting from activation of the $P2X_2Rs$ and that leaks through to the capacitance signal. Fig. 4b shows examples of TICs upon photoliberation in another 4 β-cells. Typically, a step increase in $[Ca^{2+}]_i$ elicited an initial large TIC spike followed by a series of smaller events. In some cases individual events were superimposed on the large spike,

ATP release correlated with an increase in membrane capacitance ($\Delta C_m$). The increase in membrane capacitance measured once the membrane current had decayed by >95% and the capacitance signal was stable averaged 105±13 fF (n=22). The total integrated TIC ($\Sigma Q$) measured over the same period (545±49 ms) and in the same experiments averaged 139±19 pC. When multiple experiments were done on the same cell, the mean values of $\Delta C_m$ and $\Sigma Q$ obtained were used for this analysis.

Fig. 4c summarizes the relationship between $Q$ and $\Delta C_m$ in 37 experiments. It can be seen that the $Q$ is linearly related to $\Delta C_m$ ($r$=0.8; $P$<0.001). The relationship has a slope of 1.2±0.2 pC/fF.

Spontaneous TICs were sometimes observed before photoreleasing $Ca^{2+}$. The distribution of $\sqrt[3]{q}$-values of such events is shown in Fig. 4d. The distribution can be described by a single Gaussian. The mean charge ($\bar{q}$) of these events was 4.2±0.4 pC. Combining this value with the slope of 1.2 pC/fF suggests a unitary capacitance increase of 3.5 fF. This is within 21% of that observed for LDCV exocytosis in on-cell capacitance measurements (2.9 fF; [7]).

**Modelling of ATP-release**

We attribute the initial large spike observed following photorelease of $Ca^{2+}$ to the rapid release of many vesicles and superimposition of the associated TICs. We evaluated this by mathematical modelling. Fig. 5a shows the capacitance change evoked in a representative β-cell following photorelease of caged $Ca^{2+}$. In this cell, a capacitance increase of 130 fF took place within the first 0.2 s after the flash of UV-light. This corresponds to the release of 45 LDCVs with a unitary capacitance increase of 2.9 fF. Exocytosis just after the flash is so rapid that the modelled events merge into what appears as a single large transient and that individual events superimposed on the large spike only become discernible when the current starts returning towards the baseline (compare Fig. 4b). Fig. 5b compares the time courses of the capacitance increase (red trace) and the cumulative $Q$ of the simulated response in Fig. 5a (black trace). The increase in membrane capacitance and cumulative $Q$ were half-maximal after 55 and 152 ms, respectively.

In Fig. 5c, the average changes in membrane capacitance ($\Delta C_m$) observed in a series of 9 cells not expressing $P2X_2Rs$ following a step elevation of $[Ca^{2+}]_i$ are shown (red trace). It is evident that there is a prompt increase in membrane capacitance of 170±23 fF, that the signal stabilizes at a new plateau within ~2 s and that there is no sign of ongoing exocytosis or endocytosis during the following 8 s. We compared the time courses of the increase in membrane capacitance with that of ATP released as reported by the TIC measurements. The black trace in Fig. 5d shows the integrated average charge ($\Sigma Q$) over the first 10 s after

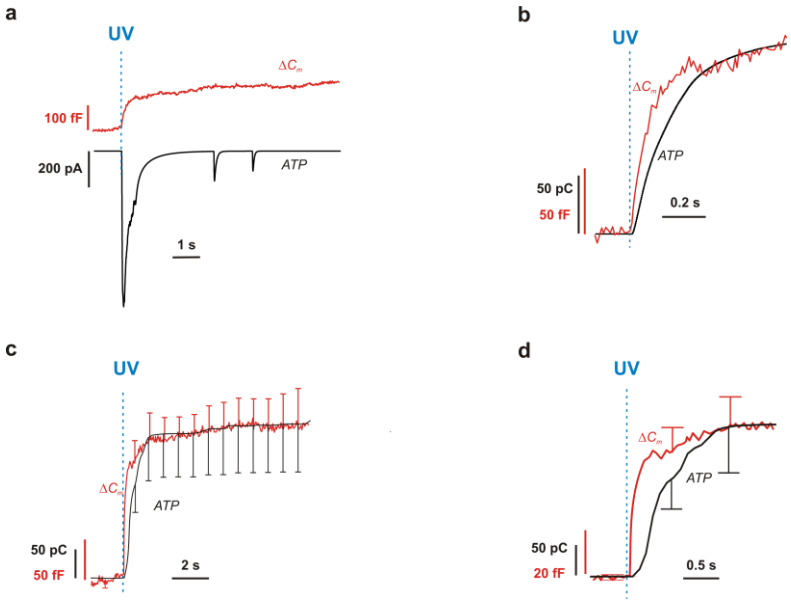


**Fig. 5.** Time course of ATP release and association with capacitance increase. a Predicted time course of ATP release (black trace) following photorelease of caged $Ca^{2+}$ based on a capacitance increase of 130 fF with a $t_{½}$ of 55 ms (red trace). **b** Comparison of time courses of capacitance increase (red trace) and cumulative TIC charge for modelled ATP trace in panel a. **c** Cumulative charge of TICs of the five cells shown in Fig. 4a-b (black) superimposed on the mean capacitance increase in untransfected cells (red). For clarity, error bars (S.E.M.) are only shown for every 20 (capacitance) and 3500 (charge) points. **d** Same data as in c but the first 2 s shown on an expanded time bases.

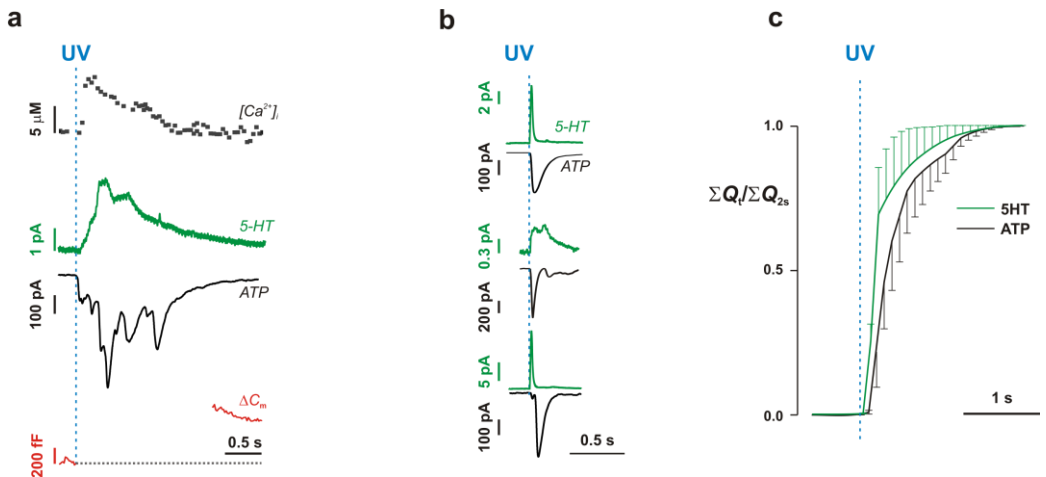


**Fig 6.** $Ca^{2+}$-evoked exocytosis monitored by 5-HT amperometry, ATP release and capacitance measurements. **a** Increase in $[Ca^{2+}]_i$ (top), amperometric transients (2nd from top), associated TICs (3rd from top) and change in membrane capacitance (*bottom*) recorded from a rat β-cell following photorelease of caged $Ca^{2+}$ by a flash of UV-light (dashed vertical line). Note that the capacitance measurements are not shown during the TICs to remove artefactual capacitance transients. **b** Similar type of recordings from another 3 cells showing. Only amperometric and TIC measurements are shown for clarity. **c** Average normalized integrated amperometric (green) and TIC charge (black) of the 4 experiments shown in a-b. Responses have been normalized to the charge recorded during the first 2 s. For clarity, error bars (S.E.M.) are only shown for every 500 points.

photoliberation of $Ca^{2+}$ in the five cells shown in Fig. 4a-b. It can be seen that both $\Delta C_m$ and $\Sigma Q$ plateau within ~2 s and then remained stable. Fig. 5d shows the responses evoked by the flash on an expanded time base. Whereas $\Sigma Q$ (reflecting ATP release) was half-maximal after 347±168 ms (n=5), the corresponding value was 59±5 ms (n=9) for $\Delta C_m$.

### Parallel measurements of exocytosis using amperometry, $P2X_2Rs$ and capacitance measurements

We examined the correlation between the capacitance increase and the release of ATP and the LDCV marker 5-HT. Fig. 6a shows an example where elevation of $[Ca^{2+}]_i$ to ~10 μM evoked a large capacitance increase (~700 fF), a prominent and protracted amperometric response and a series of TICs with a total charge of 416 pC. The responses in this cell are atypically large; the average capacitance increase and integrated TIC evoked by photoliberation of $Ca^{2+}$ in this series of experiments averaged 204±72 fF and 239±57 pC (n=8), respectively. Fig. 6b shows parallel amperometric and TIC recordings of the same type in another 3 cells. Finally, in Fig. 6c, the average time courses of 5-HT and ATP release are compared in the 4 cells shown in Fig. 6a-b. In these cells, the integrated amperometric response and TIC were half-maximal at 141±128 ms and 296±137 ms (n=4), respectively.

## Discussion

Here we have used adenoviral infection of rat pancreatic β-cells to induce expression of a high density of ATP-sensitive $P2X_2Rs$ in the plasma membrane to measure ATP release. Our technique is related to the "sniffer cell"-approach, also based on $P2X_2$ receptors, used previously by [28] with the difference that the β-cell releasing ATP is used as its own "sniffer" cell. An advantage of this method over amperometry is that exocytosis can be monitored in the entire cell whereas amperometry only detects secretion in the 30-50% of the area adjacent to the carbon fibre [23]. We have used this protocol to address two important questions in β-cell exocytosis. First, is ATP exclusively released by exocytosis of LDCVs? Second, how much of the depolarization-evoked exocytotic responses reported by capacitance measurements reflect fusion of LDCVs?

**ATP is released by exocytosis of vesicles that also accumulate 5-HT**

Fluorescence microscopy, autoradiography, electron microscopy and ultrastructural histochemistry indicate that 5-HT accumulates in insulin-containing secretory vesicles of the β-cell during preloading [29-31]. The validity of amperometry to study exocytosis of insulin-containing granules has been demonstrated [8]. Even if 5-HT accumulated in the SVs, the currents that would result from exocytosis of SVs loaded with the amine would be expected to be very small given the small volume of these vesicles (2% of that of an insulin granule as predicted from the diameters of 90 nm and 330 nm; [6]). There is a good correlation between 5-HT and ATP release and 92% of the events detected by amperometry were paralleled by a TIC. The fact that not all amperometric events are associated with ATP release can be explained by uneven loading of the vesicles with ATP and/or insufficient expansion of the fusion pore to allow the exit of ATP which is bigger than 5-HT. The latter possibility is suggested by analysis of the pedestals that sometimes precede full fusion and that are believed to reflect release via fusion pore. Although pedestals are observed in both amperometry and TIC recordings, their relative amplitude is much smaller during the latter type of measurements [23].

The parallel recordings of ATP and 5-HT release suggested the existence of a population of small TICs that did not associate with detectable co-release of serotonin (Fig. 3). It may be argued that these events reflect exocytosis of SVs that do not accumulate 5-HT. However, we do not think this is the case but rather a consequence of the lower resolution of amperometry: some events associated with the release of 5-HT will not be detected by the carbon fibre because they are too small and/or occur too far away from the carbon fibre. Indeed, when the distribution was corrected for the greater sensitivity of the $P2X_2R$-based technique and diffusional loss of 5-HT, a better agreement of the distributions was obtained. Collectively, these data argue that ATP and 5-HT are released by exocytosis of the same type of vesicles and that these are the insulin-containing LDCVs. It therefore appears that ATP should represent a good endogenous marker of insulin granule exocytosis that, unlike 5-HT, does not have to be preloaded into the cells.

**Sensitivity of the $P2X_2R$-based method for detection of exocytosis**

The smallest TICs we resolved had a peak amplitude as small as 3.2 pA. Under the conditions used in these experiments, the $P2X_2R$ single-channel amplitude is ~1 pA [24]. Thus, the smallest events involve the activation of only a few $P2X_2Rs$. It is of interest that the rise times for the smallest events are as short as for larger events (Fig. 2b). This argues that they reflect local release of ATP and rapid opening of $P2X_2Rs$ and that their activation does not involve diffusion over long distances. The smallest event observed had a charge of 33 fC, 0.7% of the mean charge (4.3 pC). Pancreatic β-cells contain 4 fmol of ATP per cell [22] of which 30% is stored in the ~10,000 insulin-containing secretory granules [14]. Thus, the ATP content per granule is 0.12 amol ($1.2 * 10^{-19}$ mol). Combining these values suggest that our technique can detect the release of $0.85 \times 10^{-21}$ mol of ATP (~500 molecules). This would correspond to an intravesicular concentration of 0.2 mM in an SV with a diameter of 90 nm and a volume of 0.4 al. This is several orders of magnitude lower than the estimated ATP concentration in classical synaptic vesicles [17]. This argues that our technique should have sufficient sensitivity to detect any SV-mediated ATP release in β-cells.

**Do SVs contribute to the observed capacitance increases?**

If the total number of SVs and LDCVs undergoing exocytosis are equivalent to *a* and *b*, respectively, the total charge (*Q*) of the

ATP-evoked current and increase in membrane capacitance ($\Delta C_m$) are given by the equations

$$\begin{cases} \Delta C_m = c_{m,SV} \cdot a + c_{m,LDCV} \cdot b & (1) \\ Q = q_{SV} \cdot a + q_{LDCV} \cdot b & (2) \end{cases}$$

Single-vesicle capacitance increases for SVs ($c_{m,\,SV}$) and LDCVs ($c_{m,\,LDCV}$) average 0.2 fF and 2.9 fF, respectively [7]. Whereas the unitary charge of the current associated with the ATP release during exocytosis of an LDCV ($q_{LDCV}$) is ~4.3 pC (Figs. 2a and 4a), the unitary charge evoked by ATP release due to exocytosis of SVs ($q_{SV}$) is not known. We therefore consider three possibilities: 1) SVs contain no ATP at all (i.e. $q_{SV}=0$); 2) SVs contain ATP at the same concentration as the LDCVs but because the volume of an SV is only 2% of the LDCVs, the amount of ATP released during SV exocytosis will be correspondingly reduced (i.e. $q_{SV}=0.02*q_{LDCV}$); and 3) SVs contain ATP at a ~50-fold higher concentration than the LDCVs so that exactly the same amount of ATP is delivered during exocytosis of SVs and LDCVs ($q_{SLMV}=q_{LDCV}$). We point out that cases (1) and (3) are consistent with the single peak in the amplitude distribution (Fig. 2a) and the rise times being constant for a wide range of TIC amplitudes (cf. [32]). However, case (2) is not supported by the experimental data. If SVs contained ATP at the same concentration as the LDCVs and if they are released at a rate comparable to that of the LDCVs as suggested by on-cell capacitance measurements [7], then a second peak should appear at 3.6-4.5 $fC^{1/3}$ in the histogram shown in Fig. 2a. However, no such peak was observed. Likewise, the analysis of the rise times provided no evidence for two distinct release pathways characterized by different time courses for ATP release as would be expected for vesicles with widely different diameters [32].

With the experimentally observed values of $\Delta C_m$ and $Q$ (105 fF and 139 pC), solving Eqs. 1 and 2 yields values for $b$ and $a$ of 32 and 56 for case 1 ($q_{SV}=0$), 30 and 87 for case 2 ($q_{SV}=0.02q_{LDCV}$) and 36 and 0 for case 3 ($q_{SV}=q_{LDCV}$). These values indicate that exocytosis of LDCV accounts for >95% of the ATP release and >85% of the observed capacitance increases. The conclusion that the capacitance changes and TICs principally reflect exocytosis of LDCVs is also consistent with the previous finding that the capacitance increase per TIC is ~3 fF [21]. The fact that a similar capacitance increase per event (3.5 fF; Fig. 4c) can be estimated from the relationship between charge and capacitance increase in the experiments involving photorelease of caged $Ca^{2+}$ provides further support of this idea.

The above analysis depends critically on the accuracy of the capacitance measurements. Changes in cell capacitance reflect the balance between the insertion of membrane during exocytosis and its recapture by endocytosis. Endocytosis is triggered with a delay after exocytosis and operates at much lower rate than exocytosis [33]. Several precautions were taken to minimise potential confounding effects of endocytosis. First, $\Delta C_m$ was measured as soon as the TICs had returned to the baseline. Second, we used moderate stimulus (peak $[Ca^{2+}]_i$ ~ 5 µM). Indeed, the capacitance measurements showed little sign of endocytosis and $\Delta C_m$ attained a new and stable plateau within ~1 s where it subsequently remained for at least 9 s. The integrated TIC charge likewise increased to a plateau within 1 s and there was no sign of ongoing exocytosis during the subsequent 9 s. These observations suggest that $\Delta C_m$ is not masked by ongoing endocytosis and that we accordingly do not underestimate the true extent of exocytosis.

**Temporal dissociation between capacitance increase and ATP release**

Interestingly, there was a 300 ms delay between $\Delta C_m$ and $\Sigma Q$ (Fig. 5b). There is a simple explanation to this delay. Whereas the capacitance increase occurs almost instantaneously upon exocytosis, the $P2X_2R$ currents activate with some delay (~5 ms; Fig. 2b) upon exposure to ATP and then decay exponentially as the agonist diffuses away from the release site. Thus, $\Sigma Q$ will plateau once the channels have deactivated and this may, depending on the amplitude and time course of the exocytotic response, take several hundred milliseconds (see Fig. 5d). Thus, it is only natural that the integrated current lags

behind $\Delta C_m$ and the dissociation is therefore not indicative of the exocytosis of vesicles containing or lacking ATP.

**Comparison with previous work**

We acknowledge that the low rate of SV exocytosis suggested by our analysis contrasts with data obtained by two-photon extracellular polar-tracer image quantification which suggest release rates as high as 4000 SVs (20% increase in FM1-43 fluorescence in 0.3 s) [34]; i.e. ~45-fold higher than the rate we observe (maximally 87 SVs over ~550 ms as in case 2 above). The functional significance of SV exocytosis is unclear. Although it was originally believed that they could mediate GABA release [5], more recent analysis suggests that most exocytotic release of GABA principally occurs during release of the insulin granules [23]. The present data also appear to exclude a role of the SVs in ATP release. The identity of the compound released during SV exocytosis (if any) therefore remains to be determined. It is even possible that SV exocytosis does not at all subserve a function in the export of molecules into the islet interstitium. Instead, rapid exo- and endocytosis of SV may provide the β-cell with a means of dynamic regulation of the cell's surface area or a mechanism for insertion of essential transmembrane proteins into the plasma membrane. Yet another possibility is that it is part of a membrane repair reaction [35]. Further work combining measurements of exocytosis by capacitance and TIC measurements with optical imaging of exocytosis are likely to be helpful in the exploration of these questions.

## Materials and methods

**Adenovirus construction**

Ad$P2X_2R$-GFP was created using Adeno-X$^{TM}$ Expression system (BD Biosciences Clontech, Erembodegem, Belgium). In short, cDNA encoding the rat $P2X_2R$ linked to GFP (kindly provided by B.S. Khakh, Cambridge, UK) was subcloned into a pShuttle vector. The expression cassette was then excised using PI-*Sce* and I-*Ceu* I and ligated into pAdeno-X, and the resulting adenoviral DNA was transfected into HEK293 cells for harvesting.

**β-cell preparation and infection**

Pancreatic islets were isolated from Sprague-Dawley or Wistar rats. The animals were sacrificed by $CO_2$ inhalation (slowly increasing the concentration of $CO_2$). The pancreas was quickly excised and pancreatic islets were isolated by collagenase digestion. The islets thus obtained were dissociated into single cells by trituration in $Ca^{2+}$-free, and the resulting cell suspension was plated on Petri dishes. The cells were maintained in tissue culture for up to 2 days in RPMI 1640 medium (10 mM glucose; Gibco BRL) supplemented with 10% FCS, 100 μg/ml streptomycin, and penicillin (100 i.u./ml). The β-cells were infected with the adenoviral construct of $P2X_2R$-GFP once they had attached to the bottom of the culture dish. Four to six hours after infection, the culture medium was replaced with fresh medium without the virus. The cells were used for experimental analysis 24-36 h after infection.

**Solutions**

During the experiment, the cells were continuously superfused with extracellular solution containing (mM) 138 NaCl, 5.6 KCl, 2.6 $CaCl_2$, 1.2 $MgCl_2$, 5 HEPES, 5 D-glucose. The pH of the medium was adjusted to 7.4 with NaOH. The osmolarity of the medium was ~290 mOsm. In the experiments in which exocytosis was triggered by intracellular dialysis, the 0.2 μM $[Ca^{2+}]_i$ media contained (mM) 110 Cs-glutamate (110 glutamic acid + 110 CsOH), 10 KCl, 10 NaCl, 1 $MgCl_2$, 3 MgATP, 0.1 cAMP, 5 HEPES, 5 $CaCl_2$ and 10 EGTA, whereas the ~2 μM $[Ca^{2+}]_i$ buffer consisted of (mM) 3 Mg-ATP, 1 $MgCl_2$, 0.1 cAMP, 10 HEPES, 120 Cs-glutamate, 10 KCl, 10 NaCl, 5 HEDTA, 0.57 $CaCl_2$. In all cases, pH was adjusted to 7.1 using CsOH. The free $Ca^{2+}$ concentration was estimated using the MAXC32 software (http://www.stanford.edu/~cpatton/maxc.html).

**Electrophysiology**

Patch electrodes (4-7 MΩ resistance when filled with the pipette solution) were pulled from borosilicate glass capillaries (Hilgenberg, Malsfeld, Germany). The electrodes were coated with Sylgard close to the tips and fire-polished. The electrophysiological measurements were made using an EPC-10 patch clamp amplifier and Pulse 8.51 software (Heka Elektronik, Lamprecht/Pfalz, Germany). All experiments were conducted using the standard whole-cell configuration at ~+34°C. The cells were voltage-clamped at -70 mV to prevent activation of voltage-gated $Ca^{2+}$ channels. Exocytosis was elicited by $Ca^{2+}$ infusion through patch electrode or by photorelease of caged $Ca^{2+}$ and the changes of capacitance caused by the fusion of secreted vesicles with the cell membrane was detected using Sine+DC method of the Pulse Lockin module. The measurements were made using an EPC-10 patch clamp amplifier and Pulse 8.51 software (Heka Elektronik, Lambrecht/Pfalz, Germany). The ATP-activated currents were filtered at 3.33 kHz and digitized at 10 kHz. When ATP release measurements were combined with recordings of membrane capacitance, the current transients were (for display purposes) filtered at 100 Hz to remove the current noise that results from the sine wave appled to measure membrane capacitance. ATP was applied using a nanoliter injector (Nanoliter 2000, World Precision Instruments, USA) with a speed of 23 nl/s. The total volume applied was 50.6 nl. All experiments were conducted on isolated β-cells far away from neighbours to ensure that currents measured reflect events in the patch-clamped cell only. In addition, the extracellular medium contained a low (5 mM) glucose concentration to prevent spontaneous action potential firing (and exocytosis) in the non-clamped cells. Successfully infected cells were identified by the presence of GFP fluorescence.

**Amperometry**

For amperometry, β-cells were loaded with serotonin by adding 0.5 mM 5-HT and 0.5 mM 5-HTP (both from Sigma, St Louis, MO, USA) to the cell culture >4 h before the experiment. A carbon fibre (tip diameter 5 μm; ProCFE, Dagan Corp., Minneapolis, MN, USA) was connected to the second headstage of an EPC-9/2 amplifier (Heka Elektronik, Lambrecht, Germany) and held at +650 mV; the other headstage was used for the measurements of ATP release and membrane capacitance. The carbon fibre was positioned in the immediate vicinity of the β-cell. The amperometric currents were filtered at 0.3 kHz and digitized at 1 kHz. The events were identified by visual inspection of the recording. Their amplitude typically was >4-fold higher than the background noise level. UV-illumination was gave rise to transient current artefacts that we removed off-line by subtraction of the responses obtained after removal of the cell from the visual field from the responses obtained during stimulation of exocytosis.

**Photorelease of caged $Ca^{2+}$ and $[Ca^{2+}]_i$ measurements**

Photolysis of the $Ca^{2+}$-NP-EGTA complex was effected by brief (~1 ms) flashes of UV-light produced by an JML-C2 flash photolysis apparatus (Rapp OptoElectronic, Hamburg, Germany). Photolysis was in most cases effected via the objective with the help of a custom-made spot illumination adaptor (Rapp OptoElectronic,) mounted on an Axiovert 200 microscope (Carl Zeiss, Goettingen, Germany). For these experiments, the cells were plated on quartz glass coverslips (UQG Optics, Cambridge, UK) to minimise loss of UV-light. The intracellular buffer for flash photolysis experiments contained (mM) 110 CsCl, 10 KCl, 10 NaCl, 2 $CaCl_2$, 1 $MgCl_2$, 25 HEPES, 3 MgATP, 0.1 cAMP, 3 NP-EGTA (*o*-nitrophenyl EGTA, tetrapotassium salt; Synaptic Systems GmbH, Goettingen, Germany) and 0.05 of the fluorescent low-affinity $Ca^{2+}$-indicator Fura-FF (Invitrogen). The measurements were made using an epifluorescence imaging system (PTI Fluorescent Master Systems, New Jersey, USA). The excitation and emission wavelengths used for Fura-FF were 340/380 and >505 nm respectively. To convert the fluorescence ratio into $[Ca^{2+}]_i$, the minimum ratio was determined at basal $[Ca^{2+}]_i$ for each

experiment. The maximum ratio was recorded immediately after rupturing the cell, by briefly clamping the membrane voltage to +500 mV. The $K_d$ for the binding of $Ca^{2+}$ to Fura-FF was assumed as 5.5 µM. (http://probes.invitrogen.com/).

**Correction of histograms for diffusion of ATP**

The $P2X_2$ receptor-based technique we have used in this study allows detection of exocytosis over the entire cell surface. By contrast, amperometry principally detects exocytosis in the close vicinity to the carbon fibre and both the time course and amplitude of events occurring in other parts of the cell will be distorted by diffusion (Fig. 1a). This complicates the comparison of histograms that include all ATP-dependent transient inward currents (TICs) with those that only include events that associated with co-release of 5-HT as detected by amperometry (Fig. 3). Inevitably, small events will be filtered out with a resultant selection bias towards larger events.

The attenuation and delay of amperometric events caused by the diffusion of released molecules to the carbon fibre have previously been analyzed in detail by Haller et al [12] using Monte Carlo methods. We used the results presented in Table 1 of that study and the original distribution of all ATP-dependent TICs (grey bars in Fig. 3b) to predict the distribution had the events instead been detected by an ATP-sensitive amperometric sensor detecting ATP in only part of the cell. To this end, the observed TICs were randomly assigned to 11 classes of release sites taking into account probabilities for events to happen at these sites (probabilities and classes of events as in [12]). The events were then scaled for the charge lost due to diffusion and their amplitudes corrected according to expected calculated half-widths. In this step it was assumed that the current transient can be approximated by an exponential with an area below it equal to a product of the spike amplitude and the half-width of the spike. Then all original events were sorted in descending order according to corrected amplitudes. Finally, the histogram of ATP events that should be detected by the carbon fibre was constructed from the *n* first sorted events, where *n* is the number of ATP events that coincide with amperometric transients. The remaining events obviously were of an amplitude below the detection level of the equipment used and were not included in the corrected histogram.

**Mathematical simulation of ATP release**

A unitary spike (amplitude ~100 pA with a rise time of 5 ms and a half-width of 18 ms) was used to simulate the current response elicited by ATP release following photorelease of caged $Ca^{2+}$ and stimulation of exocytosis. Experimentally observed spikes vary in size and kinetics. Therefore, the amplitude and half-width of the spikes were varied between 50-200 pA and 16-22 ms, respectively. Following the UV-flash and the stimulation of exocytosis, 45 granules (corresponding to a capacitance increase of 130 fF) were released at exponentially increasing times with a $t_{½}$ of 55 ms.

**Data analysis and statistical evaluation**

The current transients were analyzed using the Mini Analysis Program 6.0.3 (Synaptosoft, USA) to determine the peak amplitude, charge and rise time (10-90% of the amplitude). An event was identified as an excursion from the baseline 3 times the RMS noise (on average 2±1 pA; n=25).

The magnitude of an event (determined as the charge *q* of the current resulting from an exocytotic event) will depend on the amount of ATP released. The latter parameter is given by the product of the intragranular concentration of ATP and the volume of the granule (i.e. $4\pi r^3/3$). Electron microscopy has established that the radii of both the SVs and LDCVs are normally distributed [6]. The cubic root of the charge should also be normally distributed and the data are accordingly presented as $\sqrt[3]{q}$ in Figs. 1-3. The ATP concentration within the vesicles is also likely to be normally distributed but the product of two normal distributions (i.e. the ATP content and thus $\sqrt[3]{q}$) remains a normal distribution although the spread (coefficient of variation) will be greater.

Unless otherwise indicated, data are quoted as mean values ± S.E.M. of indicated number of experiments. Statistical significances for the observed differences were evaluated by Student's *t*-test.

## Acknowledgements

We thank Dr Baljit S. Khakh for generously providing the $P2X_2$-GFP construct and Financial support was obtained from the Wellcome Trust, the European Union (LSHB-CT-2004-005137 and LSHM-CT-2006-518153). PR is a Wolfson-Royal Society Merit Award Research Fellow.

## References

1. Wightman RM, Jankowski JA, Kennedy RT, Kawagoe KT, Schroeder TJ, Leszczyszyn DJ, Near JA, Diliberto EJ, Jr., Viveros OH (1991) Temporally resolved catecholamine spikes correspond to single vesicle release from individual chromaffin cells. Proc Natl Acad Sci U S A 88:10754-8 DOI Electronic Resource Number

2. Chow RH, Klingauf J, Neher E (1994) Time course of Ca2+ concentration triggering exocytosis in neuroendocrine cells. Proc Natl Acad Sci U S A 91:12765-9 DOI Electronic Resource Number

3. Kasai H (1999) Comparative biology of Ca2+-dependent exocytosis: implications of kinetic diversity for secretory function. Trends Neurosci 22:88-93 DOI Electronic Resource Number

4. Rorsman P, Renstrom E (2003) Insulin granule dynamics in pancreatic beta cells. Diabetologia 46:1029-45 DOI Electronic Resource Number

5. Reetz A, Solimena M, Matteoli M, Folli F, Takei K, De Camilli P (1991) GABA and pancreatic beta-cells: colocalization of glutamic acid decarboxylase (GAD) and GABA with synaptic-like microvesicles suggests their role in GABA storage and secretion. Embo J 10:1275-84 DOI Electronic Resource Number

6. Braun M, Wendt A, Birnir B, Broman J, Eliasson L, Galvanovskis J, Gromada J, Mulder H, Rorsman P (2004) Regulated exocytosis of GABA-containing synaptic-like microvesicles in pancreatic beta-cells. J Gen Physiol 123:191-204 DOI Electronic Resource Number

7. MacDonald PE, Braun M, Galvanovskis J, Rorsman P (2006) Release of small transmitters through kiss-and-run fusion pores in rat pancreatic beta cells. Cell Metab 4:283-90 DOI Electronic Resource Number

8. Aspinwall CA, Huang L, Lakey JR, Kennedy RT (1999) Comparison of amperometric methods for detection of exocytosis from single pancreatic beta-cells of different species. Anal Chem 71:5551-6 DOI Electronic Resource Number

9. Smith PA, Duchen MR, Ashcroft FM (1995) A fluorimetric and amperometric study of calcium and secretion in isolated mouse pancreatic beta-cells. Pflugers Arch 430:808-18 DOI Electronic Resource Number

10. Bokvist K, Holmqvist M, Gromada J, Rorsman P (2000) Compound exocytosis in voltage-clamped mouse pancreatic beta-cells revealed by carbon fibre amperometry. Pflugers Arch 439:634-45 DOI Electronic Resource Number

11. Smith PA, Proks P, Ashcroft FM (1999) Quantal analysis of 5-hydroxytryptamine release from mouse pancreatic beta-cells. J Physiol 521 Pt 3:651-64 DOI Electronic Resource Number

12. Haller M, Heinemann C, Chow RH, Heidelberger R, Neher E (1998) Comparison of secretory responses as measured by membrane capacitance and by amperometry. Biophys J 74:2100-13 DOI Electronic Resource Number

13. Becherer U, Pasche M, Nofal S, Hof D, Matti U, Rettig J (2007) Quantifying exocytosis by combination of membrane capacitance measurements and total internal reflection fluorescence microscopy in chromaffin cells. PLoS ONE 2:e505 DOI Electronic Resource Number

14. Detimary P, Jonas JC, Henquin JC (1996) Stable and diffusible pools of nucleotides in pancreatic islet cells. Endocrinology 137:4671-6 DOI Electronic Resource Number

15. Hutton JC, Penn EJ, Peshavaria M (1983) Low-molecular-weight constituents of isolated insulin-secretory granules. Bivalent cations, adenine nucleotides and inorganic phosphate. Biochem J 210:297-305 DOI Electronic Resource Number

16. Leitner JW, Sussman KE, Vatter AE, Schneider FH (1975) Adenine nucleotides in the secretory granule fraction of rat islets. Endocrinology 96:662-77 DOI Electronic Resource Number

17. Pankratov Y, Lalo U, Verkhratsky A, North RA (2006) Vesicular release of ATP at central synapses. Pflugers Arch 452:589-97 DOI Electronic Resource Number

18. Khakh BS, Bao XR, Labarca C, Lester HA (1999) Neuronal P2X transmitter-gated cation channels change their ion selectivity in

seconds. Nat Neurosci 2:322-30 DOI Electronic Resource Number
19. MacDonald PE, Obermuller S, Vikman J, Galvanovskis J, Rorsman P, Eliasson L (2005) Regulated exocytosis and kiss-and-run of synaptic-like microvesicles in INS-1 and primary rat beta-cells. Diabetes 54:736-43 DOI Electronic Resource Number
20. Obermuller S, Lindqvist A, Karanauskaite J, Galvanovskis J, Rorsman P, Barg S (2005) Selective nucleotide-release from dense-core granules in insulin-secreting cells. J Cell Sci 118:4271-82 DOI Electronic Resource Number
21. Braun M, Wendt A, Karanauskaite J, Galvanovskis J, Clark A, MacDonald PE, Rorsman P (2007) Corelease and differential exit via the fusion pore of GABA, serotonin, and ATP from LDCV in rat pancreatic beta cells. J Gen Physiol 129:221-31 DOI Electronic Resource Number
22. Detimary P, Dejonghe S, Ling Z, Pipeleers D, Schuit F, Henquin JC (1998) The changes in adenine nucleotides measured in glucose-stimulated rodent islets occur in beta cells but not in alpha cells and are also observed in human islets. J Biol Chem 273:33905-8 DOI Electronic Resource Number
23. Braun M, Wendt A, Karanauskaite J, Galvanovskis J, Clark A, Macdonald PE, Rorsman P (2007) Corelease and Differential Exit via the Fusion Pore of GABA, Serotonin, and ATP from LDCV in Rat Pancreatic {beta} Cells. J Gen Physiol 129:221-31 DOI Electronic Resource Number
24. Ding S, Sachs F (1999) Single channel properties of P2X2 purinoceptors. J Gen Physiol 113:695-720 DOI Electronic Resource Number
25. Whitlock A, Burnstock G, Gibb AJ (2001) The single-channel properties of purinergic P2X ATP receptors in outside-out patches from rat hypothalamic paraventricular parvocells. Pflugers Arch 443:115-22 DOI Electronic Resource Number
26. Pethig R, Jakubek LM, Sanger RH, Heart E, Corson ED, Smith PJ (2005) Electrokinetic measurements of membrane capacitance and conductance for pancreatic beta-cells. IEE Proc Nanobiotechnol 152:189-93 DOI Electronic Resource Number
27. Taschenberger H, Juttner R, Grantyn R (1999) Ca2+-permeable P2X receptor channels in cultured rat retinal ganglion cells. J Neurosci 19:3353-66 DOI Electronic Resource Number
28. Hazama A, Hayashi S, Okada Y (1998) Cell surface measurements of ATP release from single pancreatic beta cells using a novel biosensor technique. Pflugers Arch 437:31-5 DOI Electronic Resource Number
29. Ekholm R, Ericson LE, Lundquist I (1971) Monoamines in the pancreatic islets of the mouse. Subcellular localization of 5-hydroxytryptamine by electron microscopic autoradiography. Diabetologia 7:339-48 DOI Electronic Resource Number
30. Hellman B, Lernmark A, Sehlin J, Taljedal IB (1972) Transport and storage of 5-hydroxytryptamine in pancreatic -cells. Biochem Pharmacol 21:695-706 DOI Electronic Resource Number
31. Owman C, Hakanson R, Sundler F (1973) Occurrence and function of amines in endocrine cells producing polypeptide hormones. Fed Proc 32:1785-91 DOI Electronic Resource Number
32. Bruns D, Riedel D, Klingauf J, Jahn R (2000) Quantal release of serotonin. Neuron 28:205-20 DOI Electronic Resource Number
33. Eliasson L, Proks P, Ammala C, Ashcroft FM, Bokvist K, Renstrom E, Rorsman P, Smith PA (1996) Endocytosis of secretory granules in mouse pancreatic beta-cells evoked by transient elevation of cytosolic calcium. J Physiol 493 ( Pt 3):755-67 DOI Electronic Resource Number
34. Hatakeyama H, Takahashi N, Kishimoto T, Nemoto T, Kasai H (2007) Two cAMP-dependent pathways differentially regulate exocytosis of large dense-core and small vesicles in mouse beta-cells. J Physiol 582:1087-98 DOI Electronic Resource Number
35. Togo T, Alderton JM, Steinhardt RA (2000) The mechanism of cell membrane repair. Zygote 8 Suppl 1:S31-2 DOI Electronic Resource Number

Published February 12, 2007



# Corelease and Differential Exit via the Fusion Pore of GABA, Serotonin, and ATP from LDCV in Rat Pancreatic β Cells

Matthias Braun,[1] Anna Wendt,[2] Jovita Karanauskaite,[1] Juris Galvanovskis,[1] Anne Clark,[1] Patrick E. MacDonald,[1] and Patrik Rorsman[1]

[1]Oxford Centre for Diabetes, Endocrinology, and Metabolism, University of Oxford, Churchill Hospital, Oxford OX3 7LJ, UK
[2]Department of Clinical Sciences, Clinical Research Centre, Lund University, 20502 Malmö, Sweden

The release of γ-aminobutyric acid (GABA) and ATP from rat β cells was monitored using an electrophysiological assay based on overexpression $GABA_A$ or $P_2X_2$ receptor ion channels. Exocytosis of LDCVs, detected by carbon fiber amperometry of serotonin, correlated strongly (∼80%) with ATP release. The increase in membrane capacitance per ATP release event was 3.4 fF, close to the expected capacitance of an individual LDCV with a diameter of 0.3 μm. ATP and GABA were coreleased with serotonin with the same probability. Immunogold electron microscopy revealed that ∼15% of the LDCVs contain GABA. Prespike "pedestals," reflecting exit of granule constituents via the fusion pore, were less frequently observed for ATP than for serotonin or GABA and the relative amplitude (amplitude of foot compared to spike) was smaller: in some cases the ATP-dependent pedestal was missing entirely. An inward tonic current, not dependent on glucose and inhibited by the $GABA_A$ receptor antagonist SR95531, was observed in β cells in clusters of islet cells. Noise analysis indicated that it was due to the activity of individual channels with a conductance of 30 pS, the same as expected for individual $GABA_A$ $Cl^-$ channels with the ionic gradients used. We conclude that (a) LDCVs accumulate ATP and serotonin; (b) regulated release of GABA can be accounted for by exocytosis of a subset of insulin-containing LDCVs; (c) the fusion pore of LDCVs exhibits selectivity and compounds are differentially released depending on their chemical properties (including size); and (d) a glucose-independent nonvesicular form of GABA release exists in β cells.





## INTRODUCTION

Like neurons, many endocrine cells contain two classes of secretory vesicles. Large dense-core vesicles (LDCVs) contain peptide hormones, whereas the small synaptic-like microvesicles (SLMVs), store low molecular weight neurotransmitters (Kasai, 1999). In addition to insulin, pancreatic β-cell LDCVs accumulate a variety of low molecular weight substances, including ATP (Hutton, 1989) and serotonin (Ekholm et al., 1971). SLMVs in β cells are believed to contain γ-aminobutyric acid (GABA) (Reetz et al., 1991). $GABA_A$ (Rorsman et al., 1989; Wendt et al., 2004), $GABA_B$ receptors (Braun et al., 2004b), as well as purinergic receptors (Salehi et al., 2005) have been identified in islets of Langerhans. This suggests that GABA and ATP, released by regulated exocytosis from the β-cell, can serve as paracrine/autocrine regulators.

Exocytosis of LDCVs from pancreatic β cells is firmly established (for reviews see Barg, 2003; Tsuboi and Rutter, 2003). Little is known, however, about the release of SLMVs. Recently, high-resolution on-cell capacitance measurements have provided evidence that β-cell SLMVs are capable of regulated $Ca^{2+}$-dependent exocytosis (Macdonald et al., 2005). However, the identities of the molecules that are released during exocytosis of LDCVs and SLMVs have not been established conclusively. Using a technique based on the infection of β cells with $GABA_A$ receptor ion channels, we have recently reported depolarization-induced quantal release of GABA (Braun et al., 2004a). A similar approach, based on the overexpression of $P_2X_2$ receptor cation channels, can be applied to study exocytotic release of adenine nucleotides (Hollins and Ikeda, 1997) and has been successfully applied to insulin-secreting cells (Hazama et al., 1998; Obermüller et al., 2005; MacDonald et al., 2006). Based on reports that GAD65, the enzyme involved in GABA synthesis, associated with SLMVs in β cells (Reetz et al., 1991) and evidence for transmembrane transport of GABA in SLMV-enriched subcellular fractions (Thomas-Reetz et al.,1993), we postulated that the observed release of GABA was attributable to exocytosis of SLMVs although the amplitude distribution differed somewhat from that expected for exocytosis of SLMVs (Braun et al., 2004a). Moreover, contrary to our expectations (Kasai, 1999; Bruns et al., 2000), the properties of GABA release detected with this method were remarkably similar to those of LDCV exocytosis

M. Braun and A. Wendt contributed equally to this work.
Correspondence to Matthias Braun: matthias.braun@drl.ox.ac.uk
P.E. MacDonald's present address is Department of Pharmacology, University of Alberta, Edmonton T6G 2E1, Canada.

Abbreviations used in this paper: GABA, γ-aminobutyric acid; LDCV, large dense-core vesicle; SLMV, synaptic-like microvesicle; TIC, transient inward current.

Published February 12, 2007

in terms of $[Ca^{2+}]_i$ dependence, regulation by cAMP, and kinetics of the individual events (Braun et al., 2004a). Recently, ultrastructural evidence has been presented suggesting that GABA is not only stored in the SLMVs but also the insulin-containing LDCVs (Gammelsaeter et al., 2004). If this is the case, exocytosis of the latter type of vesicles may thus also contribute to GABA release, but this aspect has so far not been explored. In addition, biochemical measurements suggest that GABA is released at a very high rate (25% of its content per hour) in a seemingly unregulated fashion (Smismans et al., 1997; Winnock et al., 2002). The relationship between this form of GABA release and that which we have documented previously remains unclear.

Here we have investigated exocytosis of LDCVs and SLMVs using rat β cells engineered to express ionotropic ATP and GABA receptors. These measurements were combined with amperometric detection of serotonin preloaded into pancreatic β cells, widely used as an insulin proxy (Kennedy et al., 1993). This approach enabled us to explore the extent to which these compounds are released by the same or distinct exocytotic pathways and to provide some insight into the nature of the unregulated form of GABA release from pancreatic β cells.

## MATERIALS AND METHODS

### Adenovirus Construction

*$AdP_2X_2$-GFP.* $AdP_2X_2$-GFP was created using the Adeno-X Expression system (BD Biosciences; CLONTECH Laboratories, Inc.). In short, cDNA encoding the rat $P_2X_2$ receptor linked to GFP (provided by B. Khakh, Cambridge, UK) was subcloned into pShuttle. The expression cassette was then excised using PI-Sce1 and I-CeuI and ligated into pAdeno-X and the resulting adenoviral DNA transfected into HEK293 cells. Viral titer was determined by counting the number of green fluorescent cells.

*$AdGABA_A\alpha1$ and $AdGABA_A\beta1$.* The construction of adenoviruses containing the human $GABA_A\alpha1$ subunit ($AdGABA_A\alpha1$) and the human $GABA_A\beta1$ subunit ($AdGABA_A\beta1$) has been described elsewhere (Braun et al., 2004a). $AdGABA_A\alpha1$ and $AdGABA_A\beta1$ were cotransfected to create functional $GABA_A$ receptors (Birnir et al., 1995).

### Islet Cell Preparation and Adenoviral Infection

Sprague Dawley rats were killed by inhalation of $CO_2$ followed by cervical dislocation. All experimental procedures involving animals were approved by the ethical committee in Lund, and experiments in the UK were performed according to a Schedule 1 procedure. After excision of the pancreas, islets were isolated by collagenase digestion and dispersed into single cells essentially as detailed elsewhere (Åmmälä et al., 1993). For amperometry (Figs. 3 and 4), 0.5 mM 5-HT and 0.5 mM 5-HTP (Sigma-Aldrich) were added to the cell culture >4 h before the electrophysiological experiments. The β-cells were infected with $AdP_2X_2$-GFP and/or $AdGABA_A\alpha1$ and $AdGABA_A\beta1$ at a concentration of 10–100 pfu/cell and used 24–48 h after infection.

### Electrophysiology

Patch pipettes were pulled from borosilicate glass, coated with Sylgard and fire polished. They had a tip resistance 3–6 MΩ when filled with the intracellular solutions. All electrophysiological measurements were performed using the standard whole-cell configuration of the patch-clamp technique. The recordings were performed using an EPC9 patch clamp amplifier (HEKA Electronics) and Pulse software (version 8.53, HEKA). β cells were identified based on their size (cell capacitance >5 pF) and the inactivation properties of the voltage-gated $Na^+$ current (Hiriart and Matteson, 1988; Göpel et al., 1999). In Fig. 2, exocytosis of LDCVs was detected as changes in cell capacitance estimated by the Lindau-Neher technique (Gillis, 1995) implementing the Sine + DC feature of the lock-in module of the pulse software.

### Amperometry

A carbon fiber electrode (tip diameter 5 μm; ProCFE, Dagan Corp.) was connected to the second headstage of an EPC-9/2 amplifier (HEKA) and held at +650 mV. The carbon fiber was positioned within 1 μm of the cell membrane during all experiments. The amperometric current was filtered at 333 Hz, digitized at 1 kHz, and digitally filtered at 100 Hz before analysis.

### Solutions

The standard extracellular solution consisted of (in mM) 118 NaCl, 20 TEACl, 5.6 KCl, 2.6 $CaCl_2$, 1.2 $MgCl_2$, 5 HEPES, and 5 glucose (pH 7.4, adjusted with NaOH). The pipette solution for $Ca^{2+}$ infusion experiments and amperometric measurements (Figs. 1, A and B; Figs. 3 and 4) contained (in mM) 138 CsCl, 1 $MgCl_2$, 10 HEPES, 3 MgATP, 0.1 cAMP, 5 HEDTA (pH 7.15 with CsOH), and 0.57 $CaCl_2$. The free $[Ca^{2+}]$ was estimated to be 2 μM. For simultaneous recording of ATP release and capacitance (Fig. 2), the pipette solution was composed of (in mM) 110 glutamate, 10 KCl, 10 NaCl, 1 $MgCl_2$, 3 MgATP, 0.1 cAMP, 5 HEPES, 6 $CaCl_2$, and 10 EGTA (pH 7.2 with CsOH; estimated free $[Ca^{2+}]$ 230 nM). The intracellular solution for recording first latencies (Fig. 1, C and D) contained (in mM) 125 Cs-glutamate, 10 CsCl, 10 NaCl, 1 $MgCl_2$, 5 HEPES, 50 μM EGTA, 3 MgATP, and 0.1 cAMP (pH 7.15 with CsOH). The simultaneous recording of GABA and ATP release (Fig. 5; Fig. S2, available online at http://www.jgp.org/cgi/content/full/jgp.200609658/DC1) was performed using a pipette solution consisting of 135 Cs-glutamate, 1 $MgCl_2$, 3 MgATP, 10 HEPES, 0.1 cAMP, 10 EGTA, and 5 $CaCl_2$ (pH 7.2 with CsOH). The total $[Cl^-]_i$ was 12 mM and the estimated free $[Ca^{2+}]_i$ was 0.16 μM. For measuring tonic activity of $GABA_A$ receptors (Fig. 6), the extracellular solution consisted of (in mM) 138 NaCl, 5.6 KCl, 2.6 $CaCl_2$, 1.2 $MgCl_2$, 5 HEPES, and 1 glucose (pH 7.4 with NaOH), and the pipette solution contained 120 CsCl, 1 $MgCl_2$, 10 EGTA, 1 $CaCl_2$, 10 HEPES, 3 MgATP (pH 7.2 with CsOH).

### Electron Microscopy

Isolated rat islets were fixed in 2.5% glutaraldehyde in phosphate buffer, post-fixed in 1% osmium, dehydrated, and embedded in Spurr's resin. Ultrathin sections cut onto nickel grids were immunolabeled for GABA using optimally diluted (1/1,000) rabbit polyclonal antibody to GABA (Sigma-Aldrich) and protein A gold (15 nm; Biocell). Sections were viewed with a Joel 1010 microscope, accelerating voltage 80 kV. Gold particle density on different β-cell organelles was estimated by image analysis (Scion Image, Scion Corporation). Background labeling was obtained on pancreatic exocrine tissue and subtracted.

### Analysis and Statistical Evaluation

Data are given as mean values ± SEM unless indicated otherwise. Statistical significances were evaluated using Student's *t* test for unpaired data. The GABA- and ATP-induced transient inward currents (TICs) and the amperometric events were analyzed using the MiniAnalysis software (Synaptosoft). In Figs. 3 and 4, amperometric currents, which occurred within a period

Published February 12, 2007

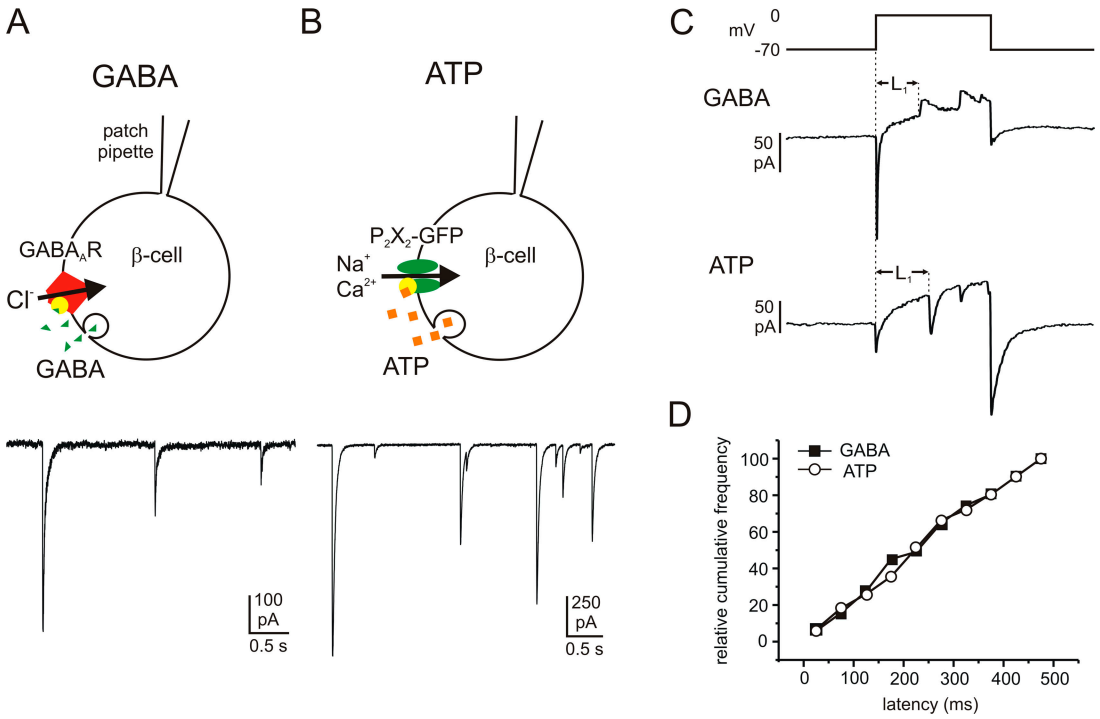


**Figure 1.** Quantal GABA and ATP release in rat β cells monitored by overexpression of the ionotropic membrane receptors $GABA_A$ and $P_2X_2$. Examples of GABA- (A) and ATP-activated (B) TICs recorded from β cells infected with $GABA_A$ and $P_2X_2$ receptors, respectively. Cells were held at −70 mV and exocytosis elicited by intracellular application of 2 μM free $Ca^{2+}$. The cartoons above the current traces illustrate schematically the protocols used. (C) Samples of GABA (transient outward currents; top trace) and ATP release events (transient inward currents; bottom trace) triggered by 500-ms depolarizations from −70 to 0 mV. The latency between the beginning of the depolarizing pulse and the onset of the first exocytotic event during the pulse ($L_1$) was measured. (D) Cumulative frequency of the first latencies of GABA release (black squares) and ATP release (open circles).

shorter than their own rise times following a purinergic or GABAergic TIC (maximally 20 ms), were regarded as simultaneous with the receptor-activated current. Stationary fluctuation analysis (Hille, 2001) was performed using MATLAB software (Mathworks Inc.).

To evaluate the temporal coincidence of GABAergic TICs and amperometric events, the two corresponding time series of transient currents were characterized with the probability density function, and the probability for an amperometric event to occur during a time interval Δt (20 ms) after a GABA-induced TIC was calculated and compared with the probability observed experimentally. A detailed description of these procedures is provided as online supplemental material.

### Online Supplemental Material

The supplemental material is available at http://www.jgp.org/cgi/content/full/jgp.200609658/DC1. Fig. S1 shows the distribution of time intervals between adjacent GABAergic TICs and amperometric events, respectively, and contains a description of the procedure for evaluating the temporal coincidence of both types of events. Fig. S2 relates to the assay for the simultaneous detection of GABA and ATP release.

## RESULTS

### Kinetics of Quantal Release of ATP and GABA from β Cells

To investigate the release of the low molecular weight transmitters ATP and GABA from pancreatic β cells, we used patch clamp–based secretion assays as described previously (Braun et al., 2004a; Obermüller et al., 2005). In brief, "autosynapses" were created in isolated rat β cells by overexpression of $GABA_A$ or $P_2X_2$ receptor ion channels using adenoviral vectors (Fig. 1, A and B). Vesicular release of GABA and ATP activates their respective receptors and thus gives rise to transient inward currents (TICs) similar to inhibitory postsynaptic currents (IPSCs) in nerve terminals. Fig. 1 (A and B, bottom) shows examples of TICs observed in β cells infected with $GABA_A$ receptor $\alpha_1/\beta_1$ subunits (Fig. 1 A) or $P_2X_2$ receptors (Fig. 1 B) when exocytosis was stimulated by intracellular application of 2 μM free $[Ca^{2+}]_i$ via the recording electrode. Some of the characteristics of these TICs (rise times and halfwidths) have been reported elsewhere (Braun et al., 2004a; MacDonald et al., 2006).

Release of both GABA and ATP can also be elicited by membrane depolarization (Braun et al., 2004a; Obermüller et al., 2005). We measured the latency between the onset of membrane depolarization and the occurrence of the first exocytotic event during 500-ms voltage clamp depolarizations from −70 to 0 mV (Fig. 1 C). No detectable difference in the first latencies of GABA and ATP release was observed. GABA was released with

Published February 12, 2007

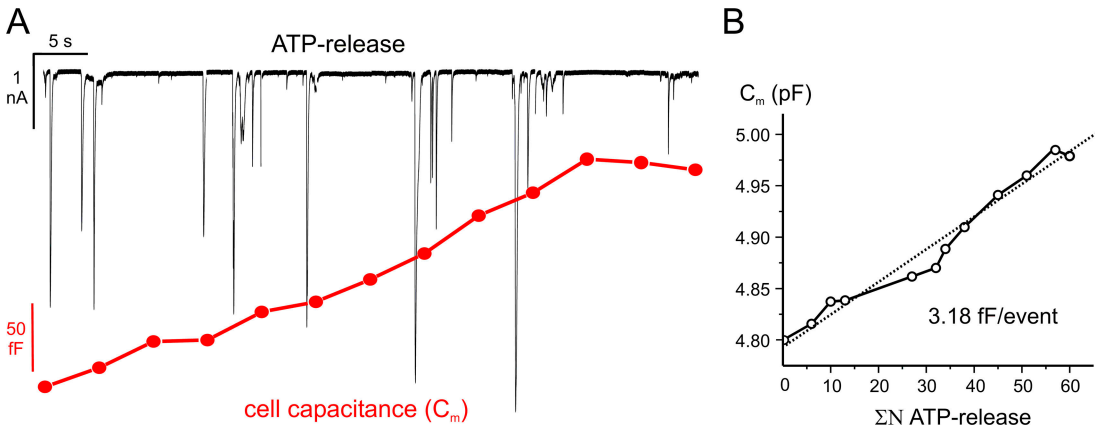


**Figure 2.** Estimation of the unitary LDCV capacitance increase. (A) $P_2X_2$ receptor–mediated TICs (top) and increase in whole-cell capacitance (bottom) recorded simultaneously in the same cell. Exocytosis was elicited by inclusion of 230 nM free $Ca^{2+}$ in the pipette solution. Each segment (5 s) was preceded by a brief prepulse with a sine wave to measure the cell capacitance. (B) Plot of the cumulative number ($\Sigma N$) of purinergic TICs vs. membrane capacitance ($C_m$) from the same experiment. A linear fit (dotted line) with a slope of 3.18 fF/event is superimposed.

an average first latency of 249 ± 19 ms ($n$ = 51 events in six cells), whereas the corresponding value for ATP was 249 ± 13 ms ($n$ = 104 events in 15 cells; Fig. 1 D).

### Parallel Recordings of $P_2X_2$ Currents and Cell Capacitance

We combined whole-cell capacitance measurements with the monitoring of ATP secretion in β cells overexpressing $P_2X_2$ receptors. The cells were held at −70 mV and exocytosis was elicited by infusion of 230 nM free $Ca^{2+}$. This $[Ca^{2+}]_i$ is sufficient to trigger exocytosis at a low rate but does not elicit endocytosis in β cells (Eliasson et al., 1996; Renstrom et al., 1997). The progressive increase in cell capacitance (Fig. 2 A, bottom trace) following establishment of the whole-cell configuration was associated with the occurrence of numerous TICs (Fig. 2 A, top trace). Fig. 2 B compares the cell capacitance ($C_m$) as a function of the cumulative number of TICs ($\Sigma N$) measured over 60 s. The slope of the linear fit (dotted line) provides an estimate of the unitary increase in cell capacitance per exocytotic event and amounted to 3.2 fF/event. In a series of eight experiments, the average capacitance increase per TIC was 3.4 ± 0.48 fF.

### Corelease of ATP and Serotonin

Serotonin is taken up by pancreatic β cells from the culture medium and selectively accumulates in insulin-containing LDCVs (Ekholm et al., 1971; Kasai, 1999). The detection of serotonin release by carbon fiber amperometry has been used extensively as an assay for LDCV exocytosis in β cells (Zhou and Misler, 1996; Takahashi et al., 1997; Aspinwall et al., 1999). We combined amperometric detection of serotonin with patch-clamp recordings of GABA or ATP release in rat β cells overexpressing either $P_2X_2$ or $GABA_A$ receptors. The cells were clamped at −70 mV and exocytosis was triggered by infusion of 2 μM $Ca^{2+}$ through the patch pipette. Fig. 3 A shows a parallel recording of ATP and serotonin release in the same cell. In this experiment, a total of 77 amperometric events and 194 $P_2X_2$ TICs were detected. Thus, the latter outnumber the former by a factor of 2.5. This is expected because the carbon fiber (d = 5 μm) only covers a fraction of this cell, whereas the $P_2X_2$ receptors will detect ATP release in the entire cell. In most cells there was a good correlation between amperometric spikes and ATP-dependent TICs. In a series of nine experiments, 77 ± 4% of all amperometric spikes were accompanied by a simultaneous ATP release event. If we instead calculated the fraction of ATP-dependent TICs associated with amperometric responses (i.e., the reverse analysis), a value of 29 ± 4% was obtained. This is again a consequence of the carbon fiber only monitoring exocytosis in ∼35–40% of the β-cell.

If ATP and serotonin are released by exocytosis of the same vesicles, then the amplitude of the associated events should correlate. We therefore compared the charges (Q) of simultaneously occurring $P_2X_2$-mediated TICs and amperometric spikes. To allow linear correlation, the data are expressed as the cubic root of the current charges ($\sqrt[3]{Q}$). This parameter is expected to be normally distributed given that the vesicle diameter follows a Gaussian distribution (Finnegan et al., 1996). To exclude exocytotic events occurring far away from the carbon fiber, with resultant diffusional loss of serotonin and distortion of the signal, only amperometric events with a rise time <15 ms were included. It is evident that $\sqrt[3]{Q}$ of purinergic TICs and amperometric currents are linearly related to each other (correlation coefficient R = 0.83; P < 0.001; Fig. 3 B). In a series of five experiments with a total of 101 events, the correlation coefficient R averaged 0.82 ± 0.05.

Published February 12, 2007

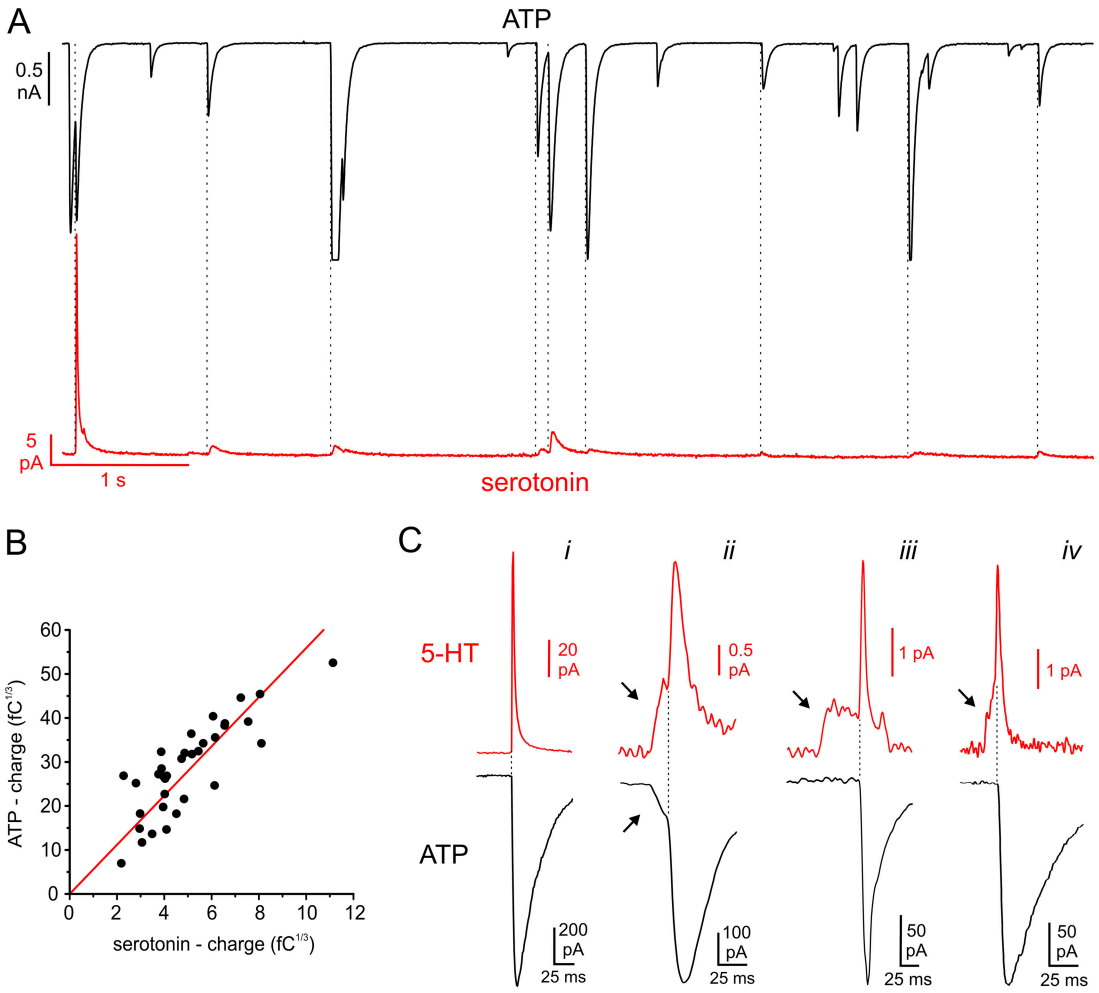


**Figure 3.** Parallel recordings of exocytotic events combining amperometry with overexpression of $P_2X_2$ receptors. The cells were held at −70 mV and exocytosis elicited by intracellular application of 2 μM free $Ca^{2+}$. (A) Parallel recording of ATP release–induced TICs (top) and serotonin release measured by amperometry (bottom) in a single β-cell. The dotted lines indicate the simultaneous occurrence of TICs and amperometric spikes. (B) Cubic root of the charge of the $P_2X_2$-mediated TICs ($n$ = 34 events recorded in the same cell) plotted against the cubic root of the charge of simultaneously recorded amperometric spikes. A linear fit is superimposed. (C) Examples of amperometric spikes (top red traces, 5-HT) and simultaneously recorded ATP release–induced TICs (bottom black trace). Prespike feet are indicated by arrows.

### Release of ATP and Serotonin during Prespike Feet

In chromaffin cells, the rapidly rising phase of amperometric events is often preceded by a small pedestal ("foot"), which represents release of transmitter through the fusion pore (Chow et al., 1992). Such prespike feet have also been described in β cells (Zhou and Misler, 1996), suggesting that serotonin can also exit via the fusion pore. It has also been argued, however, that the pedestals in β cells represent an artifact that results from the superimposition of two separate events occurring at different distances from the electrode (Smith et al., 1999). During parallel recordings of ATP and serotonin release, we observed pedestals preceding both the amperometric spikes (37 out of 124 events) and the simultaneously recorded ATP-induced TICs (17 out of 124 events; Fig. 3 C, trace *ii*). The shape of the ATP-induced TICs is independent of the localization of the exocytotic event (Obermüller et al., 2005). We can thereby discard the possibility that the pedestals result from summation of release events; if they did, we should have been able to observe two full-sized ATP-induced TICs in rapid succession. Interestingly, the foot signal of ATP-induced TICs had a lower amplitude relative to the spike phase than the corresponding amperometric currents (12 ± 2% for ATP vs. 28 ± 3% for serotonin, $P < 0.001$, $n$ = 17 in 11 cells) and contributed substantially less to the total charge of the event (3.6 ± 1% for ATP vs. 20 ± 5% for serotonin; $P < 0.001$). Moreover, many amperometric events consisting of both foot and spike signals were accompanied by simultaneous ATP-dependent TICs displaying only the rapid spike-like signal with no sign of a pedestal (traces *iii* and *iv* in Fig. 3 C; $n$ = 20 in 11 cells). Taken together, these data indicate that ATP is less readily released than

Published February 12, 2007

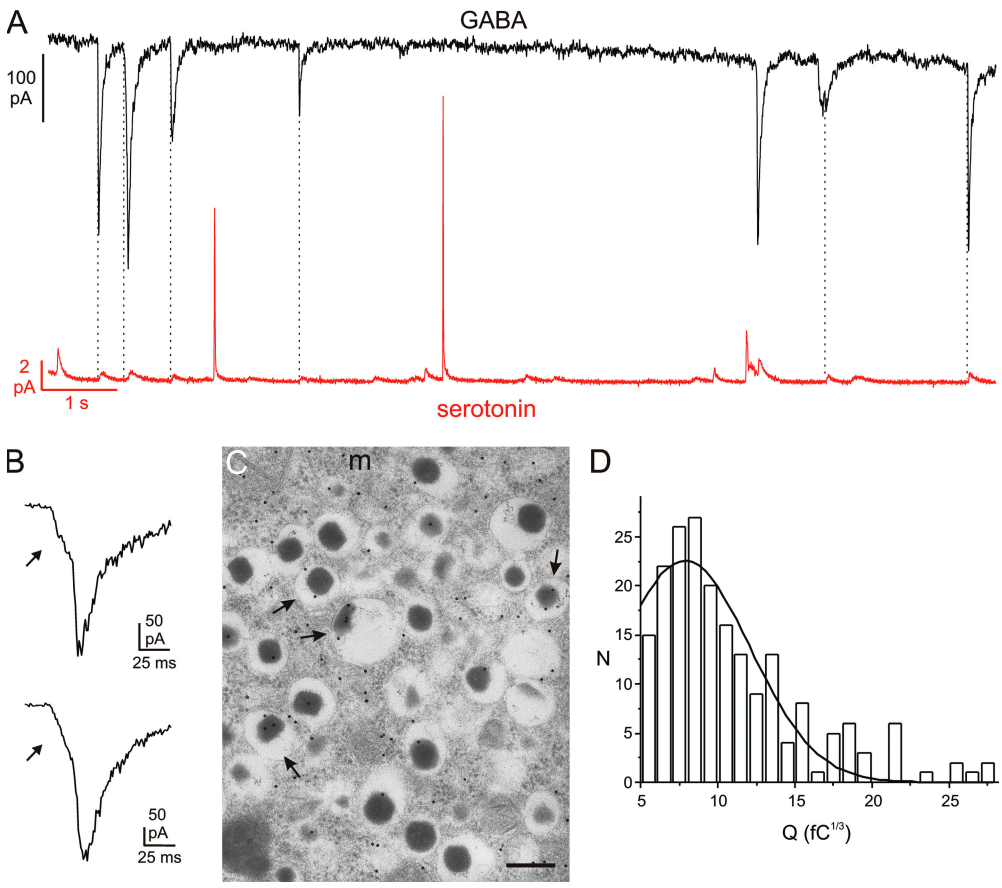


**Figure 4.** Corelease of GABA and serotonin by exocytosis of LDCVs. (A) Parallel recording of GABA-induced TICs (top) and serotonin release (bottom) in a single β-cell. The cell was held at −70 mV and exocytosis elicited by intracellular application of 2 μM free $Ca^{2+}$. (B) Examples of GABA-induced TICs displaying prespike feet. (C) Immunogold labeling of GABA in rat pancreatic β cells. Labeling over the insulin-containing LDCVs (arrows) was less than that in the cytoplasm and was variable in density. (m = mitochondria; Bar, 200 nm). (D) Distribution of cubic roots of integrated GABA-dependent TICs ($\sqrt[3]{Q}$) in a single representative experiment. A total of 200 events (N) were analyzed. A Gaussian fit is superimposed. The CV in this particular experiment was 0.49.

serotonin during the prespike feet. Amperometric feet with simultaneous ATP-induced foot signals were significantly longer than amperometric feet without ATP release (28 ± 5 ms vs. 13 ± 3 ms, $P < 0.01$) and tended to contribute more to the total charge of the event (20 ± 5% vs. 14 ± 3%).

### Corelease of GABA and Serotonin

We also combined amperometric monitoring of serotonin release with patch-clamp measurements of GABA release in β cells overexpressing $GABA_A$ receptors. Although simultaneous release of GABA and serotonin was sometimes observed (Fig. 4 A), only 6.3 ± 1.4% of the amperometric events correlated with simultaneous GABA release in a series of eight experiments. We considered the possibility that ATP appears more strongly correlated with serotonin release than GABA because ATP-dependent TICs were more frequent; normalized to the frequency of amperometric events, the number of ATP-dependent TICs was 15-fold higher than the number of GABA-evoked TICs under these experimental conditions (unpublished data). We therefore determined the fraction of GABA-induced TICs associated with simultaneous serotonin release (i.e., the reverse analysis) and obtained an average value of 22 ± 5% ($n = 8$). This value is not statistically different from the percentage of ATP-induced TICs associated with serotonin release and is sevenfold larger ($P < 0.01$) than that expected for simultaneous release of GABA and serotonin by independent events (see Materials and methods and online supplemental material).

We measured the charge of the amperometric spikes occurring simultaneously with GABAergic TICs and compared it with those that were not associated with GABA release. In a series of six experiments, the cubic root of charge of the amperometric events accompanied by GABA release averaged 94 ± 3% ($n = 44$) of that of isolated amperometric spikes. There was likewise no difference in the rise time (defined as the time required for the current to increase from 10 to 90% of its final amplitude) between amperometric events that associated with GABA release and those that did not (16 ± 3 ms vs. 16 ± 2 ms) and their half-widths (33 ± 4 vs. 32 ± 3 ms). We also compared the GABA-activated TICs that associated with serotonin release with those that did not. The cubic root of charge of GABA-activated TICs associated with serotonin release was 98 ± 7% of isolated GABAergic TICs ($n = 30$, not statistically significant).

Finally, evidence for GABA release during pedestals preceding the spike was also obtained (Fig. 4 B). We observed 22 clear pedestals with an average relative amplitude (relative to the peak) of 28.7 ± 2.5%, accounting for 6.4 ± 1% of the total charge.

Published February 12, 2007

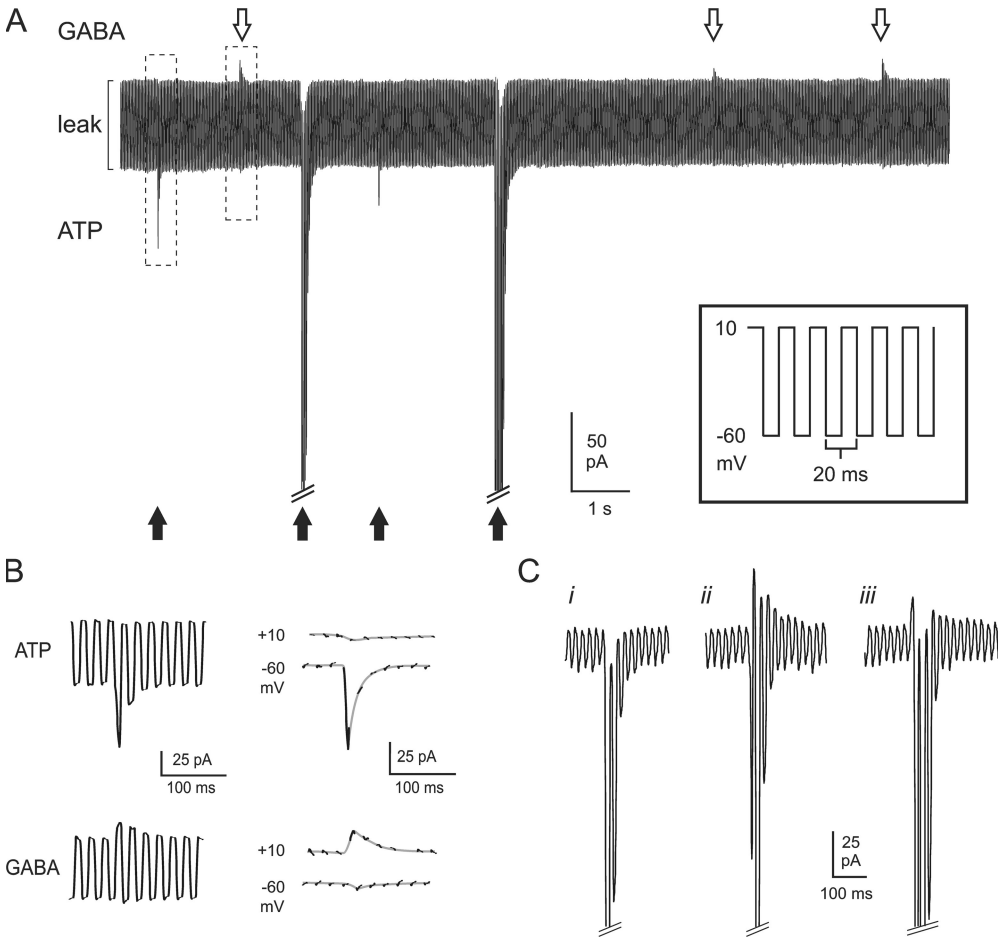


**Figure 5.** Parallel monitoring of GABA and ATP release. (A, inset) Schematic of voltage protocol used to near-simultaneously resolve GABAergic and purinergic transient currents in cells infected with both $GABA_A$ and $P_2X_2$ receptors. The membrane potential was rapidly (50 Hz) alternated between $E_{Cl}$ (−60 mV) and $E_{P2X2}$ (+10 mV). (A) Sample recording showing ATP-induced inward currents (black arrows) and GABA-induced outward currents (white arrows) in a double-infected β-cell. Exocytosis was triggered by infusion of 0.2 μM free $Ca^{2+}$ through the recording electrode. The largest inward currents have been truncated for display purposes. (B) Examples of an ATP-induced inward current and a GABA-induced outward response, marked by dashed boxes in A, shown on an expanded time base. In the right part, the current artifacts when switching between −60 and +10 mV have been removed and only current components at + 10 and −60 mV are shown. The segments of the current recordings at the respective voltages have been connected by gray lines. (C) Examples of different types of events with a dominant inward current component: (*i*) inward current in isolation; (*ii*) clear out- and inward components; (*iii*) an outward component superseded by the activation of the inward current. The inward currents at −60 mV have been truncated for display purposes.

### Subcellular Localization of GABA in Rat β cells

We reanalyzed the subcellular distribution of GABA in rat β cells (Fig. 4 C). Labeling was high in the nuclei and distributed throughout the cytoplasm. Based on the analysis of 1,017 granules from nine different cells and in agreement with our previous findings (Braun et al., 2004a), the average particle density was lower in LDCVs (6.2 particles/$\mu m^2$) than in the other compartments (15.1 particles/$\mu m^2$). The latter value does not, at variance with our previous study, include the nuclei, which contain a high density of gold particles, and this accounts for the lower intracellular density we observe here. Interestingly, 17% of the LDCVs were labeled by the antibody. This suggests that a subpopulation of LDCVs accumulates significant amounts of GABA. The particle density in these granules averaged 36 particles/$\mu m^2$.

We have also analyzed the distribution of the cubic roots ($\sqrt[3]{Q}$) of the charges of the GABA-dependent TICs. Fig. 4 D shows a representative experiment. In a series of 11 experiments including a total of 996 events, the average coefficient of variation (CV) averaged 0.43 ± 0.03. For comparison, the CV for the pooled $\sqrt[3]{Q}$ values of the amperometric spikes was 0.30.

### Simultaneous Detection of GABA and ATP Release

If GABA coreleased with serotonin reflects exocytosis of LDCVs, then GABA release should also associate with ATP release. We addressed this by overexpression of $GABA_A$ and $P_2X_2$ receptors in the same β cells. To resolve both GABA- and ATP-evoked transient currents, the intracellular medium contained 12 mM $Cl^-$, and the membrane potential was alternated between +10 and −60 mV with a period of 20 ms (Fig. 5 A, inset). With the combination of extra- and intracellular solutions used for this series of experiments, these voltages are close to the reversal potentials of the currents flowing through the $P_2X_2$ and $GABA_A$ receptors, respectively. Exogenous application of a mixture of GABA and ATP confirmed that both current types could be detected simultaneously using this protocol (Fig. S2). The peak outward (GABA) and inward (ATP) currents evoked by 0.1 mM of either agonist averaged 1.8 ± 0.4 nA and −5.4 ± 1.2 nA, respectively ($n = 7$).

Published February 12, 2007

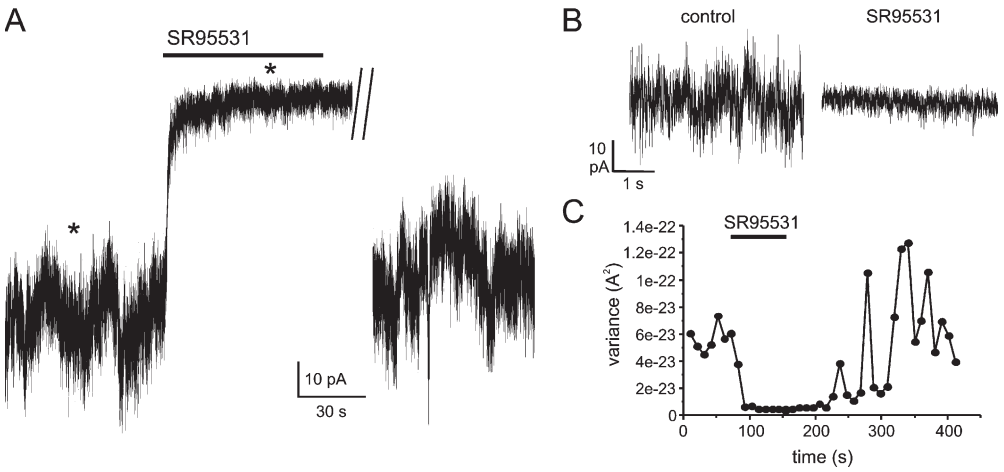


**Figure 6.** Evidence for tonic GABA release from β cells. (A) The recording was made in a β-cell overexpressing $GABA_A$ receptor $Cl^-$ channels within a cell cluster. The holding current at −70 mV was measured in the presence of 1 mM extracellular glucose with intracellular solution containing 10 mM EGTA. The $GABA_A$ receptor antagonist SR95531 (10 μM) was added to the bath as indicated by the bar. A segment of ~2 min during the washout of SR95531 has been removed. (B) Current segments marked by asterisks (*) in A shown at expanded time base. (C) Variance of current before, during, and after addition of SR95531 (as indicated by the horizontal line).

Fig. 5 A shows a recording of spontaneous events from a β-cell infected with both $P_2X_2$ and $GABA_A$ receptors. Exocytosis was stimulated by inclusion of 0.2 μM free $Ca^{2+}$ in the pipette solution. Several transient GABA-induced outward currents (white arrows) and ATP-dependent inward currents (black arrows) are superimposed on the oscillating background current. Fig. 5 B shows an outward and an inward current from Fig. 5 A on an expanded time base. In 11 cells, a total of 109 isolated outward currents at +10 mV (reflecting GABA release) and 607 isolated inward currents at −60 mV (representing ATP release) were observed. The current amplitude in the outward and inward directions averaged 25 ± 4 pA and −341 ± 98 pA, respectively. We also detected 16 events (in eight cells, 2.6% of all ATP-induced TICs), which showed both inward and outward current components (Fig. 5 C, traces *ii* and *iii*). In these 16 events, the outward and inward currents averaged 30 ± 6 and −234 ± 60 pA, respectively. In some cases, the outward current was very short-lived and rapidly superseded by the development of an inward current (Fig. 5 C, trace *iii*).

### Analysis of Tonic Activity of $GABA_A$ Receptors

Biochemical measurements have shown that β cells release 25% of their GABA contents per hour in the presence of 3 mM glucose (Smismans et al., 1997). Since insulin is not released at this low glucose concentration, exocytosis of the LDCVs is unlikely to account for this release. We have performed patch-clamp experiments on islet cell clusters overexpressing $GABA_A$ receptors in the presence of 1 mM extracellular glucose. The patch-clamped cell was held at −70 mV and infused with a high concentration of EGTA to suppress $Ca^{2+}$-dependent exocytosis. GABAergic TICs were observed extremely rarely under these conditions (<1 event/h). However, even in the absence of identifiable vesicular release, bath application of the $GABA_A$ receptor antagonist SR95531 (10 μM) reversibly blocked a part of the holding current (Fig. 6 A) and reduced the current noise (Fig. 6, B and C). In a series of five experiments, SR95531 reduced the mean holding current by 30 ± 10 pA ($P < 0.05$) and the current variance by 74 ± 6% ($P < 0.05$). No SR95531-sensitive current was observed in individual glucagon-producing α cells infected with the $GABA_A$ receptors to about the same extent as the β cells. The unitary amplitude of the events contributing to the excess (SR95531-sensitive) noise was estimated by stationary fluctuation analysis (Hille, 2001). In a series of four experiments, a unitary amplitude of 2.0 ± 0.2 pA was obtained. With a reversal potential of −5 mV (as expected for a $Cl^-$ current with the ionic gradients used in this experiment), this current amplitude corresponds to a unitary conductance of 31 ± 6 pS ($n = 4$). A similar value (27 pS) was obtained by noise analysis of the current that develops when a low concentration of GABA (1 μM) is applied to isolated outside-out patches (unpublished data).

## DISCUSSION

The role of GABA in the pancreas and the cellular processes involved in its release from the β-cell remain obscure. We have investigated whether GABA and insulin are released by the same or a distinct exocytotic pathway. Here we attempt to highlight some of the more important

Published February 12, 2007

implications of the data that have emanated from this work.

### ATP and Serotonin Are Coreleased by Exocytosis of LDCV

Using a modified carbon fiber electrode, Aspinwall et al. (1999) demonstrated corelease of insulin and serotonin. We now demonstrate that almost 80% (in some experiments being close to 100%) of the exocytotic events detected as the release of serotonin also associated with ATP release. Thus, measurements of ATP can be regarded as an endogenous reporter of LDCV exocytosis in pancreatic β cells. The fact that this $P_2X_2$ receptor-based method monitors exocytosis in the entire cell (and not just in the part of the membrane closest to the carbon fiber) makes it possible to directly correlate changes in cell capacitance to the number of exocytotic events (Fig. 2). We were thereby able to estimate that the release of one ATP quantum was associated with an average capacitance increase of 3.4 fF (Fig. 2). This value corresponds to vesicle with a diameter of 310 nm (assuming spherical geometry and a specific capacitance of 9 $fF\mu m^{-2}$), close to the 330 nm determined for β-cell LDCVs by electron microscopy (Braun et al., 2004a).

### Low Molecular Weight Granule Constituents Are Differentially Released via the Fusion Pore

We have previously reported that ATP and serotonin can be released via the fusion pore that connects the granule lumen with the extracellular space (MacDonald et al., 2006). Here we have characterized the GABA-, ATP-, and serotonin-dependent pedestals in greater detail. Based on the relative amplitudes of the pedestals, it appears that the fusion pore restricts the passage of ATP significantly more than that of serotonin and GABA. Occasionally, there was no sign of a pedestal in the ATP measurements although it was prominent in the amperometric recording. This may contribute to the finding that the correlation between serotonin and ATP release was <100% in some experiments (see above). The dimensions of ATP, serotonin, and GABA are ~1.6 × 1.1 × 0.5 nm, ~1.0 × 0.5 × 0.2 nm, and 0.75 × 0.3 × 0.2 nm, respectively. The diameter of the β-cell LDCV fusion pore is ~1.4 nm (MacDonald et al., 2006). This predicts that whereas GABA and serotonin will be easily accommodated within the fusion pore, the movements of ATP will be more restricted. The occurrence of isolated GABA-induced TICs without simultaneous ATP release (Fig. 5, A and B) we attribute to partial opening of the fusion pore, sufficient to allow the exit of the GABA but not of the bigger ATP molecule. The above "permeability sequence" ATP < serotonin < GABA for the fusion pore is precisely that predicted from their relative size. Evidence for the fusion pore to "filter" small molecules has also been obtained in synaptic vesicles (Gandhi and Stevens, 2003). Thus, exocytosis through fusion pores ("kiss-and-run") provides cells with a mechanism to differentially release small molecular weight transmitters from individual vesicles.

### Is GABA Released by Exocytosis of SLMVs, LDCVs, or Both?

Serotonin is a selective marker of the insulin-containing LDCVs (Kasai, 1999) and our value for the CV of the distribution of the amperometric charges as well as that reported by others (Finnegan et al., 1996) are consistent with this conclusion. We found that 22% of the GABA-dependent TICs associated with simultaneous serotonin release. This argues that some GABA is released by exocytosis of LDCVs. This conclusion is reinforced by the observation that there were no differences in the rise time, halfwidth, and charge between amperometric events that associated with GABA release and those that did not. If a subpopulation of the amperometric events was due to exocytosis of SLMVs, this should be reflected in different amplitudes and kinetics of the events (compare Bruns et al., 2000). The conclusion that GABA is released by exocytosis of the insulin granules is also underpinned by ultrastructural data indicating that β-cell LDCVs do contain GABA (Gammelsaeter et al., 2004; this study).

How big is the relative contribution of LDCVs to the GABA release observed? If we take the 29% of the ATP-induced TICs that associated with serotonin release as the maximum, then at least 75% of the GABA release events (i.e., 22%/29%) are attributable to exocytosis of LDCVs. Thus, we conclude that exocytosis of LDCVs accounts for most (if not all) depolarization-evoked GABA release. Three observations provide further support of this conclusion. First, GABA-induced TICs associated with amperometric events had the same charge as those occurring without release of serotonin. Second, the first latencies of the GABA- and ATP-induced TIC were the same (Fig. 1, C and D), a finding not consistent with the idea that GABA is released by exocytosis of SLMVs since exocytosis of SLMVs has been shown to give rise to a rapid phase of the capacitance response after elevation of $[Ca^{2+}]_i$ in rat β cells (Takahashi et al., 1997). Third, histograms of the charge distribution of GABA-induced TICs consistently showed only one peak (Braun et al., 2004a; this study, Fig. 4 D), compatible with one population of GABA-releasing vesicles.

This conclusion is opposed to our previous study (Braun et al., 2004a), where we postulated that the observed release of GABA is due to exocytosis of SLMVs. This was largely based on earlier publications associating these vesicles with uptake and storage of GABA and GAD65 (Reetz et al., 1991; Thomas-Reetz et al., 1993), and our own morphological data showing relative exclusion of GABA from LDCVs. While we confirmed the latter in this study (Fig. 4 C), in depth analysis suggests that a subpopulation (~15%) of LDCVs does contain

Published February 12, 2007

GABA and may therefore account for the observed current transients. Release of GABA from a subpopulation of LDCVs comprising 10–20% of the total granule number is in fact in good agreement with the earlier finding that the number of GABA-induced TICs is only ~10% of the number of LDCVs undergoing exocytosis suggested by the capacitance increase measured in parallel (Braun et al., 2004a). Uneven loading of LDCVs with the transmitter (some containing less, some more than the average) would also explain why the CV in histograms of GABA-induced TIC charges (0.43) is twice as large as that expected from the distribution of LDCV diameters (CV 0.22; Finnegan et al., 1996; Braun et al., 2004a).

The observation that corelease of GABA and ATP was rarely observed may appear in conflict with the conclusion that GABA is principally released by LDCV exocytosis. However, this may be attributable to the presence of a small inward current during ATP-induced events even at +10 mV (i.e., at the voltage used to detect GABA release), amounting to ~5% of the current amplitude at −60 mV (Fig. S2; Fig. 5 C, *i*). As the average amplitude of this component (5% of 340 pA = 17 pA) is close to the average amplitude of the GABA release–induced outward currents (25 pA), it may conceal the GABAergic signal in many cases (see also Fig. 5 C, *iii*).

### Are SLMVs Involved in Unregulated Release of GABA?

Biochemical measurements indicate that β cells release 1 amol of GABA per β-cell and second in a way largely unaffected by glucose as well as pharmacological and hormonal regulators of insulin secretion (Winnock et al., 2002). This suggests that, in addition to the vesicular release of GABA giving rise to the TICs discussed above, β cells are also equipped with a second pathway for release of the neurotransmitter. It is possible that the SR95531-inhibitable current observed in β cells within islet cell clusters in the absence of stimulatory glucose concentration (Fig. 6) reflects this background release of GABA. Our noise analysis of the SR95531-sensitive current indicates that the conductance of the unitary event is ~30 pS. This value is close to the single-channel conductance of $GABA_A$ receptor $Cl^-$ channels (Conley, 1996). Thus, background release of GABA only triggers opening of individual channels with no indication of phasic responses, which would be expected if GABA was released in a quantal fashion. It is therefore unlikely that exocytosis of SLMVs accounts for the background release of GABA.

### Concluding Remarks

The data presented here argue that GABA can be released by glucose-dependent (vesicular) and -independent (nonvesicular) pathways, and that vesicular release of GABA involves exocytosis of LDCVs. In the latter pathway, GABA is often coreleased with ATP and insulin, although we demonstrate that release through the early fusion pore is strongly molecule dependent. While evidence exists indicating that SLMVs in β cells both store GABA (Reetz et al., 1991; Gammelsaeter et al., 2004) and undergo exocytosis (MacDonald et al., 2005), the role of SLMVs in GABA release has not been possible to document. We acknowledge that if the GABA content per SLMV is <10% of an LDCV (the intravesicular concentration of GABA in the SLMVs would still be greater than fivefold higher than in the LDCVs; cf. Gammelsaeter et al., 2004), the TIC would be below our detection limit. SLMV exocytosis has been reported to proceed initially at very high rates (500 SLMVs being released over 50 ms; Fig. 2 A of Takahashi et al., 1997). Accordingly, even if every SLMV delivers only a small quantum of GABA, exocytosis of many SLMVs may, at least transiently, contribute significantly to β-cell GABA release.

Nonetheless, the observation of parallel regulated and unregulated GABA release pathways suggests roles for this inhibitory neurotransmitter in modulating both the baseline excitability of islet cells and their response to glucose stimulation. Further investigation of these two pathways will provide important insight into the intra-islet regulation of hormone release.

This work was supported by the Wellcome Trust (WT072289) and the European Union through the Network of Excellence BioSim (LSHB-CT-2004-005137) and Integrated Project Eurodia (LSHM-CT-2006-518153). P. Rorsman is a Wolfson-Royal Society Merit Award Research Fellow.

Olaf S. Andersen served as editor.

Submitted: 30 August 2006
Accepted: 26 January 2007

## REFERENCES

Ämmälä, C., F.M. Ashcroft, and P. Rorsman. 1993. Calcium-independent potentiation of insulin release by cyclic AMP in single β cells. *Nature.* 363:356–358.

Aspinwall, C.A., L. Huang, J.R. Lakey, and R.T. Kennedy. 1999. Comparison of amperometric methods for detection of exocytosis from single pancreatic β cells of different species. *Anal. Chem.* 71:5551–5556.

Barg, S. 2003. Mechanisms of exocytosis in insulin-secreting B-cells and glucagon-secreting A-cells. *Pharmacol. Toxicol.* 92:3–13.

Birnir, B., M.L. Tierney, N.P. Pillai, G.B. Cox, and P.W. Gage. 1995. Rapid desensitization of α1 β1 $GABA_A$ receptors expressed in Sf9 cells under optimized conditions. *J. Membr. Biol.* 148:193–202.

Braun, M., A. Wendt, B. Birnir, J. Broman, L. Eliasson, J. Galvanovskis, J. Gromada, H. Mulder, and P. Rorsman. 2004a. Regulated exocytosis of GABA-containing synaptic-like microvesicles in pancreatic β cells. *J. Gen. Physiol.* 123:191–204.

Braun, M., A. Wendt, K. Buschard, A. Salehi, S. Sewing, J. Gromada, and P. Rorsman. 2004b. $GABA_B$-receptor activation inhibits exocytosis in rat pancreatic β cells by G-protein-dependent activation of calcineurin. *J. Physiol.* 559:397–409.

Bruns, D., D. Riedel, J. Klingauf, and R. Jahn. 2000. Quantal release of serotonin. *Neuron.* 28:205–220.

Conley, E.C. 1996. Ion Channel Factsbook. Vol. I: Extracellular Ligand-gated Channels. Academic Press, London. 860 pp.

Published February 12, 2007

Chow, R.H., L. von Ruden, and E. Neher. 1992. Delay in vesicle fusion revealed by electrochemical monitoring of single secretory events in adrenal chromaffin cells. *Nature.* 356:60–63.

Ekholm, R., L.E. Ericson, and I. Lundquist. 1971. Monoamines in the pancreatic islets of the mouse. Subcellular localization of 5-hydroxytryptamine by electron microscopic autoradiography. *Diabetologia.* 7:339–348.

Eliasson, L., P. Proks, C. Ammala, F.M. Ashcroft, K. Bokvist, E. Renstrom, P. Rorsman, and P.A. Smith. 1996. Endocytosis of secretory granules in mouse pancreatic beta-cells evoked by transient elevation of cytosolic calcium. *J. Physiol.* 493:755–767.

Finnegan, J.M., K. Pihel, P.S. Cahill, L. Huang, S.E. Zerby, A.G. Ewing, R.T. Kennedy, and R.M. Wightman. 1996. Vesicular quantal size measured by amperometry at chromaffin, mast, pheochromocytoma, and pancreatic β cells. *J. Neurochem.* 66:1914–1923.

Gammelsaeter, R., M. Froyland, C. Aragon, N.C. Danbolt, D. Fortin, J. Storm-Mathisen, S. Davanger, and V. Gundersen. 2004. Glycine, GABA and their transporters in pancreatic islets of Langerhans: evidence for a paracrine transmitter interplay. *J. Cell Sci.* 117:3749–3758.

Gandhi, S.P., and C.F. Stevens. 2003. Three modes of synaptic vesicular recycling revealed by single-vesicle imaging. *Nature.* 423:607–613.

Gillis, K.D. 1995. Techniques for membrane capacitance measurements. *In* Single-channel recording. B. Sakmann, and E. Neher, editors. Plenum Press, New York. 155–198.

Göpel, S., T. Kanno, S. Barg, J. Galvanovskis, and P. Rorsman. 1999. Voltage-gated and resting membrane currents recorded from B-cells in intact mouse pancreatic islets. *J. Physiol.* 521:717–728.

Hazama, A., S. Hayashi, and Y. Okada. 1998. Cell surface measurements of ATP release from single pancreatic β cells using a novel biosensor technique. *Pflugers Arch.* 437:31–35.

Hille, B. 2001. Ion Channels of Excitable Membranes. Third edition. Sinauer, Sunderland, MA. 814 pp.

Hiriart, M., and D.R. Matteson. 1988. Na channels and two types of Ca channels in rat pancreatic B cells identified with the reverse hemolytic plaque assay. *J. Gen. Physiol.* 91:617–639.

Hollins, B., and S.R. Ikeda. 1997. Heterologous expression of a P2x-purinoceptor in rat chromaffin cells detects vesicular ATP release. *J. Neurophysiol.* 78:3069–3076.

Hutton, J.C. 1989. The insulin secretory granule. *Diabetologia.* 32:271–281.

Kasai, H. 1999. Comparative biology of $Ca^{2+}$-dependent exocytosis: implications of kinetic diversity for secretory function. *Trends Neurosci.* 22:88–93.

Kennedy, R.T., L. Huang, M.A. Atkinson, and P. Dush. 1993. Amperometric monitoring of chemical secretions from individual pancreatic β cells. *Anal. Chem.* 65:1882–1887.

MacDonald, P.E., M. Braun, J. Galvanovskis, and P. Rorsman. 2006. Release of small transmitters through kiss-and-run fusion pores in rat pancreatic β cells. *Cell Metab.* 4:283–290.

MacDonald, P.E., S. Obermüller, J. Vikman, J. Galvanovskis, P. Rorsman, and L. Eliasson. 2005. Regulated exocytosis and kiss-and-run of synaptic-like microvesicles in INS-1 and primary rat β cells. *Diabetes.* 54:736–743.

Obermüller, S., A. Lindqvist, J. Karanauskaite, J. Galvanovskis, P. Rorsman, and S. Barg. 2005. Selective nucleotide-release from dense-core granules in insulin-secreting cells. *J. Cell Sci.* 118:4271–4282.

Reetz, A., M. Solimena, M. Matteoli, F. Folli, K. Takei, and P. De Camilli. 1991. GABA and pancreatic β cells: colocalization of glutamic acid decarboxylase (GAD) and GABA with synaptic-like microvesicles suggests their role in GABA storage and secretion. *EMBO J.* 10:1275–1284.

Renstrom, E., L. Eliasson, and P. Rorsman. 1997. Protein kinase A-dependent and -independent stimulation of exocytosis by cAMP in mouse pancreatic B-cells. *J. Physiol.* 502:105–118.

Rorsman, P., P.O. Berggren, K. Bokvist, H. Ericson, H. Mohler, C.G. Ostenson, and P.A. Smith. 1989. Glucose-inhibition of glucagon secretion involves activation of GABAA-receptor chloride channels. *Nature.* 341:233–236.

Salehi, A., S.S. Qader, E. Grapengiesser, and B. Hellman. 2005. Inhibition of purinoceptors amplifies glucose-stimulated insulin release with removal of its pulsatility. *Diabetes.* 54:2126–2131.

Smismans, A., F. Schuit, and D. Pipeleers. 1997. Nutrient regulation of γ-aminobutyric acid release from islet β cells. *Diabetologia.* 40:1411–1415.

Smith, P.A., P. Proks, and F.M. Ashcroft. 1999. Quantal analysis of 5-hydroxytryptamine release from mouse pancreatic β cells. *J. Physiol.* 521:651–664.

Takahashi, N., T. Kadowaki, Y. Yazaki, Y. Miyashita, and H. Kasai. 1997. Multiple exocytotic pathways in pancreatic β cells. *J. Cell Biol.* 138:55–64.

Thomas-Reetz, A., J.W. Hell, M.J. During, C. Walch-Solimena, R. Jahn, and P. De Camilli. 1993. A gamma-aminobutyric acid transporter driven by a proton pump is present in synaptic-like microvesicles of pancreatic β cells. *Proc. Natl. Acad. Sci. USA.* 90:5317–5321.

Tsuboi, T., and G.A. Rutter. 2003. Insulin secretion by 'kiss-and-run' exocytosis in clonal pancreatic islet beta-cells. *Biochem. Soc. Trans.* 31:833–836.

Wendt, A., B. Birnir, K. Buschard, J. Gromada, A. Salehi, S. Sewing, P. Rorsman, and M. Braun. 2004. Glucose inhibition of glucagon secretion from rat β cells is mediated by GABA released from neighbouring β cells. *Diabetes.* 53:1038–1045.

Winnock, F., Z. Ling, R. De Proft, S. Dejonghe, F. Schuit, F. Gorus, and D. Pipeleers. 2002. Correlation between GABA release from rat islet β cells and their metabolic state. *Am. J. Physiol. Endocrinol. Metab.* 282:E937–E942.

Zhou, Z., and S. Misler. 1996. Amperometric detection of quantal secretion from patch-clamped rat pancreatic β cells. *J. Biol. Chem.* 271:270–277.

# Selective nucleotide-release from dense-core granules in insulin-secreting cells

**Stefanie Obermüller[1], Anders Lindqvist[1], Jovita Karanauskaite[1,2], Juris Galvanovskis[2], Patrik Rorsman[1,2] and Sebastian Barg[1,3,*]**

[1]Department of Experimental Medicinal Sciences, Lund University, BMC B11, SE-221 84 Lund, Sweden
[2]OCDEM, Nuffield Department of Clinical Medicine, University of Oxford, Churchill Hospital, Oxford, OX3 7LJ, UK
[3]Vollum Institute, Oregon Health and Sciences University, 3181 SW Sam Jackson Park Road, Portland OR, 97210, USA
*Author for correspondence (e-mail: bargs@ohsu.edu)

*Accepted 17 June 2005*
*Journal of Cell Science 118, 4271-4282 Published by The Company of Biologists 2005*
*doi:10.1242/jcs.02549*

## Summary

**Secretory granules of insulin-secreting cells are used to store and release peptide hormones as well as low-molecular-weight compounds such as nucleotides. Here we have compared the rate of exocytosis with the time courses of nucleotide and peptide release by a combination of capacitance measurements, electrophysiological detection of ATP release and single-granule imaging. We demonstrate that the release of nucleotides and peptides is delayed by ~0.1 and ~2 seconds with respect to membrane fusion, respectively. We further show that in up to 70% of the cases exocytosis does not result in significant release of the peptide cargo, likely because of a mechanism that leads to premature closure of the fusion pore. Release of nucleotides and protons occurred regardless of whether peptides were secreted or not. These observations suggest that insulin-secreting cells are able to use the same secretory vesicles to release small molecules either alone or together with the peptide hormone.**

Key words: Exocytosis, Endocytosis, Fusion pore, Insulin, Hormone, Kiss-and-run, Secretion

## Introduction

Pancreatic B-cells and other (neuro-)endocrine cells use large dense-core vesicles (LDCVs or granules) to store and release a variety of peptide hormones, such as insulin. In addition, these granules contain high concentrations of low-molecular-weight transmitter molecules, such as amino acids, nucleotides and amines (Hutton, 1994). Release of any granule cargo requires regulated exocytosis, which has classically been envisioned as 'full fusion' of the granule with the plasma membrane (Heuser and Reese, 1973; Viveros et al., 1969). In this mode of exocytosis, the granule fuses with the plasmalemma and the two membranes mix completely. Consequently, the entire granule content is discharged into the extracellular space, which is consistent with the finding that the mixture of secreted products is similar to that of the granule cargo (Detimary et al., 1995; Kirshner et al., 1966).

In an alternative mode of exocytosis, originally proposed for synaptic vesicles (Ceccarelli et al., 1973), a transient pore forms between the vesicle lumen and the extracellular space. This pore permits release of transmitter and uptake of tracer molecules, but reseals rapidly to reestablish the integrity of the original secretory vesicle (transient fusion or 'kiss-and-run'). A hallmark of neuronal 'kiss-and-run' exocytosis is the absence of lipid mixing between vesicle and plasma membrane (Aravanis et al., 2003). A similar mechanism may exist in dense-core granule exocytosis. Indeed, live-cell imaging of fluorescently labeled granule proteins led to the conclusion that a fraction of granules can retain their identity during exocytosis, and that these granules reseal later (Holroyd et al., 2002; Perrais et al., 2004; Taraska et al., 2003; Tsuboi et al., 2004). However, in these granules a lipid marker as well as some integral membrane proteins dispersed from the granular membrane into the plasma membrane (Taraska and Almers, 2004; Tsuboi and Rutter, 2003), indicating partial mixing of the two membranes. To indicate this difference of transient granule exocytosis to neuronal 'kiss-and-run' exocytosis, the term 'cavicapture' has been introduced (Taraska et al., 2003).

Fusion of a secretory granule with the plasma membrane begins with the formation of a narrow fusion pore (Breckenridge and Almers, 1987; Zimmerberg et al., 1987). The fusion pore has an initial diameter of 2-3 nm that widens and fluctuates in diameter, but may close again as long as it stays below a critical threshold of 10-20 nm (Alvarez de Toledo et al., 1993; Lollike et al., 1998; Spruce et al., 1990). Beyond that critical threshold the pore expands irreversibly, in a manner that is consistent with full-fusion exocytosis. Fusion pore kinetics have been shown to be affected by both cytosolic and extracellular calcium concentrations (Ales et al., 1999; Hartmann and Lindau, 1995), activation of protein kinase-C (Scepek et al., 1998), and by interventions with proteins of the exocytotic machinery, such as complexin (Archer et al., 2002), synaptotagmin (Wang et al., 2001), and syntaxin (Han et al., 2004).

Parallel amperometric recordings of membrane capacitance and catecholamine release demonstrated that at least some transmitter molecules can leak through the initial fusion pore (Albillos et al., 1997; Alvarez de Toledo et al., 1993), albeit at a slow rate. This slow initial release through the fusion pore

gives rise to a characteristic pre-spike feature ('foot') in amperometric recordings, while bulk release of catecholamine coincides with the beginning of the final and irreversible expansion of the pore (Albillos et al., 1997; Alvarez de Toledo et al., 1993). However, these findings are difficult to interpret because charged transmitter molecules are bound to a gel-like matrix within the lumen of the granule (Uvnäs and Åborg, 1988), and hydration of this matrix is a prerequisite for bulk release of the bound molecules (Marszalek et al., 1997). In contrast to catecholamines, some proteins are initially retained in the granule despite an already open fusion pore (Barg et al., 2002; Perrais et al., 2004). In insulin-secreting cells, there is a delay of up to 10 seconds after pore formation, before the entire peptide contents is rapidly released [<100 milliseconds (Barg et al., 2002; Michael et al., 2004)] and large tracer molecules can enter the granule (Takahashi et al., 2002). Since this phenomenon is reminiscent of the bulk release of catecholamine that occurs at the moment of irreversible pore expansion, the latter findings suggest that peptides with a size similar to that of the fusion pore (2-3 nm) are unable to pass the initial fusion pore at a significant rate. Notably, the molecular dimensions of many of the peptide hormones are similar to estimates of the diameter of the transient fusion pore (Lindau and Almers, 1995).

These findings raise the question whether release is regulated beyond the moment of membrane fusion, and specifically whether a transient fusion mechanism may enable cells to release selectively low-molecular-weight transmitters from LDCVs. Here we have studied exocytosis and cargo discharge from individual LDCVs in Ins1-cells, a well-established model of neuroendocrine $Ca^{2+}$-dependent secretion (Asfari et al., 1992). Exocytosis was measured in three complementary ways. First, we monitored membrane fusion using high-resolution capacitance measurements, which reports the increase in cell surface area that occurs during exocytosis. Second, the release of nucleotides was studied at the single-vesicle level as nucleotide-activated currents measured in cells transfected with ionotropic purinergic receptors (Khakh et al., 2001). Third, peptide release and vesicle fusion were investigated in individual granules by real-time imaging of fluorescent reporter proteins and dyes. We report that up to two-thirds of exocytotic events were not associated with detectable peptide release but nevertheless resulted in the release of ATP. These data suggest that the release of peptides and low-molecular-weight granule constituents is differentially regulated following membrane fusion, possibly at the level of the fusion pore itself.

## Materials and Methods

### Culture and transfection of Ins1-cells

Ins1-cells (passages 85-106) were grown in RPMI 1640 medium (10 mM glucose; Gibco BRL) supplemented with 10% fetal bovine serum, streptomycin (100 μg/ml), penicillin (100 μg/ml), Na-pyruvate (1 mM), and 2-mercaptoethanol (50 μM). Cells were transfected using Fugene 6 (Roche) or Lipofectamine2000 (Invitrogen), according to the protocols recommended by the manufacturers. Following transfection, the cells were replated on glass coverslips and used within 3 days.

### Solutions

During the electrophysiological and optical recordings the cells were constantly perfused with extracellular solution (EC) consisting of (in mM) 138 NaCl, 5.6 KCl, 1.2 $MgCl_2$, 2.6 $CaCl_2$, 1 D-glucose and 5 Hepes (pH 7.4 with NaOH). When exocytosis was elicited by voltage-clamp depolarizations, 20 mM of NaCl was equimolarly replaced with tetraethyl ammonium-chloride (TEA-Cl) to facilitate the detection of inward $Ca^{2+}$-currents. In Fig. 1C, $CaCl_2$ was increased to 10 mM. The pipette solution in the latter experiments (Figs 3-4) contained (in mM) 125 CsCl, 10 NaCl, 1 $MgCl_2$, 0.05 EGTA, 3 Mg-ATP, 0.1 cAMP, 5 Hepes (pH 7.15 using CsOH). In other experiments (Fig. 2B-D and Fig. 6), exocytosis was elicited by intracellular dialysis of the cell with a buffer containing (mM) 125 CsCl, 10 NaCl, 1 $MgCl_2$, 10 EGTA, 9 $CaCl_2$, 3 Mg-ATP, 0.1 cAMP, 5 Hepes (pH 7.15 using CsOH). The free $Ca^{2+}$ concentration was calculated to be 2.0 μM (WinMaxChelator, http://www.stanford.edu/~cpatton/). All experiments on living cells were carried out at 32-34°C. Rapid local application of high $K^+$- or $NH_4Cl$-containing solutions was achieved with a Nanoliter 2000 injector (World Precision Instruments, Sarasota, FL).

### Electrophysiology

Patch electrodes were pulled from borosilicate glass capillaries coated with Sylgard close to the tips and fire-polished. The pipette resistance ranged between 2 and 4 MΩ when filled with the

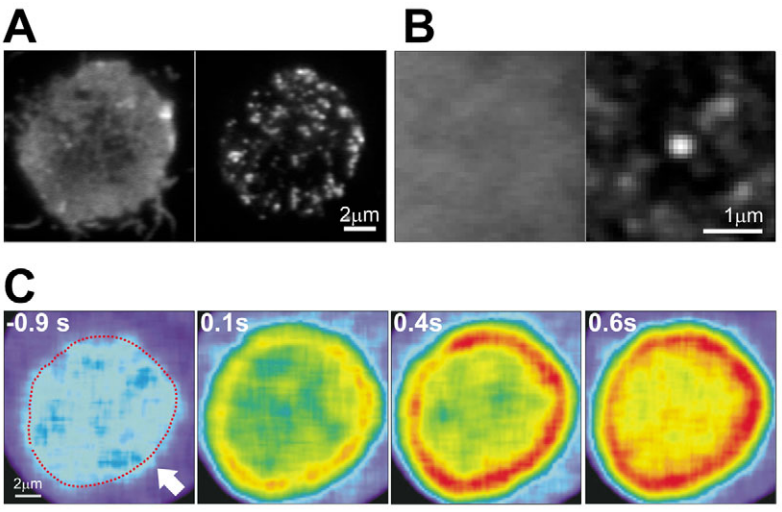


**Fig. 1.** (A) TIRF-images of a cell transfected with $P2X_2$-mRFP1 (left panel) and IAPP-EGFP (right panel). (B) Average image of 23 small frames taken from images like those shown in A and centered on the location of granules (right panel, IAPP-EGFP spots). The left panel is the average image of similar frames cut at the same locations from the red channel. Note uniform $P2X_2$-mRFP1 labeling (left). (C) Sequence of confocal images showing Fluo-5F fluorescence in a cell that expressed $P2X_2$-mRFP. At t=0 seconds, ATP (2 mM) was applied to the cell via a puffer pipette from the direction indicated with an arrow.

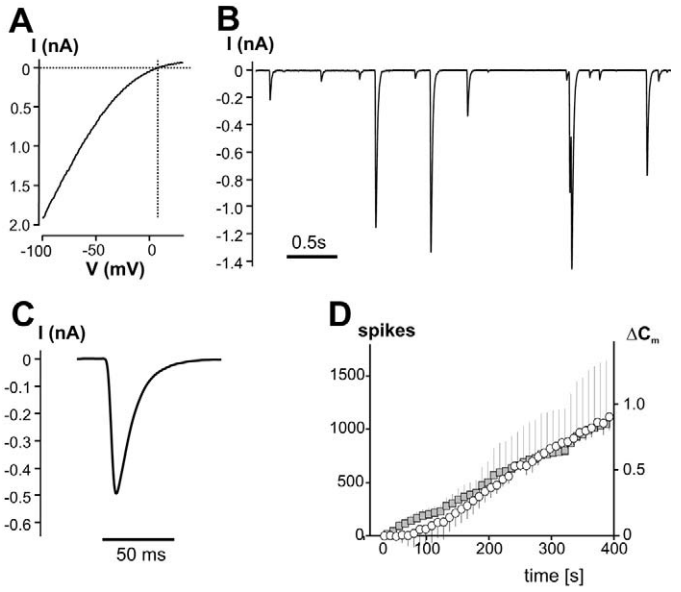


**Fig. 2.** Electrophysiological detection of nucleotide release from individual LDCVs. (A) Current (I)-voltage (V) relationship in a cell expressing $P2X_2$-EGFP. The current was activated by application of 0.2 mM ATP through a puffer pipette, and the I-V characteristics were then determined by ramping the membrane potential from –100 to +30 mV. The response obtained before application of ATP was subtracted from that recorded immediately after addition of the nucleotide to obtain the net current. The dotted horizontal and vertical lines represent the zero-current and the reversal potential, respectively. (B) Typical recording of current spikes evoked in a $P2X_2$-expressing cell by dialyzing the cell interior with a solution containing 2 μM free $Ca^{2+}$. (C) Current spike obtained by averaging 32 recorded events (black line) with an amplitude ranging between 400 and 600 pA. (D) Cumulative number of current spikes recorded in four cells as shown in Fig. 1C (gray squares) and increase in whole-cell capacitance recorded in parallel (open circles) measured at 0.1 Hz. The scaling corresponds to 0.8 fF per spike (MacDonald et al., 2005).

intracellular solution specified above. The measurements were conducted using an EPC-9 amplifier and the Pulse software (version 8.4 or later; Heka Elektronik, Lambrecht, Germany). Exocytosis was elicited by voltage-clamp depolarizations from –70 mV to zero and detected as changes in cell capacitance estimated by the 'Sine + DC'-feature of Pulse, using a 500 Hz, 20 mV sine. The experiments were performed in the whole-cell configuration with an access resistance of 10-20 MΩ. For membrane currents ⩽500 pA, the voltage error is limited to ~5 mV. In Fig. 2B,C and Fig. 3A,B, $P2X_2$-currents were filtered at 1.67 kHz and sampled at 5 kHz. Spike analysis was performed using MiniAnalysis software (Synaptosoft, Decatur, GA) setting the threshold at five times the RMS noise during event-free sections of the recordings (5-8 pA). Spikes in Fig. 3A were detected by eye. We point out that this assay provides information similar to that obtained by amperometry but that it has the advantage of detecting all release events in the entire cell whereas carbon fiber amperometry usually covers only a fraction of the cell.

### Analysis of $P2X_2$ receptor distribution on the plasma membrane

It has previously been shown that the electrophysiological properties of $P2X_2$-EGFP are similar to those of unlabeled $P2X_2$ (Khakh et al., 2001). We ascertained uniform expression of the expressed $P2X_2$ receptors using total internal reflection microscopy (TIRF; see below). In Ins1-cells expressing $P2X_2$-mRFP1 (Fig. 1A,B, left panels) and the granule marker IAPP-EGFP (Fig. 1A,B, right panels), the fluorescence intensity of $P2X_2$-mRFP1 in the footprint of the cell exhibited a standard deviation of 31±2% ($n$=7 cells) of the background-subtracted mean. This level of variation is primarily due to uneven illumination, because it was seen also in cells stained with the membrane dye FM4-64 (standard deviation 28±1%; $n$=4; not shown). There was no evidence for preferential localization of $P2X_2$-mRFP1 with regard to individual granules, and when 23 small frames each with a granule in the center were averaged, the corresponding average image in the $P2X_2$-mRFP channel appeared even (Fig. 1B, left). In the individual frames, the mRFP1 signal within a 0.5 μm circle corresponding to the site of the granule (identified by IAPP-EGFP) was the same (103±2%; $n$=23) as that of a surrounding 2 μm-wide annulus.

To test whether the observed fluorescence distribution represents functional $P2X_2$-receptors, we took advantage of the fact that $P2X_2$ is somewhat permeable to $Ca^{2+}$, and imaged ATP-evoked $Ca^{2+}$-influx in cells that expressed $P2X_2$-mRFP. Cells were dialyzed in whole-cell voltage-clamp mode (–70 mV) with a solution containing (in mM) 120 Cs-glutamate, 10 CsCl, 10 NaCl, 1 $MgCl_2$, 10 Hepes, 3 Mg-ATP 10 EGTA and 0.2 Fluo-5F (Molecular Probes, Eugene, OR), adjusted to pH 7.15 using CsOH. The combination of low-affinity $Ca^{2+}$-indicator and high concentration of $Ca^{2+}$-chelator has previously been shown to resolve $Ca^{2+}$-microdomains (Zenisek et al., 2003). A central plane of the cell was then selected and imaged with a confocal microscope at 10 Hz (Fig. 1C). At time zero, 2 mM ATP (in EC with 10 mM $CaCl_2$) was applied through a local puffer pipette to activate $P2X_2$-channels. Immediately after ATP application, the $Ca^{2+}$-signal increased uniformly in a rim below the plasma membrane of the cell (Fig. 1C), indicating uniform expression of functional $P2X_2$-channels. The lesser increase in the $Ca^{2+}$-indicator signal at the upper left corner was seen in all cells and is likely due to the larger distance from the mouth of the ATP-puffer pipette (direction of puff indicated with an arrow in Fig. 1C).

### Live cell imaging

The images in Fig. 1A-B were obtained with a custom-built lens-type total internal reflection fluorescence (TIRF) microscope equipped with a 100×/1.65 Apo lens (Olympus, Melville, NY). The 488 nm line of an Argon/Krypton laser (Innova 70C, Coherent, Santa Clara, CA) was used to excite both EGFP and mRFP1, and their emission was imaged simultaneously with an image splitter (Multispec MicroImager, Optical Insights, Santa Fe, NM) that separated the red and green components into two channels as side-by-side images on the chip of a charge-coupled device (CCD) camera (Cascade 512B, Roper Scientific, Trenton, NJ). The final spacing was 80 nm per pixel. A lens (400 mm focal length) was included in the emission path of the red channel to correct for a slight focus difference between the red and green channels. To correct for any residual mis-registration and differences in magnification caused by the lens, we acquired pictures of scattered 200 nm beads (Molecular Probes, Eugene, OR) fluorescing at both wavelengths. Beads in the two images were brought into superposition by shifting, stretching, or shrinking the image of the red channel with in-house software (Taraska et al., 2003) written in Matlab (Mathworks, Natick, MA). The parameters thus obtained were used to correct the cell images and resulted in a shift of 5 pixels or less. All images were acquired with MetaMorph software (Universal Imaging, Downingtown, PA).

All other images were obtained on inverted scanning confocal microscopes (LSM510 or Pascal, Carl Zeiss, Jena, Germany). Fluo-5F, EGFP, pHluorin and EMD were excited with the 488 nm argon line and emission was collected through a 100×/1.4 NA objective at >505 nm or 505-530 nm (Fig. 7). The theoretical optical resolution

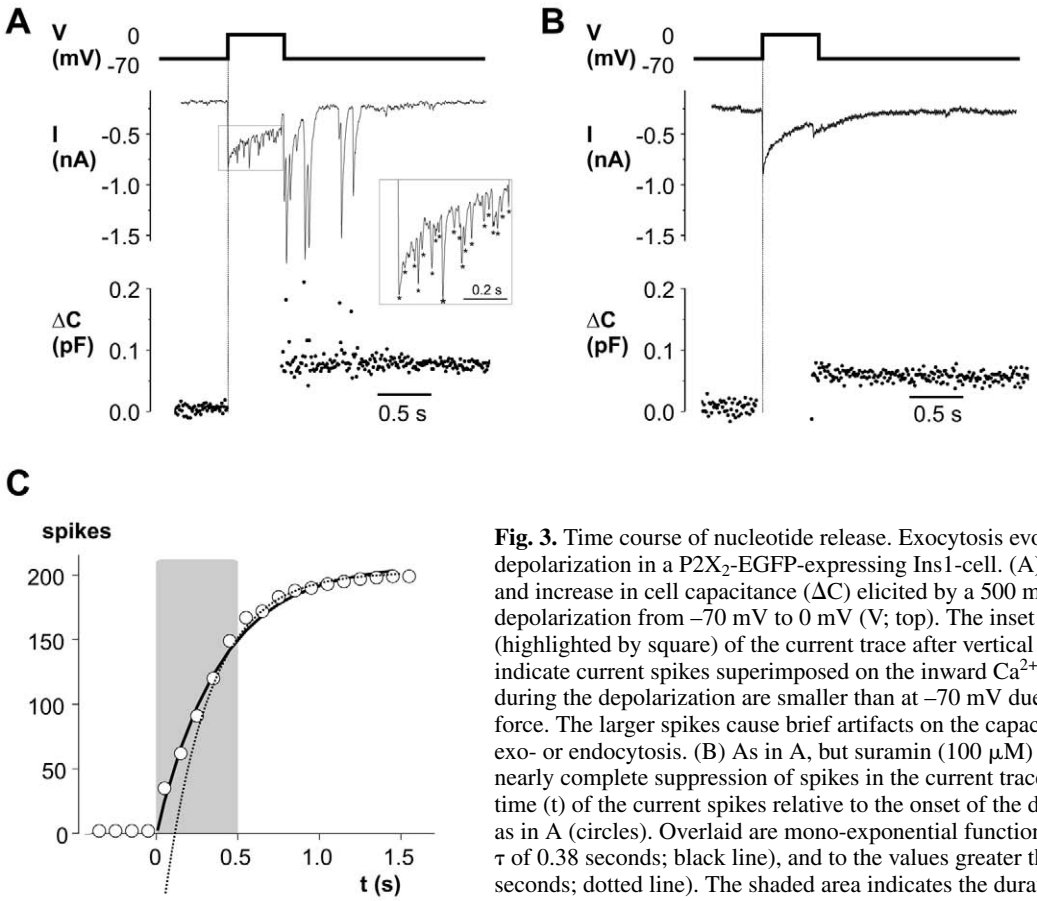


**Fig. 3.** Time course of nucleotide release. Exocytosis evoked by voltage-clamp depolarization in a $P2X_2$-EGFP-expressing Ins1-cell. (A) Membrane currents (I; middle) and increase in cell capacitance (ΔC) elicited by a 500 millisecond voltage-clamp depolarization from –70 mV to 0 mV (V; top). The inset shows the indicated part (highlighted by square) of the current trace after vertical and horizontal expansion. Asterisks indicate current spikes superimposed on the inward $Ca^{2+}$-current (identified by eye). Spikes during the depolarization are smaller than at –70 mV due to the reduced inward driving force. The larger spikes cause brief artifacts on the capacitance trace that are unrelated to exo- or endocytosis. (B) As in A, but suramin (100 μM) was applied to the cell, resulting in nearly complete suppression of spikes in the current trace. (C) Cumulative histogram of the time (t) of the current spikes relative to the onset of the depolarization in eleven experiments as in A (circles). Overlaid are mono-exponential functions fitted to all points (time constant τ of 0.38 seconds; black line), and to the values greater than 500 milliseconds (τ of 0.28 seconds; dotted line). The shaded area indicates the duration of the depolarizing stimulus.

with this configuration is 213 nm (Abbe's criterion), and we scanned at 0.12 μm/pixel (Figs 4-6), 0.6 μm/pixel (Fig. 7C,D) or 0.18 μm/pixel (Fig. 1C). In the experiment shown in Fig. 5, ECFP was excited at 458 nm and detected at 465-495 nm on the forward scan. On the return scan of each line, pHluorin was excited at 514 nm and detected at <560 nm. The scan speed was 1.5 milliseconds per line pair. At the settings used, 19±5% ($n$=16) of the signal in the pHluorin channel crosstalks into the ECFP channel. The bottom layer of granules (referred to as the footprint of the cell) was found by moving the focal plane upwards from below the cell towards the plane with the maximum intensity of the first appearing granules. For display purposes, the images shown in Fig. 5 have been averaged over four consecutive frames.

In Fig. 6, electrophysiological detection of ATP release was combined with simultaneous optical detection of IAPP-pHluorin in the entire cell. We employed a 40×/1.25W objective, the plane of focus was set in the center of the cell, and the axial resolution was reduced by opening the confocal pinhole to its maximum setting. The measured point-spread function in this configuration has an axial width of 7.3 μm at half-maximum, comparable with the height of Ins1-cells adhering to the coverslip (Barg et al., 2002). Electrophysiology and imaging were synchronized by trigger signals generated by the Pulse software or (in Fig. 6) the confocal microscope.

### Image analysis

LDCVs undergoing exocytosis were detected manually by repeatedly playing the movies fast forward and reverse. The fluorescence intensity was then determined by defining a circular region-of-interest (ROI) of about 0.5 μm diameter at the spot where an event occurred. The data are displayed either as the mean of the ROI (8-bit resolution) divided by the initial fluorescence ($F/F_0$; for EGFP, EMD and ECFP), or divided by the peak fluorescence ($F/F_{peak}$; for pHluorin). In Fig. 6A,B local background was measured in an area close to the granule and subtracted from the raw data. In Fig. 6C,D, a ROI was defined around the entire cell (see Fig. 6C,D, white line) and corrected by the average value of a background ROI defined outside the cell, for each frame.

### Dextran uptake

For uptake experiments, Ins1-cells plated on coverslips were first incubated in standard EC (see Solutions) at 34°C for 30 minutes. Exocytosis was then stimulated using a buffer containing (mM) 83.6 NaCl, 60 KCl, 1.2 $MgCl_2$, 2.6 $CaCl_2$, 5 HEPES (adjusted to pH 7.4 with NaOH), 1 glucose, and 14 μM Alexa568-hydrazine (Molecular Probes, Eugene, OR) for 30 seconds. The cells were then washed five times with ice-cold EC before fixation in formaldehyde (3%). Cells were imaged using a confocal microscope as described above. Random co-localization was estimated as 7% in image pairs in which the two channels had been brought out of register by rotation and/or mirroring. It was ascertained by imaging neighboring planes that co-localized vesicles were spherical and located in the same plane.

### Statistical evaluation

Data are quoted as the mean values ±s.e.m. of indicated number of experiments or cells as indicated. Non-linear fitting was done in Origin (OriginLab, Northampton, MA, USA). Statistical significances were evaluated using Student's $t$-test.

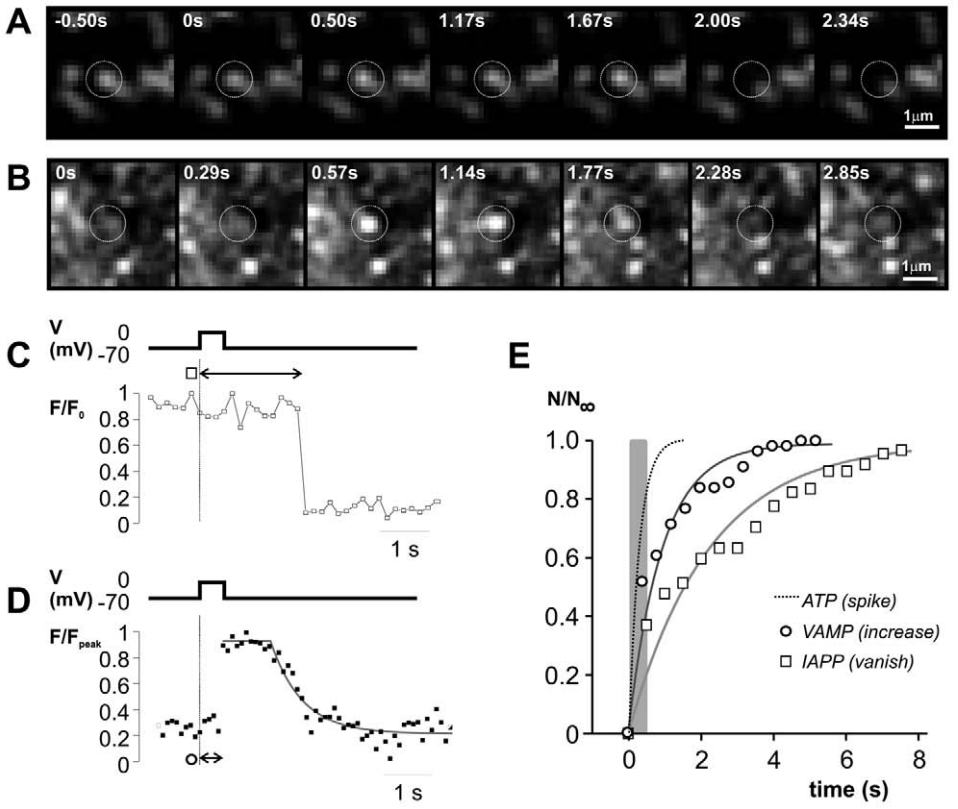


**Fig. 4.** Time course of peptide release and luminal pH changes. (A,B) Cells expressing VAMP-pHluorin or IAPP-emerald (IAPP-EMD) were voltage-clamped and their footprint imaged at 10 Hz. Example images taken in separate cells transfected with IAPP-EMD (A) or VAMP-pHluorin (B) at the indicated times relative to the onset of a 500 millisecond depolarization from –70 mV to zero mV. (C) Time course of IAPP-EMD fluorescence (lower trace) in the ROI indicated by the circle in A in response to a 500 millisecond depolarization (top trace). Note that the IAPP-EMD fluorescence disappears after a delay of ≈2 seconds. (D) As in C for the experiment shown in B. Note that the VAMP-pHluorin trace rises abruptly to a plateau from which it declines mono-exponentially after a delay of ≈1 second. The gray line superimposed on the data points represents the best fit of a discontinuous function consisting of a straight-line segment followed by a mono-exponential decay to the remainder of the trace, using the first point of the rising phase as the start of the event. (E) Cumulative histograms showing the time, relative to stimulation, of the loss of IAPP-EMD fluorescence (squares), the increase in VAMP-pHluorin fluorescence (circles) analyzed as indicated by arrows in C and D. The functions superimposed on histograms in E are exponential functions fitted to the distributions yielding τ-values of 0.9±0.1 (circles), and 2.2±0.2 seconds (squares). For comparison, the function from Fig. 3B (fit to the nucleotide release data >500 milliseconds) is included as a dotted line.

## Results

### Release of adenine nucleotides from insulin-containing LDCVs

To investigate the time course of nucleotide release from LDCVs we transfected GFP-labeled purinergic receptors ($P2X_2$-GFP or $P2X_2$-mRFP1 (Khakh et al., 2001), into clonal Ins1-cells. In these cells, release of adenine nucleotides from LDCV will evoke 'autaptic' activation of the expressed $P2X_2$-channels and give rise to transient inward whole-cell currents similar to the excitatory postsynaptic currents (EPSCs) that can be recorded from neurons. It was ascertained that functional $P2X_2$-receptors were uniformly expressed in the plasma membrane (Fig. 1A-C) (see Materials and Methods for details). Cells expressing $P2X_2$-EGFP were then voltage-clamped at –70 mV and the receptors activated by brief exposure to 0.2 mM ATP. The application of ATP evoked large and rapidly activating inward currents with an average magnitude of 3.2±0.4 nA ($n$=13, not shown). Voltage ramps from –100 to +30 mV during the application of ATP confirmed that the $P2X_2$ currents exhibited strong inward rectification and the current amplitude at zero mV was only 6±3% ($n$=8) of that seen at –70 mV (Fig. 2A).

We elicited exocytosis in cells expressing $P2X_2$-EGFP by dialyzing the cytosol with a pipette solution containing 2 μM free $Ca^{2+}$, while holding the membrane potential at –70 mV. Shortly after formation of the whole-cell configuration, inward current spikes were observed (Fig. 2B,C). Of the 1640 events recorded, 559 were single spikes were sufficiently separated from neighboring spikes to allow more detailed analysis. On average, these spikes reached a peak amplitude of 500±30 pA, had a rise time (10-90%) of 5.0±0.1 milliseconds, deactivated mono-exponentially with a time constant of 16±1 milliseconds and carried an average charge of 10±1 pC. A pre-spike feature, reminiscent of the 'foot' described in amperometric recordings from chromaffin cells (Chow et al., 1992), was observed in only 3% of the events (not shown). We repeated the experiment and recorded the increase in whole-cell membrane capacitance in parallel (Fig.

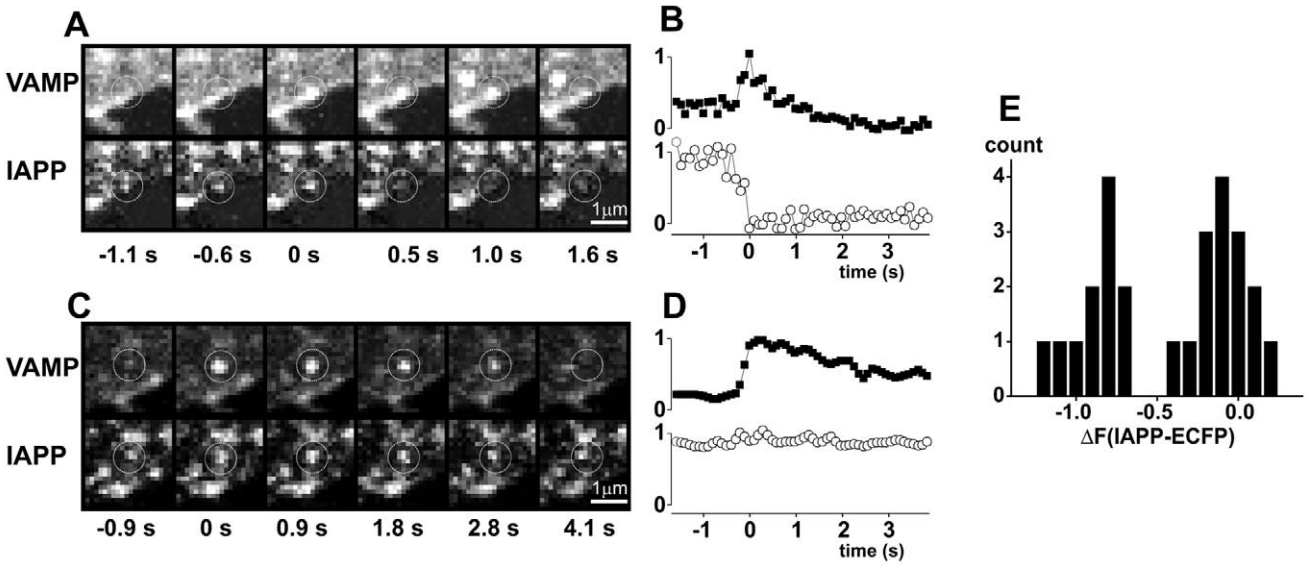


**Fig. 5.** Exocytosis does not necessarily lead to peptide release. (A,C) Simultaneous imaging of VAMP-pHluorin (top) and IAPP-ECFP (lower) in double-transfected cells. The cell (imaged at 10 Hz) was stimulated with a 3 second puff of solution containing 87 mM KCl. Times quoted below the images are relative to the peak in the VAMP-pHluorin signal. (A) Example of a granule (highlighted by a circle) that showed a transient increase in VAMP-pHluorin fluorescence and that culminated in the loss of IAPP-ECFP fluorescence. (B) Fluorescence intensities of IAPP-ECFP (open circles) and VAMP-pHluorin (black squares) within ROIs centered on the granule highlighted in A. (C) Example where the increase in VAMP-pHluorin fluorescence was not associated with the rapid loss of IAPP-ECFP fluorescence. (D) As in B, but for the granule shown in C. (E) Analysis of IAPP-ECFP fluorescence in 28 cells and in A,C. Data in the histogram were derived from traces as in B and D by subtracting the intensity measured at t=5.25 seconds from that at –1.0 second, both averaged over 0.5 second.

2D). In four separate experiments, a mean of 1000±541 spikes was observed during the first 400 seconds, and the associated capacitance increase was 895±87 fF. From these values, we estimate the unitary capacitance increase to be ~0.9 fF/spike assuming that endocytosis is negligible under these experimental conditions. However, no capacitance increase occurred during the first ~50 seconds, while spiking happened at about the same frequency during the entire 400 s. This finding is consistent with endocytosis taking place mainly during the first minute of the recoding, before necessary cytosolic factors may have been washed out. To avoid this effect, regression lines were fit to the data between 100 and 400 seconds, which yielded slopes of 2.62 fF per second for the capacitance increase, and 2.65 spikes per second for the $P2X_2$-currents. With these values the unitary capacitance increase calculates to 1.0 fF per spike, in reasonable agreement with the 0.8 fF obtained by high-resolution cell-attached capacitance (MacDonald et al., 2005). In conclusion, expression of $P2X_2$ in the cell of interest allows reliable detection of nucleotide release from single granules, with millisecond time resolution.

## Time course of nucleotide release

We exploited the $P2X_2$ receptor-based assay to determine the time course of nucleotide release in response to a single voltage-clamp depolarization. Ins-1 cells are well suited for this type of stimulus because exocytosis is tightly coupled to $Ca^{2+}$-influx and essentially limited to the duration of the stimulus (Barg et al., 2002; Yang et al., 2002). We recorded membrane capacitance and currents in cells expressing $P2X_2$-EGFP, and applied a single depolarization lasting 500 milliseconds. In the experiment shown in Fig. 3A, the observed capacitance increase of 70 fF was confined to the duration of the depolarization and no further increase occurred after the voltage was stepped back to –70 mV. This corresponds to the release of 88 granules using a conversion factor of 0.8 fF per granule (MacDonald et al., 2005). In parallel, we detected a series of transient inward currents that resembled the spikes observed during intracellular $Ca^{2+}$ infusion (cf. Fig. 2B). As shown by the inset, numerous current spikes (highlighted by asterisks) were superimposed on the $Ca^{2+}$-current and continued for ~1 seconds after the end of the stimulation. In this experiment, 12 events were observed while there was no further increase in cell capacitance. As expected from the current-voltage relationship of the ATP-gated current (Fig. 2A), the spikes observed at –70 mV were ≈20-fold larger than those seen during the depolarization. Inclusion of the purinergic antagonist suramin (100 μM) in the extracellular solution had no effect on the capacitance increase but almost abolished the current spikes (Fig. 3B), confirming that they result from activation of purinergic receptors. In a series of ten experiments as in Fig. 3A, a total of 199 current spikes were detected, 50 of which occurred after the end of the depolarization. The histogram in Fig. 3C shows the cumulative latency histogram of these events, measured from the onset of the depolarization to the peak of the spike. Approximating a single exponential function to the data suggests that ATP is released with a time constant (τ) of 385 milliseconds, which is ~4-fold slower than the time course of capacitance increase (Barg et al., 2002). However, because not all current spikes can be resolved during the depolarization, this value is likely

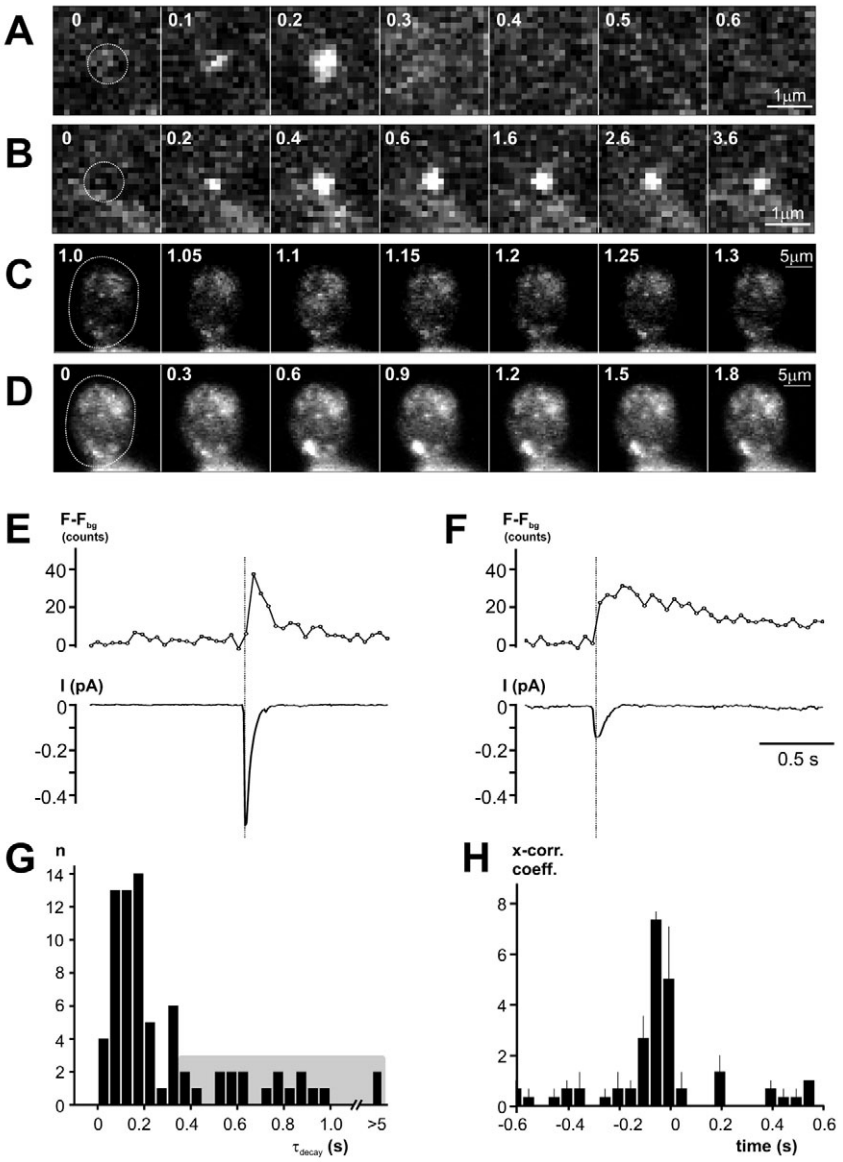


**Fig. 6.** Parallel recording of nucleotide and peptide release from individual granules. (A,B) Confocal images of a section of the footprint of a voltage-clamped cell expressing both IAPP-pHluorin and P2X$_2$-mRFP. The images were recorded at the indicated times relative the onset of the IAPP-pHluorin flash. Exocytosis was elicited by intracellular dialysis of the cell with a buffer in which $[Ca^{2+}]_i$ was set at 2 μM. Note that the highlighted granules increase their fluorescence during the displayed sequence. In A, the signal from the granule is rapidly lost, while in B it remains elevated for several seconds. (C,D) Image sequences of a cell co-transfected with IAPP-pHluorin and P2X$_2$-mRFP1 and stimulated as in A and B. The entire cell was imaged in the IAPP-pHluorin channel (see Materials and Methods), and whole-cell current spikes due to activation of the P2X$_2$ receptors were recorded in parallel. Examples of a short-lived fluorescence transient in C, and a long-lasting event in D. (E,F) Time course of the average fluorescence intensity in the ROIs indicated by the white circle in C and D (top) and inward membrane currents associated with the events (lower). Note slow decay of fluorescence in F. (G) Histogram of the decay constants of 56 events as in C and D. The shaded area indicates decay constants greater than 350 milliseconds. (H) Cross-correlation histogram of the times of fluorescence peaks vs the times of current peaks in three experiments similar to that shown in C and D.

underestimating the true rate of nucleotide release. When the fit was instead limited to only the 50 events observed after the pulse, when they could reliably be resolved, a τ of 280 milliseconds was derived (dotted line in Fig. 3C). In the latter case, the fitted curve extends below the ordinate, as expected if many events escaped detection. Both time constants are longer than that for the capacitance increase and we conclude that release of adenine nucleotides lags slightly (<200 milliseconds) behind membrane fusion.

## Time course of peptide release

We next monitored the time course of peptide release from Ins-1 cells using chimeric constructs of IAPP with various fluorescent proteins. These constructs result in soluble proteins that are correctly targeted to the granule lumen (Barg et al., 2002; Michael et al., 2004). To monitor the time course of peptide release without interference of granular pH changes, we tagged IAPP with the essentially pH-insensitive fluorescent protein emerald (EMD) (Tsien, 1998). Cells expressing IAPP-EMD were imaged in a plane adjacent to the coverslip with a confocal microscope and simultaneously voltage-clamped. We then applied the same single 500 millisecond depolarization stimulus as in Fig. 3, which resulted in the sudden loss of fluorescence from several IAPP-EMD labeled granules. Fig. 4A shows part of a cell where such an event occurred (granule highlighted by the circle). As illustrated in Fig. 4C, the fluorescence in the example of Fig. 4A was initially stable and then disappeared about 2 seconds after the onset of the stimulus. Vertical movement of the granule out of the focal plane is unlikely to account for the disappearance of fluorescence because the granule vanished within <100 milliseconds. The axial resolution of the microscope in these experiments was ~0.8 μm (estimated from the half-width at 10% intensity of the point-spread function). This suggests that the granules would have to move out of focus at speeds >8 μm per second to allow the fluorescence signal to decay by ⩾90%. This is almost ten-fold the maximum horizontal speed actually

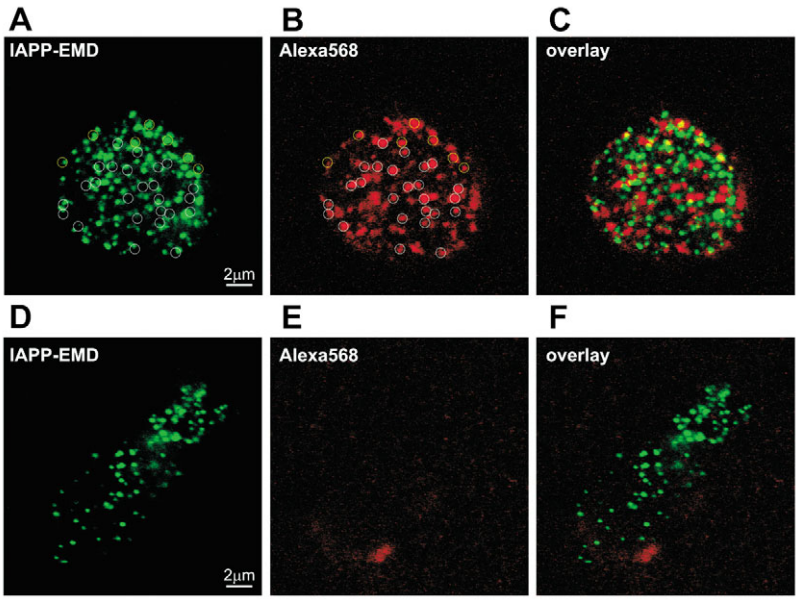


**Fig. 7.** Stimulation-dependent uptake of endocytotic tracer dye. (A-C) Uptake of Alexa563-hydrazine (red; B) in cells expressing IAPP-emerald (green; A). Vesicles containing only Alexa563-hydrazine are highlighted by white circles, and vesicles containing both labels are highlighted by yellow circles and appear yellow when the images are merged, as shown in C. Exocytosis was stimulated for 30 seconds with 87 mM KCl, followed by washing on ice. (D-F) As in A-C, but the cells were incubated in standard EC solution (5 mM KCl) containing Alexa563-hydrazine.

observed in these cells (<1 μm per second) (Ivarsson et al., 2004). From records such as in Fig. 4C we determined the time of fluorescence loss, relative to the onset of the depolarization. The data are plotted in a cumulative histogram in Fig. 4E and can be described by an exponential function with a time constant $\tau$=2.2±0.2 seconds. This is similar to the value we reported previously for the release of IAPP-EGFP (Barg et al., 2002) and ~6-fold slower than the time constant for nucleotide release determined above (dotted line).

## Time course of granule pH-equilibration

Mature granules have a luminal pH of ~5.5 that equilibrates during exocytosis with the extracellular pH. We took advantage of this feature to monitor granule fusion, by using the pH-sensitive fluorescent protein pHluorin fused to the luminal side of VAMP-2 (VAMP-pHluorin) (Miesenbock et al., 1998). In insulin-secreting cells, both endogenous VAMP and VAMP-EGFP are principally localized to granules (Regazzi et al., 1995; Tsuboi et al., 2004). We tested for co-localization in double-transfected Ins1-cells and found that 88±2% of the VAMP-pHluorin-positive vesicles also contained the granule-specific marker IAPP-mRFP1 ($n$=288 in 6 cells; data not shown). We also tested the effect of elevating the luminal pH on VAMP-pHluorin fluorescence. Bath application of $NH_4Cl$ (50 mM) resulted in an 11±2-fold increase in the fluorescence of VAMP-pHluorin-labeled granules ($n$=26 vesicle from 6 cells; not shown).

A similar increase in granule fluorescence is expected during exocytosis and should indicate fusion pore opening. We again imaged cells and subjected them to a single voltage-clamp depolarization, as in Fig. 4A. During and after the stimulus, several fluorescent puncta appeared throughout the cell. Fig. 4B shows an area of a cell in which such an event occurred (highlighted by a circle) and the dotted trace in Fig. 4D shows the mean fluorescence intensity within the circle indicated in Fig. 4B. The fluorescence in the spot suddenly increased at the end of the stimulus, stayed bright for another second and then decayed back to baseline. The initial rise occurred within a single frame (0.1 second). As discussed above, this is too quick to be accounted for by vertical granule movement. Contrary to what would be expected if the granule had collapsed into the plasma membrane, 39 of the granules (70%) retained more than two-thirds of their peak fluorescence one second after exocytosis. This confirms the previous finding in PC12 and Min6 cells that the granule stays morphologically intact at least temporally following exocytosis (Taraska et al., 2003; Tsuboi et al., 2004).

We quantified traces as in Fig. 4D by determining (1) the latency of the fluorescence increase relative to the stimulus (illustrated with an arrow in Fig. 4D), (2) the duration of the plateau period, and (3) the time constant of an exponential fit to the decay phase. The cumulative distribution of the latency for a total of 56 events (21 cells) is shown in Fig. 4E. The distribution increases monophasic and a single exponential fit yielded a time constant of $\tau$=0.9±0.1 seconds, which is intermediate between that of ATP release (<0.35) and peptide release (2.2 seconds) (Fig. 4A,C,D). The fluorescence remained then elevated for an average of 1.0±0.2 seconds (plateau phase), and the final decay phase had an average time constant of $\tau$=7.1±2.3 seconds (median 1.95 seconds). The rapid increase in fluorescence during the stimulus indicates that VAMP-pHluorin is a useful probe of exocytotic fusion. However, the decay phase is more ambiguous and may be caused either by pore closure and reacidification of the granule (Taraska and Almers, 2004) or by the escape of VAMP-pHluorin into the plasma membrane (Tsuboi and Rutter, 2003).

## Exocytosis without release of peptides

Since it is possible to detect both fusion pore opening and peptide release with fluorescent probes (Fig. 4), we next asked whether pore opening is always associated with peptide release. In these experiments, we co-transfected cells with VAMP-pHluorin and IAPP fused to the pH-insensitive enhanced cyan fluorescent protein (IAPP-ECFP). The cells

were imaged simultaneously in the ECFP and pHluorin channels and stimulated by local application of KCl (87 mM). A total of 32 exocytotic events (detected as transient increases in the pHluorin channel) were observed in 12 cells. In some of these events, the increase in pHluorin fluorescence was clearly associated with the abrupt disappearance of fluorescence from the corresponding spot in the IAPP-ECFP channel. An example is shown in Fig. 5A (granule highlighted with a circle), and Fig. 5B shows the associated fluorescence intensities in both channels for this granule. It can be seen that the IAPP-ECFP fluorescence vanished in <0.3 seconds and at the same time as the increase in VAMP-pHluorin. In other cases, the increase in pHluorin fluorescence occurred without concomitant decrease in ECFP-fluorescence. An example of such a granule is shown in Fig. 5C,D. The VAMP-pHluorin signal reached a peak within a fraction of a second, and then decayed slowly towards the original level. No significant change was detected in the IAPP-ECFP channel. We then quantified for the amount of IAPP-ECFP that was released by subtracting the granular ECFP-fluorescence immediately before the VAMP-pHluorin spike from that 5 seconds after the spike, both averaged over 0.5 seconds. In this analysis a value of zero corresponds to no release, and a value of –1 reflects complete release of IAPP-ECFP. The histogram of the 28 events that could be analyzed in this way (Fig. 5E) shows two clearly separated peaks, indicating that there was either complete release (peak around –1) or no release at all (peak around zero). This finding justifies grouping the data into eleven (39%) 'release' granules and seventeen (61%) 'no release' granules, and we conclude that in nearly two-thirds of the cases, exocytosis did not result in peptide release.

## Nucleotide release is independent of peptide release

We have found that the luminal pH can equilibrate during exocytosis without peptide release (Fig. 5), and that release of nucleotides is at least as fast as pH-equilibration (Fig. 4). By analogy, this makes it plausible that nucleotides could be selectively released from granules that retain their peptide contents during an exocytotic event. To test this possibility, we combined the electrophysiological detection of nucleotide release with $P2X_2$ and the optical detection of exocytosis and release. For the latter, we used IAPP-pHluorin as probe, which combines the advantages of being sensitive to the pH-change after pore opening and being a soluble peptide that is potentially released from the granule.

It was first ascertained that the IAPP-pHluorin reports exocytosis. We imaged the footprint of cells expressing both IAPP-pHluorin and $P2X_2$-mRFP. The cells were then voltage-clamped at –70 mV and exocytosis was evoked by dialyzing the cell interior through the patch pipette with a solution containing 2 μM free $Ca^{2+}$. Soon after establishing the whole cell configuration, discrete spots of transient increases in fluorescence were observed. The events could be classified into two classes. In the first type of events (52%), there was a rapid loss of fluorescence that often coincided with the appearance of a short-lived cloud of fluorescence centered at the original spot (Fig. 6A). In the second type, the fluorescence remained elevated for several seconds and then slowly decayed towards the baseline (Fig. 6B). We defined fluorescence increases that decayed with time constants (τ) of <350 milliseconds and >350 milliseconds as rapid and persistent events, respectively. The average time constants of the rapid and persistent events thus classified were 0.12±0.02 seconds (median 0.09 seconds; $n$=14 events from four cells) and 7.3±2.0 seconds (median 5.0 seconds; $n$=13 events). Based on the rapid decay and the association with a cloud of fluorescence (Fig. 6A, fourth frame) it seems plausible to interpret rapid events as release of IAPP-pHluorin. The persistent events are consistent with granules that retain IAPP-pHluorin after exocytosis and dim slowly because of a combination of bleaching and re-acidification.

Next, we correlated the optical measurements of IAPP-pHluorin release with electrophysiological detection of nucleotide release. Since the latter method is insensitive to the location of release events, we adapted the microscope to allow detection of fluorescence emanating from the entire cell (see Materials and Methods). When the experiment was repeated with these microscope settings, transient fluorescence increases could be still be observed. Fig. 6C,D shows examples of two such events; note that an entire cell is displayed. Events could not be reliably detected by eye in these movies, and we therefore plotted the average intensity of the entire cell (circled with a white line). Fig. 6E,F shows the fluorescence intensity for the events shown in C and D. Single exocytotic events can thus be resolved optically even at the level of an entire cell. From these traces we calculated the decay constants of all detected events, and plotted them in the histogram shown in Fig. 6G. It can be seen that 19 out of 75 events (28±6%, $n$=3 cells) had decay constants >350 milliseconds (mean value: 0.66±0.05 seconds; median 0.75 seconds) whereas the remaining 56 (72%) events had a time constant <350 milliseconds (mean value: 0.16±0.01 seconds; median 0.15 seconds).

At the same time we detected transient ATP-activated currents in these cells (Fig. 6E,F, lower), similar to those in Fig. 2B. We determined the time of every peak in the fluorescence and current traces, and stored them in separate event lists. Cross-correlation analysis (Fig. 6H) of the event lists revealed a distinct peak at –50 milliseconds, indicating that the peak of the IAPP-pHluorin fluorescence lagged behind that of the current spikes. This confirms the earlier observation that pH-equilibration during exocytosis is somewhat slower than nucleotide release (Fig. 4). To determine how many of the current spikes were associated with a fluorescence event, we scored events as coinciding when the two peaks occurred within 0.4 seconds of each other. This analysis reveales that 68±14% of the current spikes were associated with either transient or persistent changes in fluorescence. This indicates that we detect release of ATP from granules, rather than other types of secretory vesicles. The lack of complete correlation is expected because in transiently transfected cells, not all granules will contain IAPP-pHluorin. For example, 24 hours after transfection, ~30% of LDCVs identified by immunostaining for phogrin do not contain IAPP-EMD (not shown). However, the 52 granules for which exocytosis could be detected with both methods were not different from the entire sample of 75 granules, and the ratio of rapid events (71%, τ=0.15±0.01 seconds) and persistent events (29±5%, τ=0.65±0.06 seconds) was similar. We conclude that nucleotide release occurs during both rapid (72%) and persistent events (28%), the latter of which we interpret as absence of peptide release.

### Uptake of fluid phase tracer during exocytosis

Our data indicate that membrane fusion is not obligatorily associated with peptide release, and that some granules retain soluble peptides during exocytosis. We therefore tested whether such granules are able to reseal after exocytosis. To this end, we measured the vesicular uptake of the fluid phase marker Alexa568 ($M_r$ 0.7, comparable with the $M_r$ 0.5 for ATP) into cells expressing IAPP-EMD (Fig. 7A-F). Following stimulation with 87 mM external $K^+$ for 30 seconds, Alexa568 was rapidly taken up by into vesicles that were similar to IAPP-EMD labeled granules in apparent size and shape (Fig. 7B). Stained vesicles were confined to the rim just underneath the plasma membrane (not shown). Notably, 27±2% ($n$=10 cells) of all Alexa568-labeled vesicles also contained IAPP-EMD (Fig. 7C), indicating that these granules had undergone exocytosis without releasing (all of) the peptide marker. In control experiments, no uptake of Alexa-568 was detected in cells incubated in the same conditions but in a solution containing only 5 mM $K^+$ (Fig. 7D-F). Since labeling of granules with Alexa568 was resistant to extensive washing before fixation of the cells, we conclude that stained granules were no longer connected with the extracellular space.

## Discussion

### Differential release of small molecules and peptides

We have studied the time courses of membrane fusion, pH equilibration of the granule lumen, release of low-molecular-weight granule constituents and the exit of the peptide cargo associated with exocytosis in rat insulin-secreting Ins1-cells. Exocytosis in B-cells is initiated with a delay as short as 5-10 milliseconds after $Ca^{2+}$-influx (Barg et al., 2001). However, two key observations suggest that membrane fusion should not automatically be equated to instant and complete discharge of the secretory products. First, release is delayed relative to fusion of the granule with the plasmalemma. We found that release of adenine nucleotides was delayed by 0.1-0.2 seconds with respect to membrane fusion, and ATP-dependent current spikes were observed even after the capacitance had ceased to increase (Fig. 3A,C). A similar latency has been observed for serotonin release from insulin granules in experiments combining capacitance measurements and amperometry (Smith et al., 1999). Peptide release was delayed even further (~2 seconds on average) (Fig. 4A,C,E), consistent with our earlier study (Barg et al., 2002). Second, many granules stay structurally intact beyond the moment of fusion and the peptide cargo often remains within the granule after exocytosis (up to 70%, Fig. 5), confirming similar observations in neuroendocrine cells (Angleson et al., 1999; Holroyd et al., 2002; Perrais et al., 2004). In addition, we demonstrated here that nucleotides are released during exocytosis regardless of whether peptides are retained or not (Fig. 6). Taken together the data indicate that exocytosis of insulin granules can take two functionally different routes following membrane fusion: either complete emptying of the granule content, or selective release of only ions and small-molecular-weight compounds with (at most) partial release of the peptides.

### Storage and release of nucleotides

Amperometric current spikes from mast- and chromaffin cells frequently (50-70%) have a pre-spike feature (‘foot’) that is believed to result from slow release of catecholamine or serotonin through the initial fusion pore (Chow et al., 1992). Although in our experiments the $P2X_2$ receptors were uniformly distributed (Fig. 1) and thus likely to be situated in the immediate vicinity of the release sites, such pre-spike features were rarely (3%) seen. We speculate that the apparent absence of a foot results from differences in the chemical characteristics of amines and adenine nucleotides rather than differences in their size. While adenine nucleotides have a more extended molecular structure (diameter 0.9-1.5 nm) than catecholamine (<1 nm in all dimensions), efflux of these molecules is unlikely to be limited by the initial fusion pore (2-3 nm). We rather attribute the absence of a ‘foot’ to the nature of the storage of ATP in the granule. Charged transmitter molecules like ATP bind to a polyanionic matrix within the granule (Nanavati and Fernandez, 1993; Uvnäs and Åborg, 1988; Verdugo, 1991), which could prevent their release at least during the life time of the initial fusion pore. It is well established that the granule matrix of chromaffin and other cells contains chromogranins and charged proteoglycans (Kiang et al., 1982). Other proteins may be involved as well, and the luminal domain of the synaptic vesicle membrane protein SV2 has been shown to be part of the matrix of synaptic vesicles (Reigada et al., 2003). The granule matrix acts like an ion exchange resin where liberation of the bound transmitter molecules requires influx of ions into the granule lumen to replace the charged transmitter molecules (Marszalek et al., 1997; Nanavati and Fernandez, 1993; Uvnäs and Åborg, 1988; Verdugo, 1991). Such a mechanism would result in a post-fusion modulation of release, and could account for the delay in ATP release. The absence of a foot signal may therefore indicate that ATP is discharged through an already expanded fusion pore.

### Delayed peptide release

We show that the delay between fusion pore opening and peptide release is on average 2.2 seconds (Fig. 4A,C,E). It is not immediately evident why peptide release is even slower than ATP release but the bulkier nature of the peptide represents a possible explanation. This is suggested by the finding that the small tracer dye sulfonylrhodamine-B readily enters granules of B-cells, but influx of larger dextran-based tracer molecules is delayed (Takahashi et al., 2002). Thus, the rate and latency of tracer influx into the exocytosing granule depends on the molecular size of the tracer, which has been interpreted as gradual expansion of the pore. Insulin is stored in the granule as a $Zn_2$-insulin$_6$ crystal, and the dimensions of this crystal suggest that their release would require a pore diameter of at least 5 nm. Thus, the rate fusion pore dilation may determine the onset of peptide release. Alternatively, it can be envisioned that the insulin crystal has to be dissolved prior to release. This process may take some time and its rate depends on environmental factors. For example neutralization of the luminal pH, which we found to be delayed by 0.9 seconds with respect to fusion pore formation (Fig. 4B,D,E), results in decreased stability of the insulin crystal (Hutton,

1994). Aggregation of matrix and cargo proteins could therefore prevent release of peptides until their mobilization is triggered by a change in the ionic composition of the lumen.

### Is differential release mediated via transient fusion?

Traditionally, insulin granules have been thought to collapse into the plasma membrane during exocytosis (full fusion). This may have been the case for some of the granules we studied; most notably those where the VAMP-pHluorin signal had a rapid decay phase (Figs 4, 5). However, we often observed a plateau phase in the VAMP-pHluorin signal, which indicates that the granules did not collapse immediately. Indeed, there is now good evidence that a significant fraction of granules remains structurally intact after exocytosis (Barg et al., 2002; Perrais et al., 2004; Taraska and Almers, 2004; Taraska et al., 2003; Tsuboi et al., 2004; Tsuboi et al., 2000; Vo et al., 2004). Confirming these studies, we report here that in up to two-thirds of the exocytotic events the labeled IAPP remained at the site of the granule. Furthermore, the extracellular tracer dye Alexa568 was trapped in a stimulus-dependent manner in granules that still contained the release marker IAPP-EGFP (Fig. 7). Since the molecular weight of Alexa568 ($M_r$ 0.7) is comparable with that of ATP ($M_r$ 0.5), it seems probable that ATP exited the granules that were filled with the dye. Together with the fact that dye accumulation was insensitive to extensive washing, this indicates that the granules had undergone exocytosis, released small compounds like nucleotides and then closed their pores to pinch off of the plasma membrane.

How is the mode of exocytosis (full fusion vs transient exocytosis) related to the mode of release from a granule (partial or complete)? It is tempting to equate transient exocytosis with partial cargo release because the duration of the transient fusion pore openings is long in relation to the time it takes for nucleotide release (Fig. 3C and Fig. 4E). In addition, we observed nucleotide release from granules engaged in transient exocytosis (Fig. 6F). This finding is in line with previous reports that chromaffin granules completely release their acetylcholine content during transient fusion (Albillos et al., 1997). By contrast, peptide release was restricted in the majority of exocytosis events (Figs 5, 6). This finding agrees with data from PC12 and Min6 cells, where exocytosis did not necessarily lead to release (Holroyd et al., 2002; Tsuboi and Rutter, 2003). Assuming that the duration of the plateau phase in VAMP-pHluorin experiments (1 second) reports the time during which the pore remains open, premature closure of the pore is a likely mechanism by which release of peptides (delay of 2.2 seconds after exocytosis) is prevented (Fig. 4). There is evidence that granules that are retrieved intact in this manner remain fusion competent and are able to bypass the endosomal recycling pathway (Vo et al., 2004). The presence of nucleotide transporters in insulin granules supports the idea that such recaptured granules can be recycled by simple refilling with the nucleotide (Bankston and Guidotti, 1996). A similar mechanism has been postulated for chromaffin granules (Tabares et al., 2001). Granule recycling by transient exocytosis and refilling with transmitter provides the cell with a secretory pathway that avoids sorting, concentration and internalization of the granular components.

While it seems plausible that such rapid endocytic retrieval of granules is achieved simply by reversal of fusion pore opening, such a mechanism is not compatible with the experimental evidence. To accommodate the large and bulky peptide hormones, the fusion pore must expand to diameters >5-10 nm, while capacitance measurements indicate that formation of the fusion pore is reversible only as long as the diameter remains below 2-3 nm (Albillos et al., 1997; Breckenridge and Almers, 1987). Thus, whenever peptide release occurs during transient exocytosis, the pore is unlikely to close by reversal of the fusion reaction. A recent study provided evidence that in Min6 cells the GTPase dynamin, but not other endocytosis-related proteins, is required for stabilization of the granule and pore closure (Tsuboi et al., 2004). It is likely that other proteins will be implicated in this process in the future. Finally, it seems plausible that B-cells would control the differential release of nucleotides and peptides depending on the metabolic state of the body. Future work should therefore address whether a defect in this regulation could underlie certain aspects of human diabetes.

We thank W. Almers (Portland, OR; supported by NIH MH-60600) for the use of equipment, B. Khakh (Cambridge, UK), J. Rothman (Sloan Kettering, USA) and R. Tsien (San Diego, USA) for supplying plasmids, D. Machado (La Laguna, Tenerife, Spain) for helpful discussion and K. Borglid for technical assistance. Supported by the Swedish Research Council (Vetenskapsrådet) Swedish Strategic Research Foundation, the Göran Gustafssons Stiftelse for Research in the Natural Sciences and Medicine, the European Foundation for the Study of Diabetes (Albert Renold Award), the Juvenile Diabetes Research Foundation, the Swedish Diabetes Association, the Crafoord Foundation, the Novo Nordisk Foundation, the Royal Physiographic Society, and Thurings Stiftelse and the Wellcome Trust. P.R. is a Royal Society Wolfson research fellow. S.B. was a recipient of an EMBO long-term fellowship during part of this study.

## References

**Albillos, A., Dernick, G., Horstmann, H., Almers, W., Alvarez de Toledo, G. and Lindau, M.** (1997). The exocytotic event in chromaffin cells revealed by patch amperometry. *Nature* **389**, 509-512.

**Ales, E., Tabares, L., Poyato, J. M., Valero, V., Lindau, M. and Alvarez de Toledo, G.** (1999). High calcium concentrations shift the mode of exocytosis to the kiss-and-run mechanism. *Nat. Cell. Biol.* **1**, 40-44.

**Alvarez de Toledo, G., Fernandez-Chacon, R. and Fernandez, J. M.** (1993). Release of secretory products during transient vesicle fusion. *Nature* **363**, 554-558.

**Angleson, J. K., Cochilla, A. J., Kilic, G., Nussinovitch, I. and Betz, W. J.** (1999). Regulation of dense core release from neuroendocrine cells revealed by imaging single exocytic events. *Nat. Neurosci.* **2**, 440-446.

**Aravanis, A. M., Pyle, J. L. and Tsien, R. W.** (2003). Single synaptic vesicles fusing transiently and successively without loss of identity. *Nature* **423**, 643-647.

**Archer, D. A., Graham, M. E. and Burgoyne, R. D.** (2002). Complexin regulates the closure of the fusion pore during regulated vesicle exocytosis. *J. Biol. Chem.* **277**, 18249-18252.

**Asfari, M., Janjic, D., Meda, P., Li, G., Halban, P. A. and Wollheim, C. B.** (1992). Establishment of 2-mercaptoethanol-dependent differentiated insulin-secreting cell lines. *Endocrinology* **130**, 167-178.

**Bankston, L. A. and Guidotti, G.** (1996). Characterization of ATP transport into chromaffin granule ghosts. Synergy of ATP and serotonin accumulation in chromaffin granule ghosts. *J. Biol. Chem.* **271**, 17132-17138.

**Barg, S., Ma, X., Eliasson, L., Galvanovskis, J., Göpel, S. O., Obermüller, S., Platzer, J., Renström, E., Trus, M., Atlas, D. et al.** (2001). Fast exocytosis with few $Ca^{2+}$ channels in insulin-secreting mouse pancreatic B cells. *Biophys. J.* **81**, 3308-3323.

**Barg, S., Olofsson, C. S., Schriever-Abeln, J., Wendt, A., Gebre-Medhin, S., Renström, E. and Rorsman, P.** (2002). Delay between fusion pore opening and peptide release from large dense-core vesicles in neuroendocrine cells. *Neuron* **33**, 287-299.

**Breckenridge, L. J. and Almers, W.** (1987). Currents through the fusion pore that forms during exocytosis of a secretory vesicle. *Nature* **328**, 814-817.
**Ceccarelli, B., Hurlbut, W. P. and Mauro, A.** (1973). Turnover of transmitter and synaptic vesicles at the frog neuromuscular junction. *J. Cell Biol.* **57**, 499-524.
**Chow, R. H., von Rüden, L. and Neher, E.** (1992). Delay in vesicle fusion revealed by electrochemical monitoring of single secretory events in adrenal chromaffin cells. *Nature* **356**, 60-63.
**Detimary, P., Jonas, J. C. and Henquin, J. C.** (1995). Possible links between glucose-induced changes in the energy state of pancreatic B cells and insulin release. Unmasking by decreasing a stable pool of adenine nucleotides in mouse islets. *J. Clin. Invest.* **96**, 1738-1745.
**Han, X., Wang, C. T., Bai, J., Chapman, E. R. and Jackson, M. B.** (2004). Transmembrane segments of syntaxin line the fusion pore of $Ca^{2+}$-triggered exocytosis. *Science* **304**, 289-292.
**Hartmann, J. and Lindau, M.** (1995). A novel $Ca^{2+}$-dependent step in exocytosis subsequent to vesicle fusion. *FEBS Lett.* **363**, 217-220.
**Heuser, J. E. and Reese, T. S.** (1973). Evidence for recycling of synaptic vesicle membrane during transmitter release at the frog neuromuscular junction. *J. Cell Biol.* **57**, 315-344.
**Holroyd, P., Lang, T., Wenzel, D., De Camilli, P. and Jahn, R.** (2002). Imaging direct, dynamin-dependent recapture of fusing secretory granules on plasma membrane lawns from PC12 cells. *Proc. Natl. Acad. Sci. USA* **99**, 16806-16811.
**Hutton, J. C.** (1994). Insulin secretory granule biogenesis and the proinsulin-processing endopeptidases. *Diabetologia* **37 Suppl. 2**, S48-S56.
**Ivarsson, R., Obermüller, S., Rutter, G. A., Galvanovskis, J. and Renström, E.** (2004). Temperature-sensitive random insulin granule diffusion is a prerequisite for recruiting granules for release. *Traffic* **5**, 750-762.
**Khakh, B. S., Smith, W. B., Chiu, C. S., Ju, D., Davidson, N. and Lester, H. A.** (2001). Activation-dependent changes in receptor distribution and dendritic morphology in hippocampal neurons expressing $P2X_2$-green fluorescent protein receptors. *Proc. Natl. Acad. Sci. USA* **98**, 5288-5293.
**Kiang, W. L., Krusius, T., Finne, J., Margolis, R. U. and Margolis, R. K.** (1982). Glycoproteins and proteoglycans of the chromaffin granule matrix. *J. Biol. Chem.* **257**, 1651-1659.
**Kirshner, N., Sage, H. J., Smith, W. J. and Kirshner, A. G.** (1966). Release of catecholamines and specific protein from adrenal glands. *Science* **154**, 529-531.
**Lindau, M. and Almers, W.** (1995). Structure and function of fusion pores in exocytosis and ectoplasmic membrane fusion. *Curr. Opin. Cell Biol.* **7**, 509-517.
**Lollike, K., Borregaard, N. and Lindau, M.** (1998). Capacitance flickers and pseudoflickers of small granules, measured in the cell-attached configuration. *Biophys. J.* **75**, 53-59.
**MacDonald, P. E., Obermüller, S., Vikman, J., Galvanovskis, J., Rorsman, P. and Eliasson, L.** (2005). Regulated exocytosis and kiss-and-run of synaptic-like microvesicles in INS-1 and primary rat β-cells. *Diabetes* **54**, 736-743.
**Marszalek, P. E., Farrell, B., Verdugo, P. and Fernandez, J. M.** (1997). Kinetics of release of serotonin from isolated secretory granules. II. Ion exchange determines the diffusivity of serotonin. *Biophys. J.* **73**, 1169-1183.
**Michael, D. J., Geng, X., Cawley, N. X., Loh, Y. P., Rhodes, C. J., Drain, P. and Chow, R. H.** (2004). Fluorescent cargo proteins in pancreatic β-cells: design determines secretion kinetics at exocytosis. *Biophys. J.* **87**, L03-L05.
**Miesenbock, G., De Angelis, D. A. and Rothman, J. E.** (1998). Visualizing secretion and synaptic transmission with pH-sensitive green fluorescent proteins. *Nature* **394**, 192-195.
**Nanavati, C. and Fernandez, J. M.** (1993). The secretory granule matrix: a fast-acting smart polymer. *Science* **259**, 963-965.
**Perrais, D., Kleppe, I. C., Taraska, J. W. and Almers, W.** (2004). Recapture after exocytosis causes differential retention of protein in granules of bovine chromaffin cells. *J. Physiol.* **560**, 413-428.
**Regazzi, R., Wollheim, C. B., Lang, J., Theler, J. M., Rossetto, O., Montecucco, C., Sadoul, K., Weller, U., Palmer, M. and Thorens, B.** (1995). VAMP-2 and cellubrevin are expressed in pancreatic β-cells and are essential for $Ca^{2+}$-but not for GTPγS-induced insulin secretion. *EMBO J.* **14**, 2723-2730.
**Reigada, D., Diez-Perez, I., Gorostiza, P., Verdaguer, A., Gomez de Aranda, I., Pineda, O., Vilarrasa, J., Marsal, J., Blasi, J., Aleu, J. et al.** (2003). Control of neurotransmitter release by an internal gel matrix in synaptic vesicles. *Proc. Natl. Acad. Sci. USA* **100**, 3485-3490.
**Scepek, S., Coorssen, J. R. and Lindau, M.** (1998). Fusion pore expansion in horse eosinophils is modulated by $Ca^{2+}$ and protein kinase C via distinct mechanisms. *EMBO J.* **17**, 4340-4345.
**Smith, P. A., Proks, P. and Ashcroft, F. M.** (1999). Quantal analysis of 5-hydroxytryptamine release from mouse pancreatic beta-cells. *J. Physiol.* **521**, 651-664.
**Spruce, A. E., Breckenridge, L. J., Lee, A. K. and Almers, W.** (1990). Properties of the fusion pore that forms during exocytosis of a mast cell secretory vesicle. *Neuron* **4**, 643-654.
**Tabares, L., Ales, E., Lindau, M. and Alvarez de Toledo, G.** (2001). Exocytosis of catecholamine (CA)-containing and CA-free granules in chromaffin cells. *J. Biol. Chem.* **276**, 39974-39979.
**Takahashi, N., Kishimoto, T., Nemoto, T., Kadowaki, T. and Kasai, H.** (2002). Fusion pore dynamics and insulin granule exocytosis in the pancreatic islet. *Science* **297**, 1349-1352.
**Taraska, J. W. and Almers, W.** (2004). Bilayers merge even when exocytosis is transient. *Proc. Natl. Acad. Sci. USA* **101**, 8780-8785.
**Taraska, J. W., Perrais, D., Ohara-Imaizumi, M., Nagamatsu, S. and Almers, W.** (2003). Secretory granules are recaptured largely intact after stimulated exocytosis in cultured endocrine cells. *Proc. Natl. Acad. Sci. USA* **100**, 2070-2075.
**Tsien, R. Y.** (1998). The green fluorescent protein. *Annu. Rev. Biochem.* **67**, 509-544.
**Tsuboi, T. and Rutter, G. A.** (2003). Multiple forms of 'Kiss-and-Run' exocytosis revealed by evanescent wave microscopy. *Curr. Biol.* **13**, 563-567.
**Tsuboi, T., Zhao, C., Terakawa, S. and Rutter, G. A.** (2000). Simultaneous evanescent wave imaging of insulin vesicle membrane and cargo during a single exocytotic event. *Curr. Biol.* **10**, 1307-1310.
**Tsuboi, T., McMahon, H. T. and Rutter, G. A.** (2004). Mechanisms of dense core vesicle recapture following 'kiss and run' ('cavicapture') exocytosis in insulin-secreting cells. *J. Biol. Chem.* **279**, 47115-47524.
**Uvnäs, B. and Åborg, C. H.** (1988). Catecholamines (CA) and adenosine triphosphate (ATP) are separately stored in bovine adrenal medulla, both in ionic linkage to granule sites, and not as a non-diffusible CA-ATP-protein complex. *Acta Physiol. Scand.* **132**, 297-311.
**Verdugo, P.** (1991). Mucin exocytosis. *Am. Rev. Respir. Dis.* **144**, S33-S37.
**Viveros, O. H., Arqueros, L. and Kirshner, N.** (1969). Quantal secretion from adrenal medulla: all-or-none release of storage vesicle content. *Science* **165**, 911-913.
**Vo, Y. P., Hutton, J. C. and Angleson, J. K.** (2004). Recycling of the dense-core vesicle membrane protein phogrin in Min6 beta-cells. *Biochem. Biophys. Res. Commun.* **324**, 1004-1010.
**Wang, C. T., Grishanin, R., Earles, C. A., Chang, P. Y., Martin, T. F., Chapman, E. R. and Jackson, M. B.** (2001). Synaptotagmin modulation of fusion pore kinetics in regulated exocytosis of dense-core vesicles. *Science* **294**, 1111-1115.
**Yang, Y., Udayasankar, S., Dunning, J., Chen, P. and Gillis, K. D.** (2002). A highly $Ca^{2+}$-sensitive pool of vesicles is regulated by protein kinase C in adrenal chromaffin cells. *Proc. Natl. Acad. Sci. USA* **99**, 17060-17065.
**Zenisek, D., Davila, V., Wan, L. and Almers, W.** (2003). Imaging calcium entry sites and ribbon structures in two presynaptic cells. *J. Neurosci.* **23**, 2538-2548.
**Zimmerberg, J., Curran, M., Cohen, F. S. and Brodwick, M.** (1987). Simultaneous electrical and optical measurements show that membrane fusion precedes secretory granule swelling during exocytosis of beige mouse mast cells. *Proc. Natl. Acad. Sci. USA* **84**, 1585-1589.

# Global Elevations in Cytoplasmic Calcium Elicit Compound Exocytosis in Rat Pancreatic β-cells and Ins-1 Insulinoma Cells

**Michael B Hoppa[1], Jovita Karanauskaite[1], Lena Eliasson[2], Salma Hanna[3], Anne Clark[1], Patrick E MacDonald[3], and Patrik Rorsman[1*]**

[1]*Oxford Centre for Diabetes, Endocrinology and Metabolism, University of Oxford, Oxford, United Kingdom,*
[2]*Lund University Diabetes Centre, Clinical Research Center, Malmö, Sweden*
[3]*Department of Pharmacology and Alberta Diabetes Institute, Faculty of Medicine and Dentistry, University of Alberta, Edmonton, Alberta, Canada*

**Key Words**: compound exocytosis, muscarinic receptors, calcium, insulin, metabolism

**ABSTRACT**
Compound exocytosis is an event where the contents of several interconnected granules exit through a single fusion pore, but its significance as a mechanism of insulin release is unresolved. We have investigated its role in β-cells using electrophysiological, optical and ultrastructural techniques. Parallel recordings of changes in whole-cell capacitance with currents elicited by exocytosis of ATP and activation of $P2X_2$ receptors displayed a linear relationship between charge and capacitance. The capacitance increase per event estimated from these measurements was similar to that obtained by on-cell capacitance measurements and averaged 0.8 and 2.3 fF in Ins-1 and β-cells, respectively. A small proportion (~10%) of events fell outside of a normal distribution and had average magnitudes of charge and capacitance 6-fold larger than the means. On-cell capacitance measurements also detected a subset of events (7%) associated with capacitance increases 5-fold larger than the mean value. We propose that these large events reflect compound exocytosis. The electrophysiological observations were confirmed by live-cell imaging using TIRF microscopy measurements of exocytosis using the fluorescent protein chimera VAMP-pHluorin. Use of this technique also revealed that the likelihood of compound exocytosis increased 3-fold when carbachol was used to mobilize intracellular $Ca^{2+}$ stores to produce a global increase in $[Ca^{2+}]_i$. Our data suggest a mechanism of exocytosis that is consistent with granules prefusing in the cytosol prior to engagement with the plasma membrane, a conclusion underpinned by both confocal FM1-43 imaging and electron microscopy. We propose that multivesicular release becomes quantitatively important under conditions associated with a global elevation of $[Ca^{2+}]_i$ (such as muscarinic stimulation) and then accounts for up to 70% of exocytosis. .

## Introduction

Exocytosis is a process by which a cell delivers biomolecules into the extracellular space. In pancreatic β-cells, $Ca^{2+}$-dependent exocytosis is the process used to release insulin, the principal hypoglycemic hormone, in response to an elevation of the plasma glucose concentration. Insulin is stored in dense core vesicles (DCVs) with a

diameter of ~0.35 µm. Approximately 5% of the 10,000-13,000 DCVs in β-cells are situated in direct contact with the plasma membrane (Rorsman and Renstrom, 2003). Akin to neurons and chromaffin cells, exocytosis in the β-cell is triggered by $Ca^{2+}$-influx through plasmalemmal $Ca^{2+}$-channels. Traditionally, exocytosis is thought to involve fusion of individual DCVs with the plasma membrane and this appears to be the most common form of exocytosis in the β-cell. Although the $Ca^{2+}$-channel density in β-cells is only 5-10% of that in chromaffin cells (Barg et al., 2001), the β-cell is capable of exocytosis (monitored as increase in cell capacitance) at a rate approaching that seen in chromaffin cells (Fenwick et al., 1982; Gillis and Misler, 1992; Ammala et al., 1993; Klingauf and Neher, 1997).

The rapid coupling-uncoupling of $Ca^{2+}$-channels to DCVs could represent a bottleneck to maintain high rates of exocytosis in the β-cell. One way to avoid this would be multivesicular compound exocytosis, a process where prefused granules undergo exocytosis as a single entity. In this way, the interlinked DCVs would only have to have one DCV in an appropriate site for fusion and other granules can "piggy-back" through this fusion site to release their contents in response to influx of $Ca^{2+}$ through a single $Ca^{2+}$-channel (or a single cluster of channels). This would enhance the secretory responses during conditions of increased insulin requirements. There is evidence that this occurs in eosinophils (Lollike et al., 2002; Hafez et al., 2003), lactotrophs (Cochilla et al., 2000) and exocrine pancreatic cells (Nemoto et al., 2001), but the situation in electrically excitable cells is less well established. In β-cells, early ultrastructural (Dahl and Henquin, 1978; Orci and Malaisse, 1980) and electrochemical (Bokvist et al., 2000) measurements indicate that compound exocytosis does occur, albeit infrequently. More recently, attempts to resolve this by live cell imaging has produced conflicting results (Takahashi et al., 2004; Kwan and Gaisano, 2005; Takahashi and Kasai, 2007). The existence and significance of compound exocytosis in β-cells therefore remains debated.

In this study we monitored exocytosis of insulin granules using a $P2X_2$ receptor-based assay (Obermuller et al., 2005) and correlated these data with changes in membrane capacitance, microscopy and ultrastructural studies. Our data suggest that compound exocytosis, although rare under the experimental conditions studied previously, is a significant mechanism of insulin release and becomes quantitatively dominant following a global elevation of $[Ca^{2+}]_i$ such as that evoked in response to vagal (muscarinic) stimulation of insulin secretion.

## Materials and Methods

### Culture and transfection of Ins-1 Cells

Clonal Ins-1 cells were cultured as previously described (Obermuller *et al.*, 2005). Lipofectamine2000 (Invitrogen) was used for transfection according to manufacturer's instruction, and cells were used 1 day after transfection.

### Preparation of β-Cells

Pancreatic islets were isolated from Sprague-Dawley rats as previously described (Braun et al., 2007). For expression of VAMP, the cells were plated densely onto 18 mm glass coverslips coated with poly-L-lysine (Sigma) and allowed to rest for 18 hours. $P2X_2$-GFP was expressed by use of an adenovirus infection (Obermuller *et al.*, 2005).

**$P2X_2$ current and capacitance measurements**

Thick-walled patch electrodes (O.D. 1.5 mm, I.D. 0.86 mm; 5-9 MΩ resistance pulled from borosilicate glass capillaries (Hilgenberg, Malsfeld, Germany) using a heat-controlled pipette puller (HEKA Elektronik, Lambrecht, Germany). For measurements of capacitance, the electrodes were coated with Sylgard close to the tips and fire-polished. In experiments simultaneously measuring current and capacitance, capacitance measurements were achieved using Sine+DC method (Lollike and Lindau, 1999). The measurements were made using an EPC-10 patch clamp amplifier and Pulse 8.71 software (Heka Elektronik). The sine wave had a frequency of 700 Hz and an amplitude of ±20 mV. For display, currents were filtered at 100 Hz. Exocytosis was also monitored as the ATP-induced currents that can be measured in cells engineered to express $P2X_2$ receptors ($P2X_2R$) as previously described (Obermuller *et al.*, 2005). These transient inward currents (TIC) provide the same type of information as amperometry of 5-HT release from β-cells preloaded with the amine. An important advantage is, however, that exocytosis is monitored across the entire cell surface area whereas amperometry covers <40% of the cell. It has been established that 5-HT and ATP are co-released and the TICs can accordingly be taken to reflect exocytosis of insulin-containing DCV (Braun *et al.*, 2007). When capacitance measurements were combined with the $P2X_2R$-based assay, increases in cell capacitance were calculated by taking 140 points before and after a $P2X_2$ current response. All current spikes were analyzed using the Mini Analysis Program 6.0.3 (Synaptosoft, USA) to determine the charge (integrated current; *Q*) of the individual events, which depends on the amount of ATP released. Events with *Q*-values that fell outside the standard deviation of the mean were deemed to represent compound exocytosis. Small events with slow activation/deactivation kinetics, reflecting kiss-and-run events (MacDonald, 2006), were excluded from further analysis. Such events accounted for 18% in Ins-1 and 23|% in rat β-cells.

**TIRF Microscopy**

Experiments were conducted with an inverted microscope (IX-81, Olympus, UK) customized for evanescent field microscopy using a high numerical aperture objective (1.49 N.A., Apo x 60 Oil, Olympus, UK) or (1.45 N.A., Apo × 150 Oil, Olympus UK) (Fig 8). VAMP-pHluorin was imaged with the 150x objective using 12 ms exposures, excitation at 488 nm at 16.7 Hz in full 512x512 mode (Figs 4-5). In some experiments, VAMP-pHluorin was measured using a 60x objective and 45ms exposures and recorded at 10 Hz using 512x256 pixels. All excitation was done using a 488 line laser (100mW argon ion laser, Melles Griot, Bensheim, Germany). Emitted light was collected using a 515-550 filter (Olympus) via a dichroic mirror that allowed transmission at 502 - 557 nm. Images were captured using a Cascade II 512b CCD camera (bin 1x1) controlled by Cell^R software (Olympus, UK). All analysis was performed using Metamorph Software v7.1. The VAMP-pHluorin images were analyzed first by eye for fluorescence that appear as a single stationary punctate spot. For measurements of exocytosis elicited by 100μM carbachol or 70mM KCl, integrated intensity measurements from a 2x2μm (Fig. 4-5) square placed over an exocytotic event were exported 10 frames before and 90 frames after the event became detectable. Co-localization between VAMP-pHluorin and insulin confirmed by fluorescent immunohistochemistry as previously described (Tsuboi and Rutter,

2003). Compound exocytosis was identified by taking events with intensities larger than the mean +3 standard deviations for single events. In order to compare exocytotic events in cells expressing different levels of VAMP-pHluorin, fluorescence changes were normalized against the average footprint fluorescence in each cell.

**On-cell capacitance measurements**

All on-cell measurements were performed and analyzed as previously described(MacDonald et al., 2005). Compound events were identified as events that associated with a capacitance increase larger than 3x average granule size as measured (MacDonald et al., 2006); 2.52 fF and 8.7 fF respectively for Ins-1 and and β-cells, respectively.

**FM1-43FX dye staining of exocytosis**

Primary rat β- or Ins-1 cells were plated on coverslips 24-48 hours prior to experiment. The cells were superfused with $Ca^{2+}$-free extracellular solution at 34°C for 5 minutes. The solution in the bath was then quickly removed and replaced with solution consisting of (in mM) 73 NaCl, 70 KCl, 1.2 $MgCl_2$, 2.6 $CaCl_2$, 1 D-glucose and 5 Hepes (pH 7.4 with NaOH) and 5μg/ml FM1-43FX (Invitrogen). After ~30 s of stimulation, the extracellular solution was removed and the cells fixed in 4% paraformaldehyde at 4°C. Cells were scanned in 0.4 μm z-slices using a Zeiss 510LSM confocal microscope. Excitation was effected at 488 nm and emitted light collected at 515-550 nm. Control cells not exposed to high extracellular $K^+$ did not show FM1-43FX invaginations.

**Electron Microscopy**

Experiments were performed as previously described (Olofsson et al., 2002). Briefly, After stimulation (10 min), the islets were fixed in 2.5% glutaraldehyde (Merck, Stockholm, Sweden) for 1 h, treated with 1% osmium tetroxide,dehydrated and embedded in Epon 812 (Agar Scientific, Essex, England) before ultrathin sections (60–80 nm) were cut using a LKB MK III Ultratome (Leica, Vienna, Austria). The sections were contrasted with uranyl acetate and lead citrate and finally examined in an electron microscope. Sections were examined in the Joel 1010 microscope.

**Solutions**

During the $P2X_2$ recording experiment, the cells were continuously superfused with extracellular solution containing (mM) 138 NaCl, 5.6 KCl, 2.6 $CaCl_2$, 1.2 $MgCl_2$, 5 HEPES, 1 D-glucose (5 mM D-glucose for the rat β-cells). The intracellular pipette solution contained in (mM):125 CsCl, 10 NaCl, 1 $MgCl_2$, 10 EGTA, 5 (0.2 μM intracellular free $Ca^{2+}$) or 9 $CaCl_2$ (2 μM), 3 Mg-ATP, 0.1 cAMP, 5 HEPES (pH 7.15 using CsOH). The free $Ca^{2+}$ concentration was estimated using the MAXC32 software (http://www.stanford.edu/~cpatton/maxc.html). In the on-cell capacitance measurements, the extracellular medium consisted of (mM) 125 NaCl, 4 KCl, 2 EGTA, 1 $MgCl_2$, 10 glucose and 10 HEPES (pH 7.2). The pipette-filing solution was comprised of (mM): 125 NaCl, 4 KCl, 2.6 $CaCl_2$, 1 $MgCl_2$, 13 TEA-Cl, and 10 HEPES (pH 7.2). In all experiments, the temperature was maintained at 30-33°C.

## Results

**$P2X_2$ currents display much wider variation in charge than expected from normal distribution of granule diameters**

Ins-1-cells and rat β-cells were engineered to express $P2X_2$ receptors ($P2X_2R$). Insulin-containing granules contain high levels of ATP (Hutton and Peshavaria, 1983) and exocytosis will therefore be associated with

release of ATP that will activate the $P2X_2R$ and thus give rise to transient currents (Obermuller *et al.*, 2005). The currents measured from both Ins-1 and rat β-cells when exocytosis was stimulated with 0.2 μM $[Ca^{2+}]_i$ are shown in Fig. 1A,C. It is evident that there is considerable amplitude variation. Whereas some events were smaller than 100 pA, other were larger than 1 nA. Histograms showing the distribution of the cubic root of the charge associated with these events ($\sqrt[3]{q}$; see Methods) are displayed in Fig. 1B,D. The distributions could be reasonably fit by single Gaussians. The mean *q* of the events that belonged to the distributions were 3.1±0.2 pC and 27.6±2.2 pC in Ins1- and rat β-cells, respectively. However, many events fell outside the normal distributions (open bars). The mean *q* of these events averaged 31±4

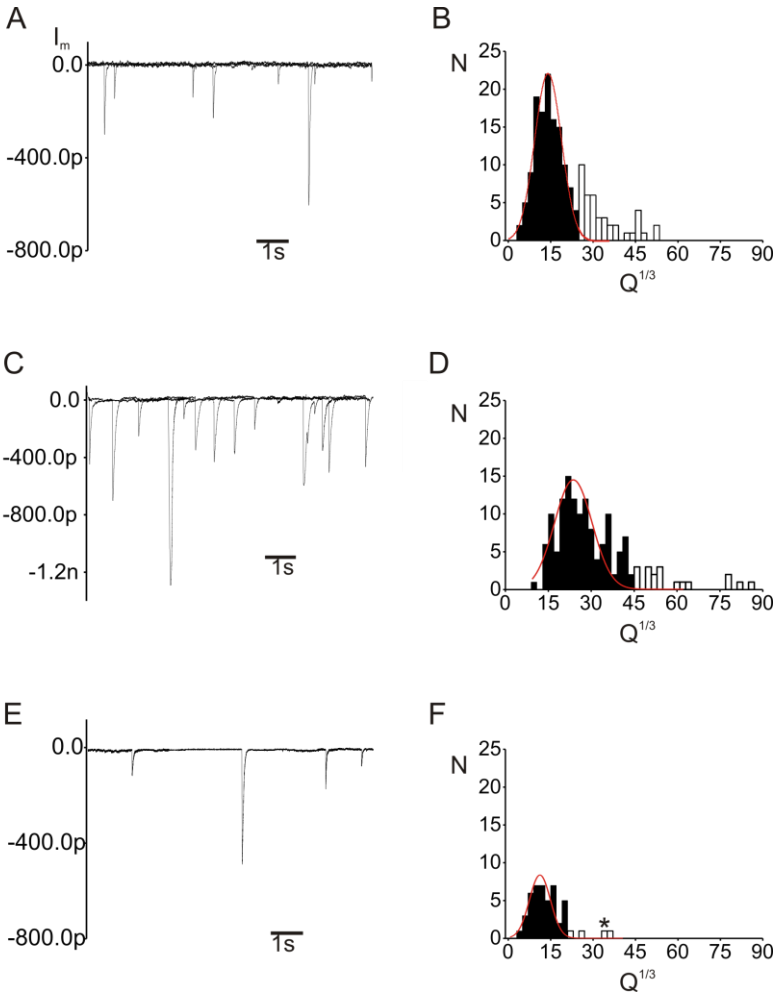


Figure 1. **Recordings of ATP release from Ins-1 and primary rat β-cells expressing $P2X_2$ receptors.** (A,C) $P2X_2R$ currents observed in Ins-1 cells (A) and rat β-cells (C) dialyzed with intracellular buffer containing 0.2 μM $[Ca^{2+}]_i$. In both (A) and (C), 3 successive sweeps have been superimposed. (B,D) Histograms showing the distributions of the cubic roots of the integrated currents associated with each current transient ($\sqrt[3]{Q}$) in Ins-1 (B) and rat β-cells (D). (E) $P2X_2R$ currents observed in an outside-out patch pulled from an Ins-1 cell. The events were recorded from thee different patches as indicated by the breaks. (F) Histogram showing the $\sqrt[3]{Q}$ of the current transients recorded in outside-out patches. The asterisks in (B,D) and (F) are the ones mentioned in Results. In B,D and F, events used for fitting the Gaussians are shown in black. The open bars (multivesicular release) were not used for these calculations.

pC (n=38) and 241±41 pC (n=21).

The larger events could be the result of many granules fusing simultaneously in different parts of the cell. To mitigate this interference, we limited our measurement area by monitoring ATP release in outside-out patches from Ins-1-cells (Fig 1E). These patches had an average capacitance of 0.67±0.10 pF (n=20 patches); only ~9% of the capacitance of the cells (7.5±1.8 pF: n=20). Again the distribution could be fit by a Gaussian. The mean *q* of the events under the curve was 2.8±0.5 pC (n=57). Also under these conditions, some of the events were bigger than expected. For example, the event highlighted by the asterisk in Fig. 1F is 35 pC,>13-fold larger than the mean *q*.

**Charge of $P2X_2$ receptor currents is linearly related to capacitance**

The data of Fig. 1E-F argue that superimposition of many small events is unlikely to account for the occurrence of the largest events. We addressed the alternative possible explanations of the large $P2X_2R$ events that either ATP content of the granules is highly variable or that compound exocytosis contributes to the amplitude variation. We examined these possibilities by simultaneous measurements of membrane capacitance and $P2X_2R$ currents. Fig. 2A-C show examples of events that were be recorded in rat β-cells when exocytosis was triggered by intracellular dialysis with 0.2 µM $[Ca^{2+}]_i$. Whereas the current transients in Fig. 2A are small (<200 pA) and associated with minute changes in membrane capacitance (<3 fF), both currents and capacitance increases are considerably larger in Fig. 2B-C. Fig. 2D-E summarize the relationship between the increases in membrane capacitance and the charge during events detected as $P2X_2$ transients in rat β- and Ins-1 cells,

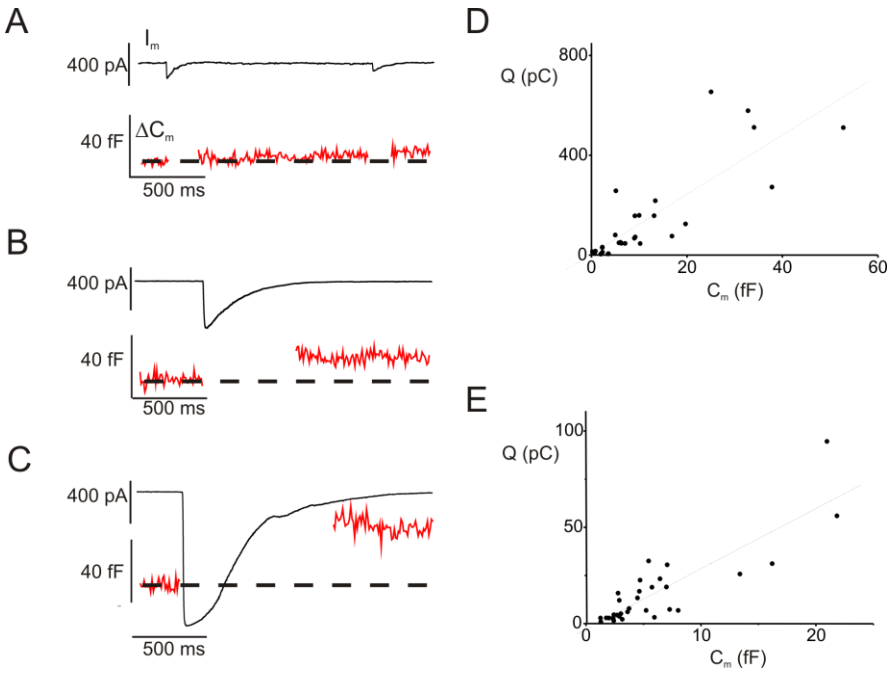


Figure 2. **$P2X_2R$ currents associated with increases in whole-cell capacitance.** (A-C) Examples of $P2X_2R$ current transients recorded from primary rat β-cells ($I_m$, black) are shown. A sinewave (800 Hz) was added to the holding potential to allow measurements of cell capacitance ($C_m$, red). (D) Relationship between the integrated $P2X_2R$-mediated current (*Q*) and the associated capacitance increase ($\Delta C_m$) for rat β-cells. The regression coefficients (*r*) were 0.69 and 0.78 in D and E, respectively ($p<0.001$ in both cases).

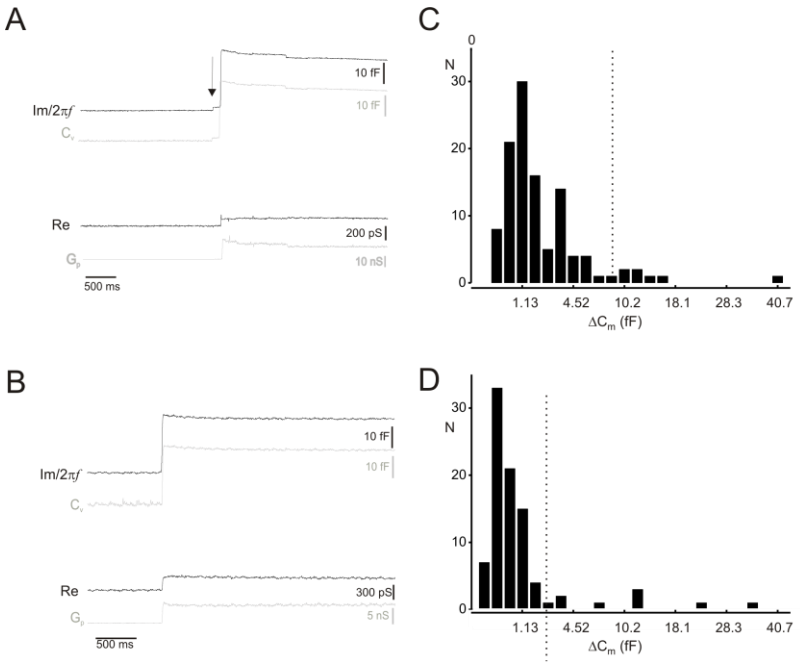


Figure 3. **Exocytosis of granules in cell-attached membrane patches of Ins-1 and primary rat β-cells have a varied distribution in single step size.** (A-B) Representative capacitance (Im/2π*f*) and conductance (Re) recordings from membrane patches of intact rat β cells stimulated with 10 mM glucose. Upward steps in Im/2π*f* result from the fusion of single vesicles within the patch. Deflections in Re during exocytosis result from the presence of fusion pores. The true vesicle capacitance ($C_v$) and fusion pore conductance ($G_p$) were calculated from the Im and Re conductance components (grey traces). The arrow in A highlights a small event (1.7 fF) preceding a large event producing a capacitance increase of 26.6 fF. (C-D) The size distribution of exocytotic events in rat β-cells (C) and Ins-1 cells (D) shown as vesicle diameter (below) and membrane capacitance (above). The vertical dashed lines indicate the diameter of a vesicle producing a capacitance increase 3-fold higher than the mean value (7.2 fF in C and 2.4 fF in D).

respectively. In both cases, the data could be described by linear relationships. The slopes of the relationships are 0.084 fF/pC and 0.29 fF/pC for the β- and Ins-1 cells. These values taken together with the mean charge of the events obtained in Fig. 1 predict unitary capacitance increases of 0.8-0.9 fF (for *q*-values of 2.8-3.1 pC) and 2.3 fF (*q*=29 pC) in Ins-1 and rat β-cells, respectively. For comparison, the average step increase in on-cell capacitance measurements average 0.8 fF in Ins-1(MacDonald *et al.*, 2005) and 2.9 fF in rat β-cells (MacDonald *et al.*, 2006).

The linear relationship between current amplitude and the capacitance step raises the interesting possibility that multiple granules prefuse and give rise to a large $P2X_2R$ currents and increases in membrane capacitance. The fact that a relationship can be observed also militates against the possibility that the wide distribution of current amplitudes solely reflects large variability of granular ATP content, although this may well contribute to the scatter of the data points.

**On-cell capacitance detects compound exocytosis.**

If granules prefuse within the cell and undergo compound exocytosis, this should be seen as a population of large capacitance steps in high-resolution on-cell capacitance measurements. We note that in on-cell capacitance measurements of exocytosis, only ~1% of the cell surface membrane area

is included in the pipette. In addition, these measurements are not offset by the large conductance changes due to activation of the $P2X_2$ receptors. Fig. 3A (arrow) shows an example of a typical single event in a rat β-cell. These events have, consistent with our previous findings (MacDonald *et al.*, 2006), an average size of ~ 3 fF. More extensive analysis revealed a small population of much larger events (Fig. 3A-B). Thus, 7% of all recorded events in rat β-cells (8 events out of 110 events in 43 cells) were associated with a capacitance jump 3-fold larger than the average event size (to the right of the dotted line in Fig. 3C). Assuming normal distribution around the mean value, it can be estimated that <0.01% of the events would have such large diameter as measured by electron microscopy (MacDonald *et al.*, 2005). In Ins-1-cells, 11% of all events (i.e. 9 out of 80 events in 22 cells) displayed capacitance steps 3-fold larger than the average size (Fig 3D). The DCV release rates were 0.34±0.03 events/min*patch (n=48) (MacDonald *et al.*, 2005) in Ins-1 cells and 0.42±0.07 events/min*patch (n=48) in rat β-cells.

**Visualizing compound exocytosis through TIRF microscopy**

The above data suggest that compound exocytosis accounts for 7-10% of all exocytotic events. This contrasts with imaging data recently reported that compound exocytosis is negligible in intact mouse islets (Takahashi *et al.*, 2004). To address this discrepancy, we used TIRF illumination to visualize exocytosis in cell expressing VAMP-pHluorin (a granule-specific transmembrane protein, pHluorin exposed to the granule lumen) (Tsuboi and Rutter, 2003). Fig. 4A shows a typical exocytotic event elicited by high-$K^+$ stimulation (70 mM). The VAMP-pHluorin signal is initially "silent" due to the low intragranular pH. Following exocytosis, there is a dramatic increase in fluorescence, reflecting the opening of the fusion pore and $H^+$ equilibration leading to an increase in granular pH. Next, the VAMP-pHluorin-labeled granule membrane spreads laterally within the plasma membrane. Figure 4C shows the corresponding time course of fluorescence change measured in the region of interest (grey trace). Most of the events were of roughly the same amplitude (Fig. 4D). Occasionally, events of larger amplitude were seen. Figure 4B shows an example of an event consisting of the simultaneous appearance of an oblong structure with the dimensions of two single granules ($4^{th}$ frame from left), which merge over the subsequent two frames into a circular shape from which VAMP-pHluroin subsequently diffuses. The black trace of Fig. 4C shows the time course of the fluorescence change associated with this event. It takes longer to peak and the amplitude is approximately twice that of the individual event in Fig. 4A (one of two events highlighted in red in Fig. 4D). We ascertained the uniformity of the evanescent field by measuring the background VAMP-pHluorin signal that results from incomplete retrieval of vesicular membrane proteins (Granseth et al., 2006; Balaji and Ryan, 2007). Every cell was scanned along both the x- and y-axis (Figure 4E) and the mean fluorescence was calculated as a function of the width of the cell footprint. This analysis (Figure 4F) illustrates that there was no significant distortion of the data due to non-uniformity of the illumination.

**Compound exocytosis is evoked by the muscarinic agonist carbachol**

Although we observed some compound exocytotic events in cells stimulated with glucose, they were much smaller than that expected from the observations made in Figs. 1-3. One important difference between electrophysiological measurements (Figs. 1-

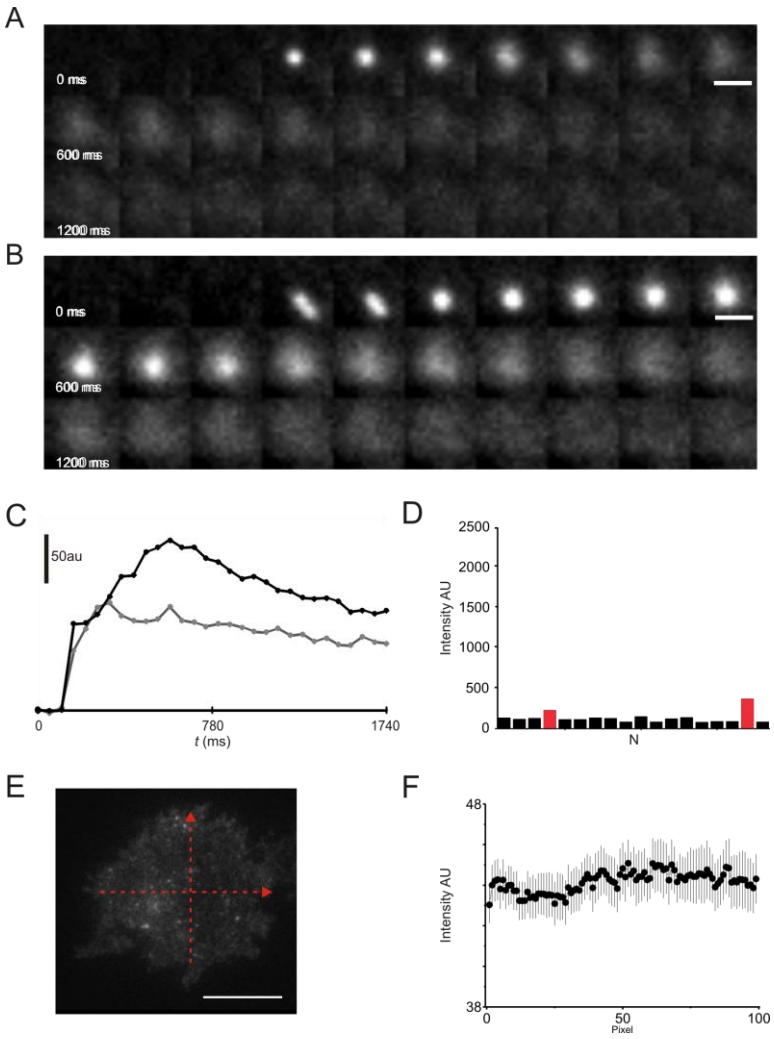


Figure 4. **Total internal reflection illuminated images of multivesicular compound exocytosis.** (A) Representative montage of a single exocytotic event (image interval: 60 ms). The red square highlights the frame of peak fluorescence, which occurred 120ms after opening of the fusion pore with resultant unquenching of pHluorin and increase in fluorescence. (B) Montage of a compound exocytotic event of two interconnected granules that both exist in the evanescent field at the onset of fusion pore formation, as shown in the frame highlighted in blue. The frame containing peak fluorescence is highlighted in red, occurring 480ms after opening of the fusion pore. 30 consecutive time-lapse images obtained by TIRF microscopy in an Ins-1 cell transfected with VAMP-pHluorin are shown. Exocytosis was evoked by superfusion with a buffer containing 70 mM $K^+$. Scale bar: 1 µm. (C) Intensity of fluorescence in the images shown in (A; grey trace) and (B, black trace) plotted against time. (D) Distribution of integrated intensity of pHlourin fluorescence. n=18 events recorded from 7 cells. The red bars show the two events associated with a fluorescence increase 2-to 3-fold greater than average.

2) and the TIRF microscopy data shown in Fig. 4 is the way the β-cells were stimulated. Whereas exocytosis was triggered by $Ca^{2+}$ influx through voltage-gated $Ca^{2+}$-channels in Fig. 4, $Ca^{2+}$ was supplied by infusion from the recording electrode in Figs. 1-2 leading to a global and uniform elevation of $[Ca^{2+}]_i$. It is well established that ACh acting through muscarinic receptors stimulates insulin secretion by mobilization of intracellular $[Ca^{2+}]_i$ stores (Gilon and Henquin, 2001). This leads to a large and global elevation of $[Ca^{2+}]_i$, thus mimicking the situation during the whole-cell

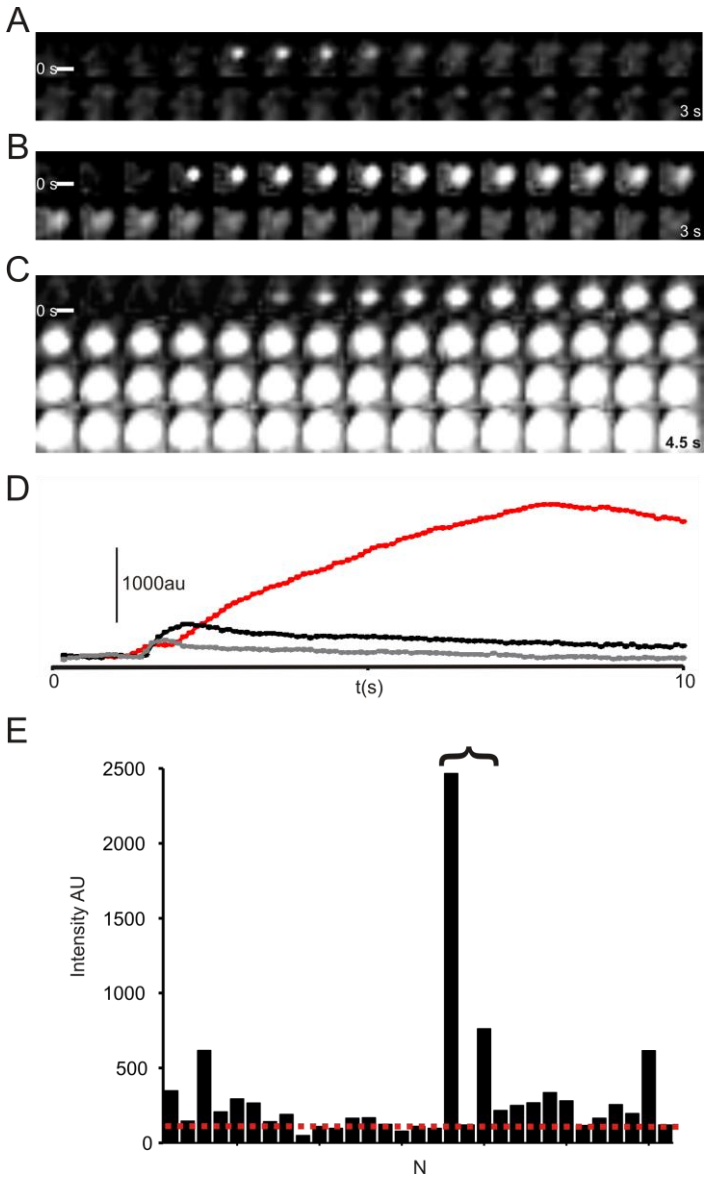


Figure 5. **Carbachol-induced stimulation of exocytosis in Ins-1 cells. (**A-C) As in fig. 4A-B but the image interval is 100 ms and secretion was evoked by puffer ejection of 60 nl of 1 mM carbachol close to the cell. (D) Intensity of fluorescence in the images shown in (A; grey trace) and (B, black trace) and (C, red trace) plotted against time. (E) Distribution of integrated intensity of pHlourin fluorescence. A total of 31 events in 9 cells were analyzed. The red line represents the average intensity from single exocytotic events evoked by $K^+$ and is overlayed for reference. The asterisk bracket highlights the three events displayed in (A-C).

capacitance measurements. Figure 5A shows an individual granule undergoing exocytosis in response to puffer application of the muscarinic agonist carbachol (grey trace in Fig. 5D). This individual event displayed characteristics indistinguishable from those evoked by high-$K^+$ stimulation. However, many more large events are observed when secretion was evoked by carbachol. Fig. 5B shows an example with a fluorescence increase corresponding to six granules of the type in Fig. 5A. Similar to what was observed in Fig. 4B, the fluorescence increased gradually over 700 ms (Fig. 5D, black trace). Finally, Fig. 5C shows an example of a very large event, with a

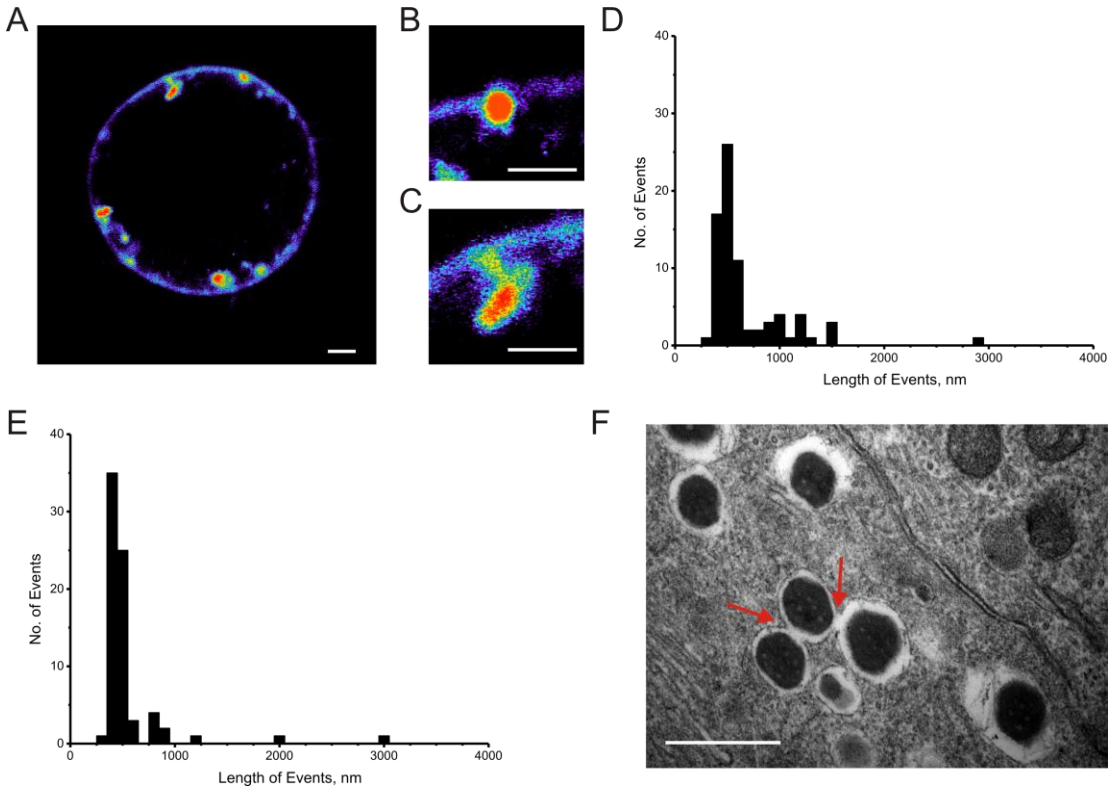


Fig. 6**. Multivesicular exocytosis detected by confocal imaging. (**A**)** Section through the center of a rat β-cell stained with FM1-43FX during a 30-s stimulation with 70 mM $K^+$ in the presence of 5 mM glucose. (B) A fusion event of a single granule. (C) A single fusion event showing 3 interconnected granules. (D) Distribution of fusion events based upon length of stained punctate-fluorescence continuous with the plasma membrane in rat β-cells (n=74). (E) Same as D but in Ins-1 cells (n=75) (F) Electron micrographs of β-cells exposed to control medium containing 16 mM glucose supplemented with 100 μM carbachol. Red arrows highlight luminal connections between granules. Note continuity of surrounding granule membranes. Scale Bar = 400nm.

magnitude corresponding to the simultaneous release of 14 secretory granules and where fluorescence increased over 7 s (Fig. 5D). Fig. 5E shows the amplitude variations of 31 separate events. The red line indicates the average fluorescence increase of the single events evoked by high-$K^+$. In the presence of carbachol, 29% of the exocytotic events were of the "compound" type (i.e. produced a fluorescence increase larger than the average amplitude + 2 standard deviations). On average, these events were 6-fold larger than the average event.

**Multivesicular and single-vesicle exocytosis imaged with FM1-43FX**

We next used the dye FM1-43FX (Cochilla et al., 1999) to observe exocytosis of secretory granules in Ins1 cells. The FM1-43FX dye only labels membranes in direct contact with the extracellular solution. Fig. 6A shows a confocal image taken through the center of the cell. Exocytotic events were identified as bright punctuate spots. Fig. 6B shows the most common (>90%; n=74) event. These events had a diameter of 500-600 nm. Fluorescent beads with a diameter of 200 nm had a measured diameter of

500±25 nm (n=12). The latter observation makes it likely that the observed FM1-43FX pucta observed following stimulation reflect exocytosis of insulin vesicles, which have a diameter of ~300 nm (Braun et al., 2004). Occasionally, FM1-43FX stained much larger and complex structures, an example of which is shown in Fig. 6C. Fig. 6D shows a histogram for the length of the axis through the structures. Whereas most events were close to the average of ~0.6 μm with 90% of the measured events ≤1 μm, some events were much longer (up to 2.8 μm in a single plane). Similar observations were made in Ins1-cells (Fig. 6E).

**Ultrastructural evidence of granule prefusion**

The existence of multivesicular structures in β-cells was also documented by electron microscopy. Fig. 6F shows an electron micrograph of a rat islet. Although it was difficult to quantify three-dimensional structures of granules using this technique due to the ultra thin two-dimensional nature of the preparation used in EM, the presence of clear connections (with continuous vesicle membrane) between the lumina between adjacent DCVs (red arrows Fig. 6F) provide ultrastructural evidence that multivesicular structures from within the cytosol under certain conditions.

## Discussion

We have detected compound exocytosis by several different techniques: TIRF imaging, on-cell capacitance measurements, parallel ATP-release and whole-cell capacitance measurements, confocal imaing and electron microscopy. Collectively, these data provide a strong case for compound exocytosis in the β-cell. We acknowledge that our conclusion is at variance with the data previously reported by others suggesting that compound exocytosis in the β-cell, if it occurs at all, is a very rare event.

It could be argued that the events we characterized as compound exocytosis in the imaging experiments were simply the fusion of granules that were more densely packed with VAMP-pHluorin. There are at least two reasons why we believe this possibility can be rejected. First, the small events showed consistent fluorescence increases both at the single-cell level and between different cells (Fig. 5E; 38 events in 11 different cells). Even if the loading of the granules varied, it remains to be explained why the time course of the fluorescence increase should be slower for the large events (Fig. 5D). It could also be proposed that the large events observed by imaging (Figs. 4-5) and the on-cell capacitance measurements (Fig. 3) reflect exocytosis of many individual events occurring temporally and spatially close to each other. Again, we think this possibility can be discarded because all events began as a punctate spot and the fluorescence spreads radially (Fig 5A-C). Such behaviour is better explained by the flow of fluorescent membrane from a single fusion pore as illustrated schematically in Fig. 7. Indeed, the multivesicular structures do not collapse into a big sack of granules but retain some of the structure and can be seen as chains of interconnected granules both in electron micrographs and in FM1-43 imaging (Fig. 6). The latter is reminiscent of what has been reported in rat lactrotropes (Cochilla *et al.*, 2000). This might be a reason for the low frequency at which these structures are seen in the electron micrograph. The luminal bridges remain quite narrow and unless they are captured in the sectioning, the granules would seem unconnected. The shape of the multivesicular structures might also be of consequence for detecting such events using optical techniques. To visualize a chain of linked DCVs undergoing compound exocytosis would only possible if the granules line up in the single focal plane under observation. This structure also would

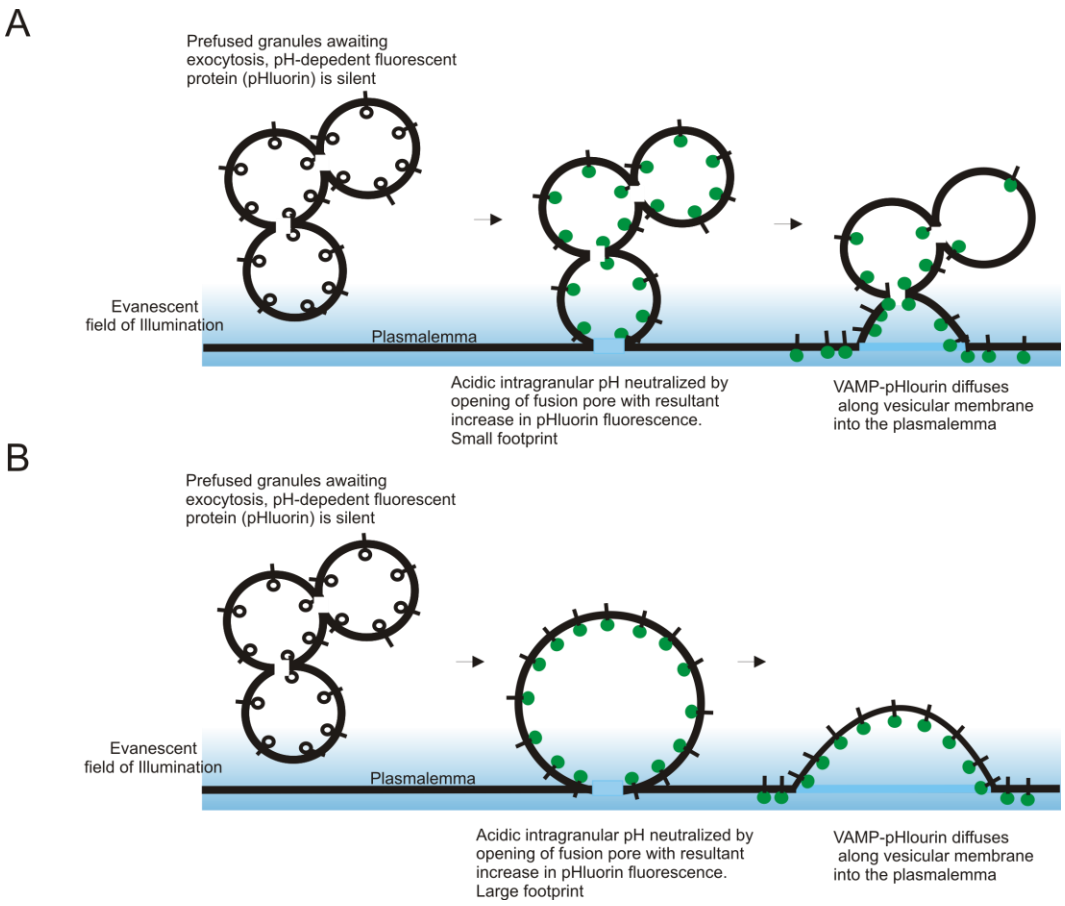


Fig. 7. **Schematic of two possible forms of compound exocytosis**. (A) The granules retain their structure and exist as a chain of vesicles interconnected via narrow pores. Upon exocytosis and pH equilibration the pHluorin fluorescence increases but because the evanescent field only extend ~100 nm into the cell, the initial footprint remains small. (B) The individual vesicles collapse into a big sack. In the latter case, fusion with the plasma membrane and resultant pH equilibration is expected to produce a large initial footprint. In both A and B, VAMP-pHluorin subsequently diffuses laterally within the membrane.

likely explain the rather slow increase in fluorescence of VAMP-pHluorin for compound events.

Statistical analysis of the on-cell capacitance measurements also makes it highly unlikely that the large events result from (close to) simultaneous fusion of granules. If we assume that exocytotic events form a stationery time series with the rate constant of λ, then the probability ($P$) that during time $t$ at least two events follow is given by the expression (Feller, 1971):

$$P = 1 - \exp(-\lambda t) - \lambda t \exp(-\lambda t)$$

With the observed release rates (0.34min-1 in Ins-1 cells and 0.42min-1 in rat β-cells), we can estimate that the likelihood of at least 2 events occurring within 25 ms (the time frame over which the membrane capacitance settles at the new level following exocytosis in on-cell measurements) is ~$10^{-8}$ in both cell types. Thus, it seems justifiable to conclude that the large steps we observe result from single multivesicular fusion events,

The fusion between DCVs prior to exocytosis is most likely explained through the action of t-SNARE proteins, syntaxin and SNAP-25. Although the t-SNAREs are

most commonly found on the plasmalemma, they are also present on secretory organelles as well (Takamori et al., 2006). We found that the frequency of multivesicular events increased following stimulation with the muscarinic agonist carbachol. Activation of muscarinic receptors in β-cells stimules insulin secretion by at least three mechanisms: i) by stimulation of electrical activity; ii) by $IP_3$-induced mobilization of intracellular $Ca^{2+}$; and iii) PKC-dependent enhancement of exocytosis (Gilon et al., 1997). The combination of these effects result in global elevation of cytosolic $Ca^{2+}$ and thereby promote fusion between insulin granules prior to exocytosis.

The multivesicular structures we observe within the β-cells retain their dense cores. The integrity of the dense cores is not completely unexpected because the stability of the $Zn_2$-$insulin_6$ complex is determined by the granular pH and there is no reason why pH should increase following fusion with other granules. However, once fusion with the plasma membrane has occurred, pH equilibration will propagate through the structure leading to the solvation of the crystal throughout the multivesicular complex. While the prefused granules retain their string of pearls shape in the cytosol, it is also likely that this shape could be retained during exocytosis. The fusion pores shown (Fig. 3A-B) are 5-10 nS, which correspond to pore diameters of 10-15 nm. Although this pore diameter is large enough to allow the flow of pHluorin and insulin molecules (~3 nm diameter), it would nevertheless be expected to limit the speed of their diffusion. This may contribute to the fact that insulin secretion (measured biochemically) is so much slower than expected from the capacitance measurements (Rorsman and Renstrom, 2003). The retention of shape during a compound fusion event would also minimize the amount of endocytotic proteins such as clathrin (Merrifield et al., 2005) needed for the retrieval of exocytosed membrane. Interestingly, large step-wise decreases in membrane capacitance during endocytosis have previously been observed in mouse β-cells (Eliasson et al., 1996). These large endocytotic events were observed when exocytosis was evoked by $Ca^{2+}$ infusion, i.e. experimental conditions similar to those employed here when compound exocytosis was observed.

Recent work using 2-photon imaging in intact mouse islets (Takahashi *et al.*, 2004) failed to reveal compound exocytosis, and instead favoured the view that the vesicles fuse to each other sequentially. However, sequential exocytosis over tens of seconds would be inconsistent with the finding that the capacitance increases seen in the on-cell measurements were instantaneous even for the largest events. Moreover, the finding that the fluorescence increases in a gradual fashion during the large events suggests that VAMP-pHluorin containing membrane is continuous. If rapid sequential exocytosis occurred, then discrete increases in VAMP-pHluorin signal would be expected. We emphasize that our measurements should not be taken as evidence that the slow form of sequential exocytosis does not occur. In this form of exocytosis, the sequential fusion of a new DCV with one that has previously undergone exocytosis would occur outside the evanescent field and thus escape detection (Tran et al., 2007). In the capacitance and $P2X_2R$ measurements, this would simply appear as a series of individual events.

What is the functional significance of multivesicular exocytosis? The low density of $Ca^{2+}$ channels in the β-cells can be envisaged to limit the number of secretory granules that are sufficiently close to the $Ca^{2+}$-channel to undergo exocytosis upon depolarization. If several granules can

prefuse, then a large exocytotic response may initiated by $Ca^{2+}$ influx via a single (cluster of) $Ca^{2+}$-channels (Barg *et al.*, 2001). The significance of this is illustrated by the decline of the exocytotic responses during repetitive stimulation with depolarizing pulses to activate the voltage-gated $Ca^{2+}$-channels. This effect was not due to the depletion of release-competent granules as evidenced by the consistency of the exocytotic responses elicited by photoliberation of caged $Ca^{2+}$ (see Fig. 5. of (Barg *et al.*, 2001)). Although compound exocytosis in the presence of glucose alone accounts for only 7% of the release events, compound exocytosis may be functionally more significant under other conditions. For example, in the presence of carbachol, 29% of the events were of the multivesicular type and associated with fluorescence increases ~6-fold larger than the average event size. If these data can be extrapolated to amounts of insulin secretion, then it can be estimated that 70% of the hormone released during muscarinic stimulation may be released by compound exocytosis.

## Acknowledgements

We thank Dr. Stephen Arch (Reed College, Portland, OR) for helpful comments in the preparation of this manuscript and Dr Juris Galvanovskis for advice on the statistical analysis. This work was supported by grants from the Wellcome Trust (WT072289) and the Integrated Project Eurodia (LSHM-CT-2006-518153) as well as OXION (Ion Channels and Disease Initiative) to PR, the Canadian Institutes of Health Research (MOP81350) to PEM and the Swedish Research Council to LE. P. MacDonald is a CDA and AHFMR Scholar and the Canada Research Chair in Islet Biology. P. Rorsman is a Wolfson-Royal Society Merit Award Research Fellow.

## Abbreviations

ATP = adenosine triphosphate
$InsP_3$ = inositol trisphosphate
TIRF = total internal reflection
SNARE = soluble NSF attachment receptor
ACh = acetylcholine

## References

Ammala, C., L. Eliasson, K. Bokvist, O. Larsson, F.M. Ashcroft, and P. Rorsman. 1993. Exocytosis elicited by action potentials and voltage-clamp calcium currents in individual mouse pancreatic B-cells. *J Physiol*. 472:665-688.

Balaji, J., and T.A. Ryan. 2007. Single-vesicle imaging reveals that synaptic vesicle exocytosis and endocytosis are coupled by a single stochastic mode. *Proc Natl Acad Sci U S A*. 104:20576-20581.

Barg, S., X. Ma, L. Eliasson, J. Galvanovskis, S.O. Gopel, S. Obermuller, J. Platzer, E. Renstrom, M. Trus, D. Atlas, J. Striessnig, and P. Rorsman. 2001. Fast exocytosis with few Ca(2+) channels in insulin-secreting mouse pancreatic B cells. *Biophys J*. 81:3308-3323.

Bokvist, K., M. Holmqvist, J. Gromada, and P. Rorsman. 2000. Compound exocytosis in voltage-clamped mouse pancreatic beta-cells revealed by carbon fibre amperometry. *Pflugers Arch*. 439:634-645.

Braun, M., A. Wendt, J. Karanauskaite, J. Galvanovskis, A. Clark, P.E. Macdonald, and P. Rorsman. 2007. Corelease and Differential Exit via the Fusion Pore of GABA, Serotonin, and ATP from LDCV in Rat Pancreatic {beta} Cells. *J Gen Physiol*. 129:221-231.

Cochilla, A.J., J.K. Angleson, and W.J. Betz. 1999. Monitoring secretory membrane with FM1-43

fluorescence. *Annu Rev Neurosci*. 22:1-10.

Cochilla, A.J., J.K. Angleson, and W.J. Betz. 2000. Differential regulation of granule-to-granule and granule-to-plasma membrane fusion during secretion from rat pituitary lactotrophs. *J Cell Biol*. 150:839-848.

Dahl, G., and J.C. Henquin. 1978. Cold-induced insulin release in vitro: evidence for exocytosis. *Cell Tissue Res*. 194:387-398.

Eliasson, L., P. Proks, C. Ammala, F.M. Ashcroft, K. Bokvist, E. Renstrom, P. Rorsman, and P.A. Smith. 1996. Endocytosis of secretory granules in mouse pancreatic beta-cells evoked by transient elevation of cytosolic calcium. *J Physiol*. 493 ( Pt 3):755-767.

Feller, W. 1971. An introduction to probability theory and its applications. Vol. 1, 2nd edition. John Wiley & Sons, Inc., 536 pp.

Fenwick, E.M., A. Marty, and E. Neher. 1982. Sodium and calcium channels in bovine chromaffin cells. *J Physiol*. 331:599-635.

Gillis, K.D., and S. Misler. 1992. Single cell assay of exocytosis from pancreatic islet B cells. *Pflugers Arch*. 420:121-123.

Gilon, P., and J.C. Henquin. 2001. Mechanisms and physiological significance of the cholinergic control of pancreatic beta-cell function. *Endocr Rev*. 22:565-604.

Gilon, P., J. Yakel, J. Gromada, Y. Zhu, J.C. Henquin, and P. Rorsman. 1997. G protein-dependent inhibition of L-type Ca2+ currents by acetylcholine in mouse pancreatic B-cells. *J Physiol*. 499 ( Pt 1):65-76.

Granseth, B., B. Odermatt, S.J. Royle, and L. Lagnado. 2006. Clathrin-mediated endocytosis is the dominant mechanism of vesicle retrieval at hippocampal synapses. *Neuron*. 51:773-786.

Hafez, I., A. Stolpe, and M. Lindau. 2003. Compound exocytosis and cumulative fusion in eosinophils. *J Biol Chem*. 278:44921-44928.

Hutton, J.C., and M. Peshavaria. 1983. Nucleotide and bivalent cation specificity of the insulin-granule proton translocase. *Biochem J*. 210:235-242.

Klingauf, J., and E. Neher. 1997. Modeling buffered Ca2+ diffusion near the membrane: implications for secretion in neuroendocrine cells. *Biophys J*. 72:674-690.

Kwan, E.P., and H.Y. Gaisano. 2005. Glucagon-like peptide 1 regulates sequential and compound exocytosis in pancreatic islet beta-cells. *Diabetes*. 54:2734-2743.

Lollike, K., and M. Lindau. 1999. Membrane capacitance techniques to monitor granule exocytosis in neutrophils. *J Immunol Methods*. 232:111-120.

Lollike, K., M. Lindau, J. Calafat, and N. Borregaard. 2002. Compound exocytosis of granules in human neutrophils. *J Leukoc Biol*. 71:973-980.

MacDonald, P.E., M. Braun, J. Galvanovskis, and P. Rorsman. 2006. Release of small transmitters through kiss-and-run fusion pores in rat pancreatic beta cells. *Cell Metab*. 4:283-290.

MacDonald, P.E., S. Obermuller, J. Vikman, J. Galvanovskis, P. Rorsman, and L. Eliasson. 2005. Regulated exocytosis and kiss-and-run of synaptic-like microvesicles in INS-1 and primary rat beta-cells. *Diabetes*. 54:736-743.

Merrifield, C.J., D. Perrais, and D. Zenisek. 2005. Coupling between clathrin-coated-pit invagination, cortactin recruitment, and membrane scission observed in live cells. *Cell*. 121:593-606.

Nemoto, T., R. Kimura, K. Ito, A. Tachikawa, Y. Miyashita, M. Iino, and H. Kasai. 2001. Sequential-replenishment mechanism of exocytosis in pancreatic acini. *Nat Cell Biol*. 3:253-258.

Obermuller, S., A. Lindqvist, J. Karanauskaite, J. Galvanovskis, P. Rorsman, and S. Barg. 2005. Selective nucleotide-release from dense-core granules in insulin-secreting cells. *J Cell Sci*. 118:4271-4282.

Olofsson, C.S., S.O. Gopel, S. Barg, J. Galvanovskis, X. Ma, A. Salehi, P. Rorsman, and L. Eliasson. 2002. Fast insulin secretion reflects exocytosis of docked granules in mouse pancreatic B-cells. *Pflugers Arch*. 444:43-51.

Orci, L., and W. Malaisse. 1980. Hypothesis: single and chain release of insulin secretory granules is related to anionic transport at exocytotic sites. *Diabetes*. 29:943-944.

Rorsman, P., and E. Renstrom. 2003. Insulin granule dynamics in pancreatic beta cells. *Diabetologia*. 46:1029-1045.

Takahashi, N., H. Hatakeyama, H. Okado, A. Miwa, T. Kishimoto, T. Kojima, T. Abe, and H. Kasai. 2004. Sequential exocytosis of insulin granules is associated with redistribution of SNAP25. *J Cell Biol*. 165:255-262.

Takahashi, N., and H. Kasai. 2007. Exocytic process analyzed with two-photon excitation imaging in endocrine pancreas. *Endocr J*. 54:337-346.

Takamori, S., M. Holt, K. Stenius, E.A. Lemke, M. Gronborg, D. Riedel, H. Urlaub, S. Schenck, B. Brugger, P. Ringler, S.A. Muller, B. Rammner, F. Grater, J.S. Hub, B.L. De Groot, G. Mieskes, Y. Moriyama, J. Klingauf, H. Grubmuller, J. Heuser, F. Wieland, and R. Jahn. 2006. Molecular anatomy of a trafficking organelle. *Cell*. 127:831-846.

Tran, V.S., S. Huet, I. Fanget, S. Cribier, J.P. Henry, and E. Karatekin. 2007. Characterization of sequential exocytosis in a human neuroendocrine cell line using evanescent wave microscopy and "virtual trajectory" analysis. *Eur Biophys J*. 37:55-69.

Tsuboi, T., and G.A. Rutter. 2003. Multiple forms of "kiss-and-run" exocytosis revealed by evanescent wave microscopy. *Curr Biol*. 13:563-567.